THE MACHINE CASTING OF
HIGH TEMPERATURE SEMI-SOLID METALS

By

DANIEL GUSTAV BACKMAN

S.B., Massachusetts Institute of Technology
(1972)

S.M., Massachusetts Institute of Technology
(1972)

Submitted in partial fulfillment of the requirements

for the degree of

DOCTOR OF SCIENCE

at the

Massachusetts Institute of Technology
September, 1975

Signature of Author...
Department of Materials Science and
Engineering , August 11, 1975

Certified by..
Thesis Supervisor

Certified by..
Thesis Supervisor

Accepted by...
Chairman, Departmental Committee on Graduate
Students

MASS. INST. TECH.
OCT 8 1975
LIBRARIES

THE MACHINE CASTING OF
HIGH TEMPERATURE SEMI-SOLID METALS

by

DANIEL GUSTAV BACKMAN

Submitted to the Department of Materials Science and Engineering on August 11, 1975 in partial fulfillment of the requirements for the degree of Doctor of Science.

ABSTRACT

A new process developed for machine (die) casting of high melting temperature alloy has been investigated. The process employs a partially solidified, vigorously agitated, alloy as charge material. Interest in this new development is stimulated by the predicted longer die lives and improved quality of the parts fabricated. The casting system includes; a continuous slurry producer, a reheat furnace, and a die casting machine. Efforts have been directed toward understanding the effect of process variables in the slurry producer and the die casting machine on the structure and porosity content of the castings. Die thermal behavior has been studied by direct thermal measurement and computer heat flow analysis.

Microstructures of a variety of semi-solid alloys, including: copper-base alloy 905, eutectic cast iron (Fe-2.6%-C-3.2%Si), 440 and 304 stainless steels, and cobalt-base alloy H.S. 31 produced in the continuous slurry producer have been studied. Average primary solid particle size varied from 100 to 350 microns. The average cooling and shear rates during primary solidification were 40°C/min and 350 sec^{-1}. Microprobe work showed that the primary solid particles have essentially flat concentration profiles with abrupt concentration variations at the particle boundaries and veins of entrapped liquid.

X-ray radiograph ratings were used to evaluate casting quality. The copper-base alloy 905 castings produced from semi-solid charge material have significantly less entrapped air and shrinkage porosity than those produced from the fully liquid alloy. The semi-solid slurry shrinks less. It is viscous, hence it convects less during die filling, resulting in reduced air entrapment in the castings.

A uniform distribution of primary solid particles was observed throughout the cross-section of die castings made from the partially solidified slurries.

Experimental measurements and computer simulations of die thermal behavior during casting of all liquid and partially solid copper-base alloy 905 and all liquid eutectic cast iron were carried out. In both the low and the high pressure casting machines used, the maximum die temperature and initial rate of temperature change in the die were significantly lower when a partially solid charge material was used. For example, measured die temperatures in the high pressure commercial machine were 475°C and 150°C above the initial die temperature when the copper-base alloy was cast in the 100°C superheated state and the partially solid (volume fraction solid ~0.5) state, respectively.

Correlation of computer predictions and measured die temperatures have been used to calculate values of the heat transfer coefficient at the casting-die interface. Using these values, the maximum die surface temperature and die surface temperature gradients are calculated. The values of maximum surface temperature obtained are 800°C and 315°C for a superheated (100°C) liquid charge and a partially solid (volume fraction solid ~0.5) state, respectively. The corresponding surface temperature gradients are 5640°C/cm and 718°C/cm, respectively.

The reduced thermal shock experienced by the die when a partially solid metal alloy is cast should improve die life considerably over conventional practice. With this added incentive, machine (die) casting of high temperature alloys may become competitive with alternate casting or forming processes.

Thesis Supervisors: Robert Mehrabian
Associate Professor of Materials Science & Engineering

Merton C. Flemings
Abex Professor of Materials Science & Engineering

TABLE OF CONTENTS

Chapter Number		Page Number
	ABSTRACT	2
	FIGURE CAPTIONS	6
	ACKNOWLEDGEMENTS	12
I	INTRODUCTION	13
	1. The Casting of Semi-Solid Slurries	20
	2. The production of Semi-Solid Slurries	21
	3. The Areas of Concentration	22
II	LITERATURE SURVEY	24
	A. Structure, Rheology, and Casting of Semi-Solid Alloys	24
	1. Formation of Rheocast Structures	25
	2. The Effect of Process Variables on Structure	26
	3. Rheology of Rheocast Structures	28
	4. Casting of Rheocast Alloys	30
	B. Die Heat Flow Analysis	32
	1. Analytical Solutions	33
	2. Computer Simulation	38
	3. Die Casting Heat Flow Studies	43
	4. Surface Heat Transfer Coefficient	45
	C. Die Failure	48
	1. Theoretical Study	48
	2. Experimental Studies	52
III	APPARATUS	57
	1. The High Temperature Slurry Producer	57
	2. The Collection System	60
	3. The Reheat System	61
	4. The Low Pressure Casting System	61
	5. High Pressure Die Casting System	63
	6. Thermal Measurement System	64
IV	EXPERIMENTAL PROGRAM	65
V	RESULTS	68
	1. The Structure of Semi-Solid Slurries	68
	2. Castings	72

Chapter Number		Page Number
	3. Die Thermal Analysis	75
	(a) Low Pressure System	75
	(b) High Pressure System	76
VI	HEAT FLOW SIMULATION	79
	1. Computer Results	86
	(a) Surface Die Temperature	89
VII	DISCUSSION	92
	1. Introduction	92
	2. The Structure of Semi-Solid Slurries	93
	3. Castings	98
	4. Die Thermal Analysis	101
VIII	CONCLUSIONS	106
IX	SUGGESTIONS FOR FUTURE WORK	110
	REFERENCES	112
	Table I - Life of Core and Die Materials	117
	Table II - Number of Cycles for Crack Initiation	118
	Table III - Summary of Microprobe Results	119
	Table IV - Casting Conditions for Castings No. 72 - No. 89	120
	Appendix A - Electron Beam Microanalyzer	163
	Appendix B - Computer Program and Flow Diagram	164
	BIOGRAPHICAL NOTE	185

FIGURE CAPTIONS

Figure Number		Page Number
1	Measured apparent viscosity versus volume fraction solid of four Sn-15%Pb alloy samples sheared continuously and cooled from above the liquidus temperature at a constant cooling rate of $\varepsilon = 0.33^{\circ}$ C/min.	122
2	Measured apparent viscosity versus volume fraction solid of three Sn-15%Pb samples sheared continuously at a rate of $\dot{\gamma} = 750$ sec^{-1} and cooled from above the liquidus temperature at constant cooling rates.	123
3	Average size of primary solid particles versus shear rate in Sn-15%Pb alloy samples sheared continuously and cooled from above the liquidus at constant cooling rates.	124
4	Schematic of the low pressure casting system showing the continuous slurry producer, the collection chamber, and the casting machine.	125
5	Photograph of the low pressure casting system for high temperature alloys.	126
6	Schematic of the apparatus for producing partially solid slurries of high temperature alloys.	127
7	Schematic of the high pressure casting system including the reheat furnace and the shot chamber.	128
8	Photograph of the high pressure casting system. Top: overall view of B&T die casting machine. Bottom: close view of shot chamber and reheat furnace.	129
9	Schematic of thermocouple assembly in the low pressure die casting machine. Figure on top shows position of the thermocouple in the die cavity.	130

Figure Number		Page Number
10	Schematic of thermocouple assembly in the high pressure die casting machine. Figure on top shows position of the thermocouple in the die cavity.	131
11	Microstructures of conventionally solidified 440C stainless steel alloy. Top: slow furnace cooled ingot, 50X. Bottom: rapidly cooled, water quenched sample, 50X. Cupric Chloride etch.	132
12	Comparison of microstructures for Rheocast and conventionally cast 440A stainless steel alloy. Top: Rheocast water quenched droplet, 50X. Bottom: conventional slowly cooled liquid ingot, 50X. Cupric Chloride etch.	133
13	Microstructure of a water quenched semi-solid 440C stainless steel sample made in the high temperature slurry producer. Top: 50X. Bottom: 100X. Cupric Chloride etch.	134
14	Microstructures of continuously produced semi-solid 440C stainless steel alloy slurries. Top: rapidly cooled, water quenched sample. Bottom: slowly cooled ingot, 100X.	135
15	Microstructure of continuously produced semi-solid copper base alloy 905, 88%Cu-10%Sn-2%Zn. Samples were directly water quenched. Top: 50X. Bottom: 100X.	136
16	Microstructure of continuously produced semi-solid eutectic cast iron, Fe-2.6%C-3.2%Si. Samples were directly water quenched. (a) and (b) structure showing martensite plates in primary solid particles, 50X, 200X; (c) and (d) structures showing cementite plates, 50X, 100X.	137
17	Microstructures of continuously produced semi-solid HS-31 superalloy. Samples were directly water quenched. Top: 50X; Bottom: 100X.	138

Figure Number		Page Number
18	Microstructures of continuously produced semi-solid 304 stainless steel. Samples were directly water quenched. Top, 50X; Bottom, 100X.	139
19	Microstructures of continuously produced semi-solid alloy. Samples were slowly cooled. Top: microstructure of HS-31 superalloy. Bottom: microstructure of M-2 tool steel. 50X.	140
20	Microprobe data showing composition variation in semi-solid copper base alloy 905, 88%Cu-10%Sn-2%Zn. Sample was directly water quenched. The black line represents the path of the microprobe beam.	141
21	Microprobe data showing composition variation in semi-solid copper base alloy 905, 88%Cu-1-%Sn-2%Zn. Sample was slowly cooled. The black line represents the path of the microprobe beam.	142
22	Microprobe data showing composition variation in semi-solid 440C stainless steel. Sample was directly water quenched. The black line represents the path of the microprobe beam.	143
23	Castings produced in the low and high pressure casting systems. Top: 440C stainless steel casting produced in the low pressure casting machine, IX. Bottom: copper base alloy 905, 88%Cu-10% Sn-2%Zn, casting produced in the high pressure die casting machine, ~2X.	144
24	Photomicrographs showing homogeneous distribution of primary solid particles in various regions of a eutectic cast iron, Fe-2.6%C-3.2%Si, casting produced in the low pressure casting machine, 50X.	145

Figure Number | Page Number

25 Photomicrographs showing homogeneous distribution of primary solid particles in various regions of a 440C stainless steel casting produced in the low pressure casting machine, 50X. 146

26 Microstructures of conventionally solidified (from the liquid state) copper base alloy 905, 88%Cu-10%Sn-2%Zn. Top: sample directly water quenched. Bottom: sample slowly cooled. 100X. 147

27 Microstructure of continuously produced semi-solid copper base alloy 905, 88%Cu-10%Sn-2%Zn. Top: sample directly water quenched, 100X. Bottom: sample slowly cooled. 148

28 Comparison of the microstructures of semi-solid copper base alloy 905, 88%Cu-10%Sn-2%Zn showing correlation between water quenched samples and castings. (a) and (b) are water quenched samples, (c) and (d) are the corresponding castings, 100X. 149

29 Photomicrographs showing homogeneous distribution of primary solid particles in various regions of a copper base alloy 905, 88%Cu-10%Sn-2%Zn, casting produced in the high pressure die casting machine, 50X. 150

30 Radiographs and microstructures of conventionally cast and Rheocast copper base alloy 905, 88%Cu-10%Sn-2%Zn, made in the high pressure casting system. (a) and (c) show the radiographs of castings made from superheated liquid and semi-solid metal, respectively; (b) and (d) show the corresponding microstructures at 100X. 151

31 Measured die temperature during the casting of liquid and semi-solid copper base alloy 905, 88%Cu-10%Sn-2%Zn, in the low pressure die casting machine. Thermocouple was located at node 12, 0.0139" from casting-die interface. Dotted lines represent the calculated temperature variation produced by computer simulation. 152

Figure Number		Page Number
32	Measured internal die temperatures during the casting of semi-solid copper base alloy 905, 88%Cu-10%Sn-2%Zn, in the low pressure die casting machine. Dotted line represents the calculated temperature variation produced by computer simulation. Thermocouples located at nodes 12 and 13, 0.0139" and .0278" from the casting-die interface, respectively.	153
33	Measured internal die temperatures during the casting of liquid eutectic cast iron, Fe-2.6%C-3.2%Si, in the low pressure die casting machine. Thermocouple located at node 12, 0.0139" from the casting-die interface. Dotted line represents the calculated temperature variation produced by computer simulation.	154
34	Oscilloscope display showing the actual thermocouple millivoltage measured during the casting of liquid (top) and semi-solid (bottom) copper base alloy 905, 88%Cu-10% Sn-2%Zn, in the high pressure die casting machine. Thermocouple located at node 12, 0.0139" from the casting-die interface.	155
35	Measured internal die temperatures during the casting of liquid and semi-solid copper base alloy 905, 88%Cu-10%Sn-2%Zn, in the high pressure die casting machine. Thermocouple located at node 12, 0.0139" from the casting-die interface.	156
36	Schematic diagram showing the one dimensional computer model.	157
37	Computer simulated die surface temperatures as a function of time for the liquid and semi-solid copper base alloy 905, 88%Cu-10%Sn-2%Zn, cast in the low pressure system.	158
38	Die surface temperatures as a function of time for liquid and semi-solid copper base alloy 905, 88%Cu-10%Sn-2%Zn, cast in the high pressure die casting machine.	159

Figure Number		Page Number
39	Die surface temperatures as a function of time for liquid and semi-solid eutectic cast iron, Fe-2.6%C-3.2%Si, cast in the low pressure die casting machine.	160
40	Die surface temperatures as a function of time for liquid and semi-solid eutectic cast iron, Fe-2.6%C-3.2%Si, cast in the high pressure die casting machine.	161

ACKNOWLEDGEMENTS

After eight years at M.I.T., there have been many people (both professors and technical staff) whose help has been invaluable. Unfortunately, it is impossible to thank all of these people individually.

I would like to express deep appreciation to Professor Robert Mehrabian, whose skillful guidance and support was essential to the completion of this thesis. Also, I thank Professor Merton C. Flemings for helpful suggestions and discussion throughout the course of my graduate education.

As this work formed part of a larger group effort, many co-workers provided invaluable assistance. Therefore, I would like to thank Bruce Bond, Tom Piness, Rod Riek, and Ken Young as well as all others in the Rheocast group. In addition, I would like to express my appreciation to Miss Jane Morse and Miss Susan Fabyan for the preparation of the manustript.

Finally, I would like to thank my family and friends. Specifically, I would like to express my heartfelt appreciation to my father Edwin H. Backman - who introduced me to metallurgy - for his understanding, guidance, and support. Also, I thank my wife Susan for her continued patience and understanding.

CHAPTER I

INTRODUCTION

During the last three years, research has been conducted in the solidification group at M.I.T. to develop a machine process to cast high melting temperature metals. This project - engaging a significant proportion of the group's personnel - is part of a joint industrial-university program sponsored by the Advanced Research Projects Agency. The specific aim of this program has been to conceive, assess, and develop innovative casting approaches to overcome the processing and materials problems, currently encountered by ferrous die casters. Proposed solutions to these problems have included both radical changes in machine concept and design, and modification of the metal charged into the casting machine. The most significant approach has been the development of the Rheocasting and Thixocasting processes. These processes involve the casting of partially solidified alloys.

Despite extensive research, current ferrous die casting processes are subject to numerous problems limiting the number and type of parts that can be cast economically. Among the major difficulties encountered are die cracking, soldering (the adhesion of casting to die), and die surface wear. The characteristics of each phenomena are governed by the nature of heat and fluid flow within the die and the material properties of the die and the metal cast. Basically, the degree of die cracking depends upon the magnitude of the thermal gradient at the die surface and the thermal fatigue characteristics of the die material. The extent of soldering and surface wear is dependent on the die surface temperature (and subsequent surface hardness) as well as the metal flow velocity within the die.

Previous attempts to improve die life have concentrated on the development of high temperature materials capable of withstanding severe thermal fatigue. Among the contributions in this area has been the use of refractory metal dies (e.g., molybdenum TZM alloy). These alloys are difficult and costly to machine, and furthermore, they have not improved die life significantly enough to make die casting of ferrous alloys competitive with alternate manufacturing processes.

Thermal problems also arise in the shot sleeve when conventional close tolerance die casting machines are used to cast molten ferrous alloys. These difficulties - no less severe than those present within the die cavity - include seizure of the plunger in the shot sleeve due to either differences in thermal expansion or warpage. Also, soldering of the biscuit to the shot sleeve and plunger is prevalent. Again, industrial research efforts to remedy these problems have relied upon modifying existing machinery. Among the design modifications - principally proposed by General Electric and the Doehler Jarvis Companies are the following:

1) use of a large clearance (.005") TZM (coated with molybdenum dichloride) shot sleeve and Berylco-10 plunger.
2) use of an "isothermal" shot sleeve (heated by induction).
3) the use of an air fin cooled alumina shot sleeve and an alumina plunger tip.
4) the use of disposable asbestos shot sleeve liners.

Unfortunately, with the adoption of each of the above alterations, additional problems emerged. For example, the replaceable asbestos protection system reliably protected the shot sleeve and plunger from chemical and thermal damage; however, the system suffered the disadvantage that asbestos was entrapped within the casting and adhered to the biscuit (thus decreasing its scrap value).

When liquid metals (either high or low melting temperature) are die cast, defects arise which are characteristic of the fluid flow pattern formed during die filling. The most common defects encountered are entrapped air, cold shuts, laping, and surface streaking. Conventional attempts to correct these defects have relied upon manipulation of gate, runner, and vent design and variation of die temperature. However, because no formal treatment is available (especially in ferrous casting) to predetermine these factors, selection is made by empirical methods resulting in inferior casting quality. Ferrous die casters - constrained already by materials limitations - do not have the flexibility to extensively vary the heat and fluid flow variables for production of sound parts.

Additionally, because metal shrinks upon solidification, shrinkage porosity develops during die casting. Located either in the casting bulk or on the casting surface, this phenomena detracts from both the mechanical strength and physical appearance of the part. Furthermore, conventional risering techniques designed to feed shrinkage in castings are not compatible with the die casting process. Consequently, special low melting temperature alloys have been developed which do not shrink appreciably during freezing. In general, low temperature alloy (e.g., zinc, aluminum) die castings are not heat treated. Porosity, gas and shrinkage, is well distributed and reduced in size under the large pressures prevailing during solidification. Similar porosity in ferrous parts would seriously limit their subsequent heat treatment.

Attempts to date to solve the materials problems encountered in ferrous die casting have met with limited success at best, while process alterations have been restricted to relatively minor machine modifications. The Rheocasting and Thixocasting processes recently developed in the Solidification Laboratory at the Massachusetts Institute of Technology provide an alternate solution. The basis of these approaches is that when a partially solidified metal is cast, its temperature and "effective" heat of fusion is lower than the corresponding superheated liquid. Furthermore, there are distinct advantages to casting a more viscous partially solid alloy which will be discussed later. However, a semi-solid alloy requires specific processing during solidification to insure its castability.

When an engineering alloy solidifies, dendrites form and develop an interconnected network of solid surrounded by liquid. When sheared - as in the shot sleeve of a conventional die casting machine - the solid dendritic network collapses and mobile liquid is squeezed preferentially from the interdendritic region. Attempts to die cast in this manner result in poor die filling and extensive macrosegregation.(16)

If, however, an alloy is vigorously sheared during solidification, the solidifying dendrites do not form an interconnected network.(2-8) Instead, small independent dendritic fragments are created which subsequently spheroidize by mechanical wear between fragments and by chemical coarsening processes. The production of such slurries - spheroidal solid particles suspended in a liquid - constitutes the essense of the Rheocast and Thixocast processes.

In the Rheocast process, an alloy is simultaneously cooled from the liquidus temperature and vigorously agitated. As the fraction of the primary solid particles increases, there is a gradual rise in apparent viscosity.(2,3) In general, at a given fraction solid this apparent viscosity is a function of the structure of the primary solid particles themselves - which is effected by the shear and cooling rates employed. Earlier work on low temperature alloys has shown that the viscosity is approximately 1 - 5 poise - similar to heavy machine oil - at a volume fraction solid of ~.4.(3) At this volume fraction solid, the slurry can flow in a homogeneous manner with no distinct preferential flow of either liquid or primary solid particles. Hence, the liquid-solid mixture can be die cast successfully.(4-6) At high fractions solid, larger than ~0.6, however, adjacent particles interact causing a drastic rise in apparent viscosity. These mixtures are more difficult to die cast, but could be amenable to other fabrication techniques.

Partially solid metal slurries exhibit thixotropic behavior; that is, their viscosity decreases with increasing shear rate and is time dependent.(2) For example, when a Rheocast slurry is left at rest, welds form between adjacent particles and the viscosity increases. In the Thixocasting process, a semi-solid slurry is formed into a cylindrical shape and held isothermally at the desired casting temperature. The cylindrical slug maintains its shape and may be transported easily to the shot sleeve of a die casting machine. However, upon the initiation of shear, the inter-particle welds are broken and the material behaves as a low viscosity slurry - flowing homogeneously to fill the die cavity.

1. The Castings of Semi-Solid Slurries

In both processes outlined above, the semi-solid charge possesses special attributes which offer distinct advantages over superheated liquid. First, considering thermal aspects, the temperature of the slurry is lower, and the effective heat of fusion - the heat of solidification released to the die cavity - is reduced. In addition, the higher viscosity of the semi-solid charge results in reduced forced convection during flow. Because of these three factors, less heat is transferred to the die cavity and the shot sleeve, thus reducing deterioration of each.

The high viscosity of semi-solid slurries also affects the nature of fluid flow during die filling. Solid front filling conditions are achieved more easily - rather than spraying at the ingate obtained when superheated liquid metals are die cast.(9) The more gentle and uniform die filling should result in less entrapped air. Moreover, since the metal is partially solid as it enters the die cavity, the solidification shrinkage within the casting is reduced. Thus, sounder castings can be produced by casting semi-solid metals in a die casting machine.

2. The Production of Semi-Solid Slurries

The two methods have been developed for producing semi-solid slurries. One, the static method, is a batch operation requiring a rotating paddle and crucible and temperature control of the melt.(5) The pattern of heat flow is such that dendrites form on the crucible wall and are then churned into the melt by the action of the stirring paddles. Bulk fluid motion then enables coarsening of the dendrites to proceed as described above. This method of production has several disadvantages. Air is entrapped in the slurry. The slurry is not produced continuously and therefore, castings can not be produced on a continuous schedule. Removal of the slurry from the crucible is difficult and the charge volume is uncontrolled.

To counteract these shortcomings, a continuous slurry producer was designed and built as shown in Figure 6(7). The temperature of the top reservoir is held above the liquidus, and a temperature gradient is maintained along the length of the mixing tube such that the temperature at the exit port corresponds to the desired fraction solid. In the mixing tube, rotation of the stirring rod produces the necessary shear. In order to maintain continuous operation, material can be added to the system by feeding metal into the top reservoir. The flow of metal through the system is controlled by moving the stirring rod along its axis of rotation thus changing the exit port size.

3. The Areas of Concentration

It must be emphasized that the ferrous machine casting program in the solidification group at M.I.T. has been a group effort. As such, many of the machines described and used in this thesis have been built and operated by other researchers within the group. Additionally, some of the topics of interest to this thesis have been shared by other members of the program.

However, the topics of concentration reported here form a distinct subset within the program and are the author's contribution to the over-all effort. These areas of concentration are:

1) the characterization of the structures produced in the continuous apparatus and relationship of these structures to process variables,
2) the evaluation of die castings produced and correlation of casting quality to casting condition and the structure of the semi-solid charge,
3) the development of a thermal analysis to assess the impact of semi-solid slurries on die thermal history and longevity.

II. Literature Survey

A. Structure, Rheology, and Casting of Semi-Solid Alloys

Virtually all research on the Rheocast and Thixocast processes to date has been conducted in the Solidification Laboratory at M.I.T.(1-10) These studies can be categorized into two groups. The first group is comprised of basic scientific investigations dealing with the formation and rheology of semi-solid slurries. This research has attempted to correlate process variables with the microstructure of vigorously agitated semi-solid alloys and their rheological behavior. The second group of studies is more applied in character. These investigations have been directed principally towards developing a machine casting technique for high temperature alloys and has evolved in the casting of partially solid alloys in conventional die casting machines. A small portion of this work has been in flow studies (die filling characteristics) of low temperature semi-solid alloys using high speed photography and transparent dies.

1. Formation of Rheocast Structures

To date, there has been no direct conclusive evidence showing the exact mechanism by which semi-solid slurries form. Because the solidification of metallic slurries can not be viewed directly, observations are limited to metallography of samples after complete solidification. In one recent study, the formation of solid particles under high rates of shear were observed directly in a transparent non-metallic system.(1)

In another recent investigation principally aimed towards an understanding of the rheology of partially solid slurries, Joly(2) has proposed several mechanisms to explain the formation of metallic semi-solid slurries. He postulates that as temperature in the alloy drops below the liquidus, dendrites begin to form in the vigorously agitated melt. At still lower temperatures (higher fraction solid), dendrite multiplication occurs by one of two possible mechanisms. The two modes of multiplication are:

(1) dendrite arm remelting caused by variations in radius of curvature or thermal pulses;

(2) mechanical fracture caused by stresses imposed by

the mechanical agitation of the slurry. Furthermore, Joly(2) proposes that the dendrite fragments thus produced grow and coarsen either by particle collision and coalescence or by an Ostwald ripening mechanism. He concludes that spheroidization is diffusion controlled - the driving force being the reduction in surface energy between the solid and liquid phases.

Using a transparent non-metallic alloy (H_2O - 30 wt% NH_4Cl), Nyhat(1) has directly observed the formation of semi-solid slurries. Motion pictures taken during preliminary experiments reveal that dendrites fragment to produce the slurry structure through the remelting or fracture of dendrite arms and subsequent spheroidization. Also, he observed that spherical primary solid particles collide and weld together. Both of the observations confirm the mechanisms proposed by Joly(2) on metallic systems.

2. The Effect of Process Variables on Structure

The structure of partially solid slurries is strongly dependent upon the process variables under which they form. The principal variables are the shear rate, and the time spent in the liquid-solid region. Variation of these parameters affects the particle size, shape, and the amount of entrapped liquid within the primary solid particles. Currently, the correlation between the process variables and the resulting structure is confined to the behavior of Sn-15%Pb semi-solid alloys as observed by Joly.(2)

Joly produced semi-solid Sn-Pb slurries in a high temperature Couette viscometer with the capability of controlling and recording temperature and shear rates during the course of the experiments. He found that the size of the primary solid particles in the slurry decreases with increasing cooling rate. In addition, for the highest cooling rate studied (dT/dt = 25°C/minute), the average size of primary solid particles is independent of the shear rate; whereas the amount of entrapped liquid decreases with increasing shear rate. On the other hand, for slow cooling rates (e.g., dT/dt = 0.33°C/minute), both the size of primary solid particles and the amount of entrapped liquid decrease with increasing rate of shear. Joly also showed that the size distribution of primary solid particles decreases with increasing shear rate and decreasing cooling rate. Finally, all evidence indicated that the amount of entrapped liquid within the primary solid particles of a slurry is principally a function of the total time spent in the liquid-solid region.

3. Rheology of Rheocast Structures

Employing a high temperature Couette viscometer, Spencer(3) and Joly(2) have studied the rheological behavior of semi-solid tin-lead alloys. The apparatus allows variation of rotation speed (shear rate) and temperature (volume fraction solid), and simultaneous recording of the resultant torque (viscosity).

In experiments designed to determine the relationship between apparent viscosity and volume fraction solid, the alloy was simultaneously cooled and sheared at constant rates while in the solidification range. After converting the measured torque and temperature, curves relating the apparent viscosity to volume fraction solid within the slurry were obtained. A number of such curves for a variety of shear and cooling rates are reproduced in Figure 1. Joly(2) found that the apparent viscosity decreases with both increasing shear rate and decreasing cooling rate, all other variables being held constant. Also, he concluded that the apparent viscosity of a Sn-15%Pb alloy is below 5 poise over a significant range of volume fractions solid thus making the slurry amenable to casting processes.

In addition, Joly observed that semi-solid slurries display thixotropic behavior. The degree of thixotropy was determined by measuring the apparent viscosity as the shear rate within the slurry was increased, held constant, and then decreased to the initial level. For Sn-15%Pb alloy slurries (as with other known thixotropic materials), the apparent viscosity decreases with increasing shear rate and is time dependent. The dependency of apparent viscosity upon processing history is revealed by the presence of a hysteresis loop during the measurement of torque versus shear strain. The area of the hysteresis loop is a measure of the degree of thixotropy of the system. This area is a function of the parameters and procedure used for generating the loop as well as the initial structure and extent of thixotropy of the system. Joly(2) postulated that at steady state (during relatively high rates of shear - 100 to 750 sec^{-1}), there is an equilibrium between structure build-up (welding of primary solid particles) and separation and fracture of bonds between the particles. At zero or low shear rates, partial welding of primary solid particles prevails resulting in high viscosities.

4. Casting of Rheocast Alloys

Several casting trials have been conducted to assess the feasibility of die casting semi-solid slurries. In the first test conducted at the Newton-New Haven Die Casting Company on a 400 ton KUX horizontal machine, Mehrabian and Flemings(4) report that excellent castings were produced from partially solid slurries of A380 aluminum alloy. During the experiments, plunger speed, intensifier position, and gate size were varied. It was found that increasing the plunger speed had the adverse effect of increasing the amount of porosity in the castings even though the surface quality was improved. Similarly, an increase in the gate area produced an identical effect.

In the second production trials employing the same die casting machine and dies, Fascetta et al.(6) successfully die cast reheated thixocast slugs of copper base alloys 836 and 905. For comparison, one conventionally cast slug of each alloy was reheated to an equivalent temperature in the liquid-solid range and die cast. Contrary to the results obtained with thixocast slugs, the castings produced from these conventional slugs were of poor quality indicating the non-homogeneous deformation of partially solidified non-Rheocast metal. Radiographs of the thixocast die castings, on the other hand, revealed only small amounts of porosity, comparable to that obtained in commercial bronze die castings produced from liquid alloy. Also, metallographic examination revealed a homogeneous distribution of primary solid particles throughout the casting bulk.

Riek et al.(7) produced a number of bronze castings from semi-solid slurries using a low pressure laboratory die casting machine. Results from these tests duplicate those previously outlined.(5) However, they determined that both shrinkage and the size and distribution of porosity decreases with increasing volume fraction solid. Again, the castings possessed a homogeneous distribution of primary solid particles.

Schottman(9) has studied the die filling characteristics of both liquid and semi-solid tin-lead alloys. Using a high speed movie camera and a transparent die, he has found that a liquid charge entering the die at high velocity breaks up splashing off the walls of the die cavity, thus entrapping air. Conversely, the partially solid slurry enters the die in a smooth continuous manner. He concludes that "solid front" fill causes a lower amount of entrapped gas within castings produced with semi-solid slurry. These predictions were verified when copper base alloy castings were made under identical conditions to the above in the same geometry die cavities(6).

B. Die Heat Flow Analysis

Many researchers have analyzed heat flow during the solidification of castings. The majority of investigations have dealt with solidification in sand and investment molds with emphasis directed toward control of the cast structure (e.g., dendrite arm spacing, macro- and microsegregation). These general studies have contributed significantly to the development of computational techniques for incorporating solidification into standard heat flow analyses.

In recent years, the nature of heat flow during the solidification of die and permanent mold castings has received specific attention in the literature. The methods and motivations of these heat flow analyses have been varied.

Analytical solutions (exact and inexact) and computer simulation with various degrees of sophistication have been utilized to determine the temperature distribution within both the casting and die in die casting. The objectives of these studies have included:

(1) the determination of the "optimum fill time" to improve the casting surface and reduce porosity.(18)

(2) the understanding of die failure mechanism (cracking and erosion) in order to select new or improve existing die materials.(13,26)

(3) the determination of machine parameters to increase the efficiency of die casting operations (e.g., water cooling line location and cycle time).(16,17)

1. Analytical Solutions

Analytical solutions to the heat flow equation involving solidification are limited. The most important solution to the problem of freezing - classically known as the problem of Stefan - is the exact solution of Neumann. One important extension of this solution, introduced by Schwartz(11) and summarized by Carslaw and Jaeger(12), will be described. In this model, the metal is assumed to freeze at a single temperature. The mold occupies the semi-infinite region $X < 0$ and mold properties are denoted with the subscript o. Material properties for the solidified and molten metal are designated by the subscripts 1 and 2, respectively. The temperature distribution _within the mold_ is stipulated by the following two equations.

$$\frac{T-T_R}{T_M-T_R} = \frac{k_1\alpha_o^{\frac{1}{2}}}{k_1\alpha_o^{\frac{1}{2}} + k_o\alpha_1^{\frac{1}{2}} \operatorname{erf} \gamma} \left(1 + \operatorname{erf} \frac{x}{2(\alpha_o t)^{\frac{1}{2}}} \right) \qquad (1)$$

where γ is the root of the following characteristic equation:

$$\frac{k_o\alpha_1^{\frac{1}{2}}\, e^{-\gamma^2}}{k_1\alpha_o^{\frac{1}{2}} + k_o\alpha_1^{\frac{1}{2}} \operatorname{erf} \gamma} - \frac{k_2\alpha_1^{\frac{1}{2}}(T_oT_M)\, e^{-\alpha_1\gamma^2/\alpha_2}}{k_1\alpha_2^{\frac{1}{2}} T_M \operatorname{erf} c\, \{\gamma(\alpha_1/\alpha_2)^{\frac{1}{2}}\}} =$$

$$= \frac{\gamma\, L\, \pi^{\frac{1}{2}}}{c_1\, T_M} \qquad (2)$$

and where α, k, c_1 represent the thermal diffusivity, thermal conductivity, and heat capacity, respectively. Also, L equals the latent heat of fusion, and T_o, T_R, and T_M represent the initial melt temperature, the initial mold temperature and the solidification temperature.

In order to qualitatively analyse the nature of this solution, it is convenient to make the simplifying assumption that the properties of the solidified and liquid metal are equivalent. Under these conditions, the above two equations reduce to the following:

$$\frac{T-T_R}{T_M-T_R} = \frac{1}{1 + \left(\frac{\rho_o c_o k_o}{\rho_1 c_1 k_1}\right)^{\frac{1}{2}} \text{erf } \gamma} \left(1 + \text{erf } \left(\frac{x}{2\alpha_o^{\frac{1}{2}} t^{\frac{1}{2}}}\right)\right) \tag{3}$$

and

$$\underbrace{e^{-\gamma^2}}_{\text{term 1}} \left[\underbrace{\frac{1}{\left(\frac{\rho_1 c_1 k_1}{\rho_o c_o k_o}\right)^{\frac{1}{2}} + \text{erf } \gamma}}_{\text{term 2}} - \underbrace{\frac{T_o - T_M}{T_M \text{ erf } \gamma}}_{\text{term 3}} \right] = \underbrace{\frac{\gamma \, L \, \pi^{\frac{1}{2}}}{c_1 \, T_M}}_{\text{term 4}} \tag{4}$$

Now, considering γ as the independent variable of the characteristic equation,$^{(4)}$ an increase in γ results in a decrease in terms 1 and 2 and an increase in terms 3 and 4. In order to maintain the equivalence between both sides of the equation, the increase in γ must be compensated for by a decrease in either the ratio of heat diffusivities $(\frac{\rho_1 c_1 k_1}{\rho_o c_o k_o})^{\frac{1}{2}}$, the latent heat of fusion L, or the ratio $\frac{T_o - T_M}{T_M}$. Of course, the opposite is also true, decreases in any one of the above three parameters yields an increase in γ.

Combining this deduction with equation (3), we find that given a particular mold material with fixed material properties (ρ_o, c_o, k_o), a decrease in either the heat diffusivity $(\rho_1, c_1, k_1)^{\frac{1}{2}}$, the latent heat of fusion L, or the amount of superheat $T_o - T_M$ produces a lower temperature at any given location within the die at anytime.

The above deductions can also be obtained by purely physical arguments. The use of the solution, equations (3) and (4), is restricted since it was assumed that the metal solidifies at a single temperature, and there is no resistance to heat flow at the metal-mold interface.

Furthermore, further inadequacy includes the use of an infinite die with material properties independent of temperature.

Despite these shortcomings, Noesen et al.(13) have applied this thermal analysis to the selection of die materials suitable for casting high temperature metals. For example, they found that when 304 stainless steel is cast in a molybdenum die, the ratio (T_S-T_R/T_M-T_P) is reduced to 70% of the value obtained when H-13 hot worked dies are used. T_S denotes die surface temperature. They concluded that the reduced die surface temperature will prolong fatigue life in the molybdenum die.

By introducing the simplifying assumption that the mold-metal interface maintains a constant temperature throughout solidification, Adams(14) has developed an approximate solution which includes an assumed finite heat transfer coefficient at the interface. Unfortunately, this solution is complicated and is difficult to use without resorting to detailed computation. In addition, the inexactness of the results detracts from the applicability of the analysis. In work predating the modern computer, Reynolds applied this solution to solidification in finite metallic molds with qualitative success.(15)

Several investigators have utilized simple(17-19) lumped parameter heat flow models to determine gross operational characteristics such as die preheat time, optimum fill time, and water cooling line location. Typically, bulk heat flow resistances are ascribed to the casting, the mold-metal interface, and the mold; then the mean temperature change with time is determined for each of the three components under consideration. Generally, this approach yields the necessary information for determining the gross operational parameters and is justified when one considers the complexity of a detailed quantitative solution.

In conclusion, we find the use of analytical methods are severely restricted. Some solutions are tractable and may be used to qualitatively assess the influence of process and material variables. However, those solutions more closely approaching the exact solution suffer from the handicap that they require complicated computation and are limited by the assumption made.

2. Computer Simulation

The problems inherent to analytical solutions have been circumvented through use of computer simulation. Employing finite difference techniques originally applied by Dusinbure(20,21) to the solution of transient heat flow problems, several investigators have developed computer programs to characterize heat flow during solidification.

All computer simulations require that the physical system be sectioned into incremental segments. Subsequently, a heat balance is conducted at the center of each segment, termed a node, resulting in a finite difference equation. Depending on whether forward or backwards differences are used to represent the differentials of the thermal diffusion equation, two types of difference equations may be obtained.(21) The use of forward differences - also called the standard explicit method - results in the following equation applicable for each interior regular node.

$$T(x,t+\Delta t) = T(x,t) + \frac{\Delta t\alpha}{\Delta x^2}\{T(x-\Delta x,t) - 2T(x,t) + T(x+\Delta x,t)\} \qquad (5)$$

where Δx and Δt represent the node spacing and time increment, respectively. Other equations are obtained for boundary nodes. These equations are then applied repetitively at each node yielding the temperature at each location as a function of time.

Use of the standard explicit method requires that both the time increment and nodal spacing be selected properly. The most common restriction placed upon these increments for one-dimensional problems is that:

$$M = \frac{(\Delta x)^2}{\alpha \Delta t} \geq 2 \tag{6}$$

where M, a dimensionless time constant, is the reciprocal of the Fourier number. Adherence to this condition is necessary to avoid violation of the second law of thermodynamics.$^{(21)}$ Often, however, boundary nodes and temperature dependent material properties have a destabilizing effect upon the simulation,forcing one to resort to trial and error methods in selection of Δx and Δt.

The second approach, the implicit method using backwards differences, is unconditionally stable but requires that all nodal equations for any given time be solved simultaneously to produce the variation of temperature with time.(21) Because of the complexity of the resulting computer program, this method is generally reserved for problems involving severe instability.

The critical issue in all computer simulations of freezing processes has been the determination of a method to account for the release of the latent heat of fusion.(22,23) Probably the most simple and straightforward technique has been the use of an "effective" heat capacity. In this procedure, the heat capacity of an alloy at a temperature between its liquidus and solidus is augmented by an amount equal to the heat of fusion divided by the temperature range of solidification. Written mathematically, the following expression is used:

$$(C_p)_{\text{effective}} = C_p + \frac{\Delta H_f}{T_{\text{Liq}} - T_{\text{Sol}}} \qquad (7)$$

where T_{Liq} and T_{Sol} represent the liquidus and solidus temperatures, respectively. The limiting assumption is that the variation of fraction solid with temperature is linear - which is often the most reasonable approximation possible for complex, multi-component alloys.

In some instances, this method results in certain computational dificulties, particularly when heat flow within the casting is of interest.(22) For example, if the mushy zone is small compared to node spacing of the computer program, heat liberation is confined to one nodal segment of the casting. As solidification proceeds, the solid-liquid front advances in discrete steps. Depending on the mesh size, this may not be a reasonable approximation.

A number of techniques(22,24) have been developed to avert this shortcoming. One common procedure, the "moving freezing front" method, assigns a floating node which follows the movement of the liquid-solid interface.(24) The velocity of the node is determined by a heat balance conducted on an incremental volume element located on the melting point isotherm. This model of solidification is best applied to the freezing of pure metals. A further refinement applicable to the solidification of alloys replaces the one floating node with a sub-mesh, the nodes of which follow the advancement of the mushy zone.(22)

3. Die Casting Heat Flow Studies

Few die casting researchers have applied computer techniques to the study of heat flow. Kaiser(25) et al. have developed a program utilizing Dusinbure's forward difference technique and an effective heat capacity to simulate solidification. The computer program also considers heat losses from the injected liquid during die filling and thermal resistance at the die-metal interface. The simulation output includes the effect of these variables on the temperature as a function of both time and position within the die and the casting. The computer model is applied to the determination of solidification times for thin walled zinc castings.

Samuels(26) has written a program to analyze thermally induced stresses in the die encountered during the casting of high temperature alloys. The thermal portion of this model includes a floating freezing front model of solidification and employs a backward difference technique to represent the flow of heat. Furthermore, he employs one node at the casting-die interface to represent the presence of a die coating.

Scholl(27) has studied heat flow in die casting using a hybrid computer which interfaces a digital and an analog computer to minimize the time and cost of simulation. His approach is particularly amenable to the qualitative study of the thermal effects produced by changes in process variables and die materials. In comparing his model with the model developed by Samuels,(26 he found that although the numerical magnitude of results did not agree, thermal trends produced by one model could be correlated to the other. The chief advantage of the hybrid computer procedure is that steady state die casting operations can be simulated for long times at a reasonable expense.

In conclusion, a number of varied methods (both analytical and computer simulation) have been applied to the study of heat flow in die casting. From each, information may be drawn which is valuable in characterizing and solving a specific problem. It is further recognized that the degree of model sophistication - and hence complexity - must be determined by the required accuracy of the results and the limitations of the assumptions made.

4. Surface Heat Transfer Coefficient

In all engineering heat flow studies, the surface heat transfer coefficient, h, is a critical parameter. Despite this fact, few investigations have addressed themselves to the experimental determination of h in systems involving a liquid metal-solid interface. Furthermore, no theoretical analysis is available to predict h owing to difficulties in the accurate characterization of the interface and the lack of measured thermal conductivities of surface oxides. Therefore, out of necessity, researchers usually select a value for the surface heat transfer coefficient which produces the best correlation between their theoretical and experimental results. Therefore, the accuracy of the h values obtained depends strictly upon the accuracy of the theoretical model proposed.

Adams(14) has found that the value of h ranges from .027 to .11 cal/cm^{2}sec°C for steel poured in a steel mold. He further states that if an air gap forms between the casting and the mold, the radiative surface heat transfer coefficient will be ~.013 cal/cm^{2}sec°C. Reynolds(15) studied the thermal behavior of several metals during their solidification in steel molds. By measuring the rate of solidification, he found that the values of h are .066, .0936, and .127 cal/cm^{2}sec°C for iron, lead, and aluminum, respectively. During this investigation, the highest measured value of h was .32 cal/sec cm^2 °C. This value was obtained for aluminum solidifying on the outside of a polished copper cylinder - with pressurization occurring at the interface due to solidification shrinkage. In experiments designed to study the fluidity of liquid tin in glass tubes, Ragone, Adams and Taylor(28) calculated values of ~0.16 cal/sec cm^2 °C. Their analysis assumes that heat flow was h controlled. In a similar manner, Flemings et al.(29) calculated an h value between 0.15 and 0.30 cal/sec°C cm^2 for aluminum solidifying in a glass tube.

The determination of the heat transfer coefficient at the casting-die interface in the die casting process is fraught with several difficulties. Generally, die coatings are applied between shots. The thickness and adherence characteristics are a function of time and position on the die surface. Also, high pressures develop within the solidifying metal and influence the contact area between the casting and the die. Finally, as in other casting processes, solidification shrinkage can result in the formation of an air gap and thus alter the value of the heat transfer coefficient.

Despite these complexities, several investigators have managed to estimate a value for the surface heat transfer coefficient from their heat flow analyses. Using a graphical analysis of thermal data, Nelson(19) calculated that $h \approx 1.5$ cal/cm^2 °C sec. Lindsey and Wallace(18) employed a lumped parameter model of a die and a casting to determine the optimum fill times for zinc and aluminum alloys. In analyzing this data, Kaiser et al.(25) reported an h value approximately equal to 0.214 cal/cm^2 sec °C.

C. Die Failure

Common tool steels (e.g. H-13) have failed to provide adequate die lives for the casting of high melting point metals (e.g. copper base and ferrous alloys). For these metals, the predominant mode of die failure is thermally induced fatigue cracking. Therefore, in order to achieve increased die longevity - and thus economic viability - considerable research has been devoted to the selection and development of alternate die materials capable of withstanding severe thermal-stress environments. A number of these alloys with composition are listed in Table I . Also, research has been directed towards the improvement of the H series tool steels through control of both composition and heat treatment. To accomplish these goals, both experimental and theoretical techniques have been employed.

1. Theoretical Study

Theoretical methods have been developed by Noesen (13) and Samuels (26) to predict and compare the life expectancy of metal dies. The mode of failure in each analysis is thermal fatigue cracking. As metal is injected in a die casting machine, the die surface heats rapidly causing severe thermal gradients within the die. Owing to thermal expansion, the temperature gradient produces compressional stresses within the surface layers of the die. During ejection of the casting, the gradients of both temperature and stress reverse themselves - producing tension stresses at the die surface. If during the casting cycle the stress level exceeds the elastic limit, yielding will occur. Because of the repetitive application of stresses, failure ultimately occurs by a fatigue mechanism.

Noeson(13) employed the analytical solution of Schwarz(11) (as presented earlier) to determine the die surface temperature, T_s. He then assumed that the temperature change, ΔT, of the die surface layers during the casting cycle equals $T_s - T_D$, where T_D represents the mean die operating temperature. This temperature change produces a thermal strain $\Delta\varepsilon_t$:

$$\Delta\varepsilon_t = \frac{\beta\Delta T}{1-\nu} \qquad (8)$$

where β is the coefficient of linear thermal expansion and ν is Poisson's ratio. Furthermore, he calculated the cyclic elastic strain with the following expression:

$$\Delta\varepsilon_e = \frac{2\sigma_Y}{E} \qquad (9)$$

where σ_Y and E represent the 0.1% offset yield stress and Young's modulus, respectively. Because the thermal strain is the sum of both plastic and elastic components, the cyclic plastic strain, $\Delta\varepsilon_p$, is defined:

$$\Delta\varepsilon_p = \Delta\varepsilon_t - \Delta\varepsilon_e = \frac{\beta\Delta T}{1-\nu} - 2\sigma_Y/E \qquad (10)$$

Finally, Noesen(13) utilized Coffin's(30) modified low cycle fatigue equation to calculate the number of cycles to failure, N_f:

$$N_f = \varepsilon_f / \Delta\varepsilon_p \qquad (11)$$

where ε_f equals the true fracture ductility in simple tension. The calculated life expectancy for various die materials are tabulated below for iron cast at 1536°C into a die operating at 500°C.

	T_s	N_f
Tungsten	958°C	∞
18 Ni(250) Maraging Steel	1131°C	∞
Titanium alpha-beta alloy	1262°C	∞
H-12 die steel	1120°C	7,110,000
Molybdenum	960°C	599,987
AFC77 PH stainless steel	1130°C	551,398
H-13 die steel	1107°C	17,103

Samuels(26) developed a computer program (as previously described) to calculate the temperature distribution within a die during the casting cycle. He then determined, in a manner similar to Noesen (13), the stress and strain throughout the die with the following two relationships:

$$\sigma = \frac{E\beta(\Delta T)}{1-\nu} \qquad (12)$$

$$\varepsilon = \frac{1+\nu}{1-\nu}\,\beta\,\Delta T \qquad (13)$$

where ΔT represents the difference between the die temperature at a specific location and time and the mean die temperature. Also, σ and ε are the biaxial tensile stress and strain in a plane parallel to the casting - die interface. Accordingly, the biaxial stress within the die can be represented as an equivalent shear stress:

$$\tau_s = \sigma/2 = \frac{E\beta\Delta T}{2(1-\nu)} \qquad (14)$$

Finally, yielding will occur when τ_s exceeds the shear yield stress. Though Samuels(26) made no attempt to predict die life quantitatively, the relative effectiveness of a candidate die material can be determined by examining the depth of the plastically effected zone developed during the casting cycle.

Neither of the two analyses presented above(13,26) provides a definitive prediction of die life. Both methods fail to use actual temperature gradients to calculate the resulting stress and strain fields. Futhermore, exact analysis is difficult owing to the lack of information on high temperature properties for most die materials. Consequently, these approaches (particularly that of Noesen) have been utilized to rank the relative merits of individual die materials. In addition, examination of each analysis reveals the critical material properties determining die life. In order to minimize the surface temperature and thermal gradient, a die material should have a high thermal conductivity, k, heat diffusivity, $(k\alpha\ C_p)^{\frac{1}{2}}$, and thermal diffusivity, $(k/\alpha\ C_p)$. To achieve low levels of plastic strain, the material should have a low coefficient of thermal expansion, β, a high yield stress, σ_Y, and a low value of Young's Modulus. Finally a successful die material should have a high value of fracture ductility to maximize N_f. Optimization of the above parameters will result in an improvement in die life. However, as Noesen(13) points out, there are additional factors which should be considered while selecting a die material. These factors include the presence of a phase transformation during die heating, changes in material composition (e.g., decarburization of steel), and factors controlling the extent of mechanical erosion and chemical attack.

2. Experimental Studies

Several studies have been conducted to evaluate the thermal fatigue behavior of die materials. Generally, candidate material in these programs have been selected through implementation of the physical arguments presented above. Among the metals investigated are TZM, Mallory Anveloy, H13, as well as others listed in Table I. The test procedures utilized include flame heating of a test block, dip testing of a water cooled rod of rectangular cross-section, and actual die casting of a commercial part.

Most significantly, Elam and Hopper (31) conducted production tests using a copper base alloy cast in a cold chamber die casting machine. The experimental program was divided into two sections - one portion conducted by Cerro Corporation and the other by American Standard. At Cerro Corporation, initial screening was achieved by testing the life of cylindrical die cores made from each of the 12 candidate materials. This test indicated that TZM molybdenum base alloy was superior to all others tested. However, Mallory 3950, MAR-M 200, and Gyromet 1100 each showed promise. The number of shots to failure for these materials are presented in Table I. As an extension to this study dies incorporating sharp corners and changes in cross-sectional area were made from TZM in three metallurgical conditions and H20 steel and tested. Again the results are shown in Table I. In the American Standard project, (31) a more comprehensive comparative die evaluation was conducted using 17 die materials. Of these TZM and Mallory 3950 were rated superior. The number of cycles to die failure or die removal are listed in Table I for those materials showing promise.

Benedyk et all(32) investigated the thermal fatigue behavior of die material to be used in the die casting of aluminum alloys. Their test consisted of a water cooled rod of square cross section which was repetitively dipped into molten aluminum. Both the heating and cooling cycles were controlled to simulate the heat flow conditions experienced in a die casting machine. During the tests, cracks were observed to form on the edge of the test specimen. The number of cycles necessary to initiate cracks for the materials studied are shown in Table II. The test indicated that TZM and Alloy 25 (a BeCo copper base alloy) are resistant to crack development. In addition, an extensive evaluation of H-13 in a variety of conditions was performed. Their results indicate that increasing austenizing temperature to 2050°F, hardening to $R_c\tilde{}48$, and the prevention of either a carburized or a decarburized surface layer produced improved thermal fatigue resistance.

Kasak and Stevens(33) have also investigated the fatigue cracking of die steels. Using disc specimens alternately dipped into molten lead and hot water, they found that the austenite grain size of H-13 steels has no effect on fatigue resistance. In addition, their findings indicate that though alumina inclusions accelerate failure, sulferizing of H-13 up to 0.22 percent sulfur was not detrimental. Wollering and Oertle(34) evaluated a number of die steels with a fatigue device incorporating flame heating. The steels studied showed that at a common hardness of $R_c \tilde{}52$ the resistance to crack initiation improved through the series H-21, H-19, H-13, H-12, H-11, and D-9. Suzuki et al(35) also used alternate gas flame heating and water quenching to study the effect of residual surface stresses upon the thermal fatigue resistance of H-13 steel. By comparing the cracking behavior of conventionally machined and electric discharge machined test specimens, they concluded that heat checking is prevented by large amounts of compressive residual stress. Furthermore, the measurement of surface residual stress can enable prediction of the degree of crack initiation and propagation.

Though not directly involving thermal fatigue, Draper and Samuels(36,37) have conducted extensive experiments determining the surface behavior of die materials when used to cast ferrous alloys. Employing graphite die blocks incorporating disc inserts of each test material, they studied both specimen weight loss and surface roughness as a function of the number of casting cycles. Based primarily on weight loss, they determined that molybdenum base alloys oxidize severely when subjected to molten stainless steel.

However, tungsten base alloys (i.e., Anviloy 1150 and WN-103) had much lower weight losses. In addition, Samuels and Draper(37) found that soot die coatings dramatically reduced the surface roughness of metallic dies. These coatings were smoother than coatings applied in the vapor phase. Finally, they noted die materials in order of decreasing resistance to surface deterioration when coated with soot - tungsten base alloys, molybdenum base alloys, heat resistant nickel base alloys, graphite, silicon nitride, and H-13 steel.

III. Apparatus

The high temperature machine casting system consists of an apparatus that produces partially solidified slurries of high temperature alloys, a collection chamber, and a die casting machine. Two distinct system configurations have been used in this study. In the first, slurry exiting from the Rheocaster (slurry producer) is held within the collection chamber at the casting temperature. After a sufficient amount of material has been collected, the charge is die cast in a low pressure laboratory die casting machine. This mode of operation is shown schematically in Figure 4 . In the second, semi-solid slurry is collected and solidified in a cylindrical ingot mold. Subsequently, the ingot is reheated in a furnace to the casting temperature in the liquid-solid range and die cast in a high pressure commercial die casting machine.

1. The High Temperature Slurry Producer

Partially solid slurry is produced either continuously or semi-continuously by the machine shown in Figures 5 and 6 . The crucible made from Vesuvius #235 (58% Al_2O_3, 26%C, and 12%SiO_2) is functionally divided into two regions. The top portion serves as a reservoir of molten metal, whereas the lower region - the mixing chamber - houses the mixing rotor.

The top chamber (3-5/8" diameter by 8" high) can hold ~18 pounds of molten ferrous alloy. The melt surface is partially protected from oxidation by a firebrick cover and an Argon blanket. Also, the cover contains a hole through which solid alloy rod may be fed continuously to recharge the system. This reservoir is heated by induction with a 4.2 KC, 30 KW Inductotherm motor generator set. The temperature of the top chamber is maintained above the liquidus of the alloy and is monitored continuously with a Pt-Pt 10% Rh thermocouple suspended in the melt.

The lower, mixing chamber, is cylindrical in shape (1¼" diameter by 6" long). A separate induction heating coil is wound around the outside of this chamber. Finally, the entire lower assembly is encased in a transite shroud which provides support and containment to the unit. The induction coil is powered by a 5 KW, 200 KC Lepel power supply, and the turn density of the coil is such that the desired temperature gradient is produced along the length of the mixing chamber. A 3/8" diameter exit port formed by a machined ceramic piece is located at the bottom end of the mixing chamber. A Pt-Pt 10% Rh thermocouple is inserted in the crucible at this position and is continuously monitored to insure that the desired fraction solid is obtained in the exiting slurry.

The mixing rotor is an 18" long cylinder (1" outside diameter) and runs concentrically to the bottom of the mixing chamber. Two rotor materials are used. For brass heats, a solid graphite rod (with axial grooves cut along the surface) is employed; whereas, for ferrous runs, a hollow (1/8" wall) alumina tube with hemispherically closed bottom end is used. The rotor is driven by a variable speed 3/4 H.P., D.C. motor capable of rotation speeds between 0 and 1000 rpm. This rotation provides the necessary agitation within the mixing chamber to create the semi-solid slurry. Flow of the slurry through the exit valve is controlled by raising or lowering the mixing rotor along its axis of rotation. At its fully lowered position, the rotor rests on the exit port ceramic, thus stopping flow.

Slurry from the machine is either fed into the isothermal collection chamber of cast into ingot molds. The isothermal collection chamber will be described later. The ingot molds consist of stainless steel tubes (6" x 1¼" I.D.) insulated on the inside wall with Fiberfrax paper. Seven tubes are encased in a transite shell. Each tube, in turn, is filled with semi-solid slurry producing a solid ingot upon cooling.

2. The Collection System

The isothermal collection system consists of an induction heated collection chamber, a fiberfrax crucible, and a delivery mechanism. The system is shown in Figure 4. Basically, the collection chamber is a tube furnace (1¼" I.D. by 5" long) incorporating a graphite susceptor and induction coil. The inside bore of the furnace is comprised of a Vycor tube encased by a cylindrical ceramic shell. The slurry is collected in the fiberfrax paper crucible which rests on a graphite pedestal positioned inside the Vycor tube. During filling, the temperature of metal within the crucible is monitored and held at constant temperature to avoid either solidification or remelting of the semi-solid slurry. Upon completion of filling, the graphite pedestal and crucible are lowered from the collection chamber with the aid of a manually operated mechanism consisting of a guided slide rod and locking screw.

3. The Reheat System

The reheat system consists of an induction powered reheat furnace and a transfer mechanism. The apparatus is shown in Figure 8. The reheat furnace and transfer mechanism are identical in concept to the collection chamber and delivery system previously described. The reheat furnace (2½" I.D. by 10" high) is powered by a 4.2 KC, 50 KW Inductotherm motor generator set. The ingot charge is contained in a CO_2 bonded silica sand crucible which is supported on a marinite pedestal. The ingot is heated directly by the induction field (there is no susceptor within the reheat furnace), and temperature is monitored with a Chromel/Alumel thermocouple, positioned in the center of the ingot. Upon reaching the temperature corresponding to the desired fraction solid the crucible and ingot are removed from the furnace by activating the foot operated transfer mechanism.

4. The Low Pressure Casting System

The low pressure die casting machine has a vertically aligned shot sleeve and plunger which is pneumatically driven by air cylinder powered with compressed nitrogen at a maximum pressure of 80 psi - resulting in a maximum injection pressure of ~1400 psi. The shot cylinder (1¼" I.D. steel) may be independently moved. Prior to casting, the shot cylinder is maintained in its lowered position thus allowing placement of a fiberfrax crucible filled with semi-solid slurry on the injection piston. Prior to casting, however, the cylinder is driven upwards and butted against die blocks at the ingate to the die cavity.

The two die halves (6" square by 1" thick) are made from mild steel and are each heated with a tubular resistance heater (500 watts). The parting line of the die assembly is vertically aligned with the shot sleeve and piston. The two halves are clamped together with a hydraulic jack with a maximum locking pressure of 2000 psi. The bulk temperature of the die is monitored with a chromel/alumel thermocouple located in the interior of the die.

The die geometry is shown in Figure 9 and is connected to the shot sleeve via a runner of .125 sq. in. cross section. The cavity geometry was selected to provide a modified form of a commercial part. When perpared for operation with slurry positioned in the closed shot sleeve, the injection piston is activated, resulting in the destruction of the Fiberfrax crucible and the injection of the semi-solid slurry through the runner to the die cavity.

5. High Pressure Die Casting System

A B & T Greenlee horizontal cold chamber die casting machine was used in this study. The machine, pictured in Figure 8, provides 125 tons of locking force to the dies and is equipped with a 4" diameter hydraulic injection cylinder and a 1-3/8" diameter shot sleeve. The shot piston is water cooled and can be operated with variable intensification pressure and timing during the injection stroke. After activation, the hydraulic cylinder can obtain a peak pressure of 2000 psi (17,000 psi within the casting cavity). The shot sleeve is heated with a resistance jacket coil, and the temperature is continuously monitored via a chromel/alumel thermocouple located within the sleeve.

The two die halves are machined from H-13 steel (5 CO, 1,35 Mo, 1 Si, I V, .4 C, .3 Mn). Each half is heated with two tubular resistance heaters and is thermally insulated from the back-up plates by a sheet of 1/16" thick fiberfrax paper. The dies can be maintained at 400°C - the temperature being monitored by chromel/alumel thermocouples positioned in both the stationary and moving die halves. Opening of the dies after completion of a shot is controlled by an automatic cycle timer. The casting geometry, designed to simulate a commercial part, is shown in Figure 10. The part is fed by a branched runner and is provided with two overflows and vents around each of two ejection pins.

6. Thermal Measurement System

Two miniature thermocouples are used to measure temperature near the casting-die interface. The location of these couples with respect to the die cavity is shown in Figure 9. The distance from the bead of each to the cavity surface is .0139" and .0278", respectively. The detail of the thermocouple assembly is shown in Figure 9. Chromel/alumel wire (38 gauge) is sheathed in a 35 mil two hole alumina protection tube which in turn is encased in a mild steel plug. The bead at the tip of the couple is formed by spot welding the two wires and clipping off the excess.

The steel plug and thermocouple are fitted in a close tolerance hole drilled from the back of the die cavity. Contact between the thermocouple bead and the die is insured by adjusting the forcing bolt which applies pressure to the steel plug. The leads from the thermocouple are insulated with high temperature glass tape and are extended to the cold junction of the measurement system.

The cold junction is of standard construction. The output of the junction is fed into a two channel D.C. amplifier (gain = 100). The amplified signal is subsequently displayed in a Tektronix #533A dual trace and photographed to produce a permanent record of the temperature measurement.

A similar thermocouple assembly, Figure 10, and the same measurement system was employed to measure die temperatures in the high pressure die casting machine.

IV. EXPERIMENTAL PROGRAM

The aim of this thesis has been to analyze the high temperature machine casting system - a compound system consisting of a high temperature slurry producer and a conventional die casting machine. To satisfy this objective, an experimental program has been designed to develop the relationship between process variables and both semi-solid structure and die casting quality. In addition, die temperature measurements and thermal computer simulation were employed to assess the impact of partially solid slurries upon die thermal history and longevity.

The six alloys produced by the high temperature slurry producer were eutectic cast iron (2.6 wt% C, 3.2 wt% Si), 440C and 304 stainless steels, M-2 tool steel, cobalt-base alloy H.S. 31, and copper-base alloy 905. For each alloy system, chosen experiments were carried out where the rotation speed of the mixing rotor, the temperature at the exit port, and the material flow rate were varied and measured (as described in the preceeding Apparatus section). In order to analyze the resulting high temperature structure of each alloy as it exited from the slurry producer, the semi-solid slurry was discharged directly into a water quench tank. Subsequent matallographic examination of these specimens revealed a structure composed of primary solid particles delineated by the fine dendritic structure of the quenched liquid.

In the cast iron runs, the semi-solid slurry was discharged into the induction heated collection chamber, Figure 4, and was subsequently die cast in the low pressure die casting machine, Figure 5. In the brass alloy runs, partially solid slurry was discharged into ingot molds and solidified. The ingots were then sectioned into 2" lengths, and one thin section was removed for metallographic analysis. These 2" slugs were later reheated in the reheat furnace, Figure 7, and die cast in the high pressure die casting machine, Figure 8.

The shot plunger pressure is the only machine parameter of the low pressure die casting machine which can be varied. However, in early tests, it was determined that the maximum plunger pressure produced the best casting quality. Therefore, in cast iron castings, the semi-solid slurry structure (particularly volume fraction solid) was the only variable investigated. For brass and stainless steel casting produced by the high pressure die casting machine, the effect of additional variables was explored. These included shot plunger speed, intensification pressure, and intensification timing. All castings produced by either machine were radiographed in order to assess porosity content. Furthermore, each casting was examined metallographically - some quantitative metallography was also performed, In addition to the structural work described above, two other studies were conducted. In the first, die temperature measurements were performed in both the high and low pressure die casting machines using the thermocouples and procedure outlined in the Apparatus Section. Measurements were made for cast iron and brass in the low pressure system and brass in the high pressure die casting machine. These measurements provide a collaborative input to the thermal computer program which in turn was employed to generate the entire die thermal history. The second study involved a microprobe analysis of both ingot and water quenched structures. The machine and calculations employed are summarized in Appendix A. The samples analyzed are water quench and ingot structures of copper base alloy 905 and 440C stainless steel.

In summary, the process variables enumerated above control slurry and casting structures and the thermal behavior of the die in high temperature machine casting system. This information will be used in the following sections to develop predictive models between each variable - cast structures and die thermal history.

V. RESULTS

1. The Structure of Semi-Solid Slurries

During the past twelve months, a number of high melting temperature alloys have been Rheocast in the continuous slurry producer. These alloys have included eutectic cast iron (Fe-2.6%C-3.2%Si), copper base alloy 905 (88%Cu-10%Sn-2%Zn), 440 stainless steel, and others listed in Table V. Also tabulated are the compositions of each alloy. Subsequent to production of these materials, the microstructures of water quenched and slowly cooled semi-solid samples were analysed to determine the general morphology of the primary solid particles and the phases present within each sample.

The microstructure of a water quenched semi-solid sample of 440A stainless steel is shown in Figure 12. The cooling rate during the solidification of primary solid particles was $40^{o}C/min$. The liquid surrounding these particles was solidified during quench at a calculated rate of $\varepsilon \simeq 1.0 \times 10^{5}\ ^{o}C/min$. The mean diameter of the primary solid particles - white spheres surrounded by the darker matrix - is approximately 105 microns.

For comparison, two fully liquid samples of 440 stainless steel were conventionally solidified at cooling rates of $\varepsilon = 40^{o}C/min$ (measured) and $\varepsilon \simeq 1.0 \times 10^{5}$ (calculated). These rates were achieved by furnace cooling and water quenching the samples, respectively. The resulting photomicrographs, Figure 11, indicate that the slowly cooled sample has a much coarser structure characterized by a dendrite arm spacing of ~50 microns. The water quenched liquid sample has a dendrite arm spacing of ~7.7 microns.

The microstructure of water quenched semi-solid samples of 440C stainless steel, Figure 13, is somewhat more complicated. Each photomicrograph shows several large white primary solid particles composed of martensite with a hardness of $R_c = 52$. The mean diameter of these particles (some having white carbide veins) is approximately 215 microns. Also the microstructure posesses numerous darker primary solid particles composed of austenite, $R_c = 36$. The mean particle diameter of these particles is 115 microns. The dendrite arm spacing of the surrounding dendritic water quenched liquid is approximately 10 microns.

The microstructure of a slowly cooled ($\varepsilon \simeq 25^{o}C/min$; measured) semi-solid sample of 440C stainless steel is shown in Figure 14. The photomicrograph shows a carbide network enveloping austenitic grains. The mean grain diameter is ~165 microns. In some regions of the microstructure, the grain boundaries are devoid of carbide.

The microstructure of water quenched semi-solid samples of copper base alloy 905, 88%Cu-10%Sn-2%Zn, is shown in Figure 15. Here the external boundaries of the primary solid particles (predominantly copper rich α brass)are smooth indicating a greater degree of coarsening during primary solidification than that of water quenched 440C stainless steel, Figure 13. Also, the primary solid particles of the bronze sample, Figure 15, possess a signigicant amount of entrapped liquid. The average primary solid particle diameter is ~155 microns. The measured dendrite arm spacing of the darker water quenched liquid region is ~3.0 microns.

The microstructure of water quenched semi-solid samples of eutectic cast iron (Fe-2.6%C-3.2%Si) is shown in Figure 16. The primary solid particles are composed of martensite - the needles of which are revealed distinctly at 200X. These particles contain no detectable entrapped liquid. The mean diameter of the primary solid particles is ~115 microns. However, the microstructure seems to be duplex having numerous small particles (mean diameter ~80 microns) interspersed among larger particles (mean diameter ~210 microns). The interparticle matrix, solidified during quenching, is white cast iron with numerous cementite needles (white in the photomicrographs).

The microstructures of water quenched semi-solid samples of HS-31 cobalt base superalloy and 304 stainless steel are shown in Figures 17 and 18, respectively. The mean diameter of the primary solid particles for each alloy is larger than those previously reported (HS-31, mean diameter ~350 microns; 304 stainless steel, mean diameter ~250 microns). The photomicrographs of HS-31 show coarse primary solid particles with veins of entrapped liquid similar to the primary solid particles of copper base alloy 905, Figure 15. The microstructure of slowly cooled ($\varepsilon \simeq 25^{\circ}C/min$) samples of semi-solid HS-31 superalloy and M-2 tool steel are shown in Figure 19. These microstructures are both finer and less coarsened than the slowly cooled sample of 440C shown earlier, Figure 14.

The variation of solute concentration throughout the microstructure of water quenched semi-solid samples of copper base alloy 905 and 440C stainless steel was determined by microprobe analysis. The solute concentration profiles for tin in copper base alloy 905 and for chromium, manganese, molybdenum, and silicon in 440C stainless steel are plotted in Figures 20 and 22, respectively. For copper base alloy 905, the tin concentration maintains a constant level within the α solid solution regions of the microstructure. The sharp peaks (upwards to ~20 wt% Sn) of the composition profile correspond to the presence of entrapped liquid within the primary solid particles. For 440C stainless steel, the concentration of each solute element is constant throughout the primary solid particles - there being no entrapped liquid. For both alloys studied, the solute concentration (with the exception of silicon in 440C stainless steel) rises sharply in the matrix surrounding each primary solid particle. A numerical summary of these findings is shown in

Table III.

One slowly cooled ($\varepsilon \approx 25^0$C/min) semi-solid sample of bronze 905 was analysed on the microprobe. The resulting tin concentration profile is shown in Figure 21. The plot indicates that the entrapped liquid present in water quenched samples has fully dissolved in the α solid solution. However, the tin concentration is not uniform within the grain. Rather, the concentration profile possesses two small peaks (3.5 wt% Sn) between the grain center and the grain boundary. The tin concentration in the grain at these two locations is approximately 2.0 wt%. The tin concentration between grains is quite high approaching 25 wt% Sn.

2. Castings

Cast iron, stainless steel, and bronze die castings were made in both the low and high pressure casting systems. The eutectic cast iron (Fe-2.6%C-3.2%Si) and 440C stainless steel castings were produced in the low pressure casting machine. A sample part cast (excluding runner and biscuit) is shown in Figure 23. Both semi-solid and fully liquid charge material was used. The surface appearance of the majority of castings made was good. However, due to the low pressures employed, ~1,000 psi, and the lack of adequate venting, a large amount of air was usually entrapped within the castings. The semi-solid particles (for Rheocast castings) did enter and fill the die uniformly, Figures 24 and

25. In addition, no region of any casting produced from semi-solid charge was found to be devoid of primary solid particles. The microstructure of the casting arm for 440C stainless steel, Figure 25, shows several primary solid particles which possess a central core of δ ferrite, hardness $R_B = 98$. This section of the casting experiences the fastest cooling rate during solidification.

Eighty-nine castings were made from copper base alloy 905, 88%Cu-10%Sn-2%Zn, in the high pressure die casting machine, Table IV. The part cast is shown in Figure 23. The charge for the die casting machine was prepared by reheating (Thixocasting) cylindrical ingot slugs in the reheat furnace to the desired casting temperature. The microstructures of the starting charge material, slowly cooled liquid and semi-solid bronze 905, are shown in Figures 26 and 27, respectively. Slowly cooled liquid slugs were heated to 1100°C (~100°C above the liquidus temperature) and cast. Slowly cooled semi-solid slugs were reheated to various temperatures and cast (lowest temperature was ~960°C corresponding to a fraction solid, $f_s \approx 0.60$).

The microstructures of two of the castings are shown in Figure 28. For comparison, the microstructures of the corresponding water quenched sample made during the production of ingot slug charge material is also shown in Figure 28. In both casting photomicrographs, the entrapped liquid has spheroidized to some extent. However, the bottom casting microstructure has a considerable amount of entrapped liquid despite expected diffusion during the reheating operation.

Examination of the casting cross-sections revealed that the primary solid particles filled the casting cavity uniformly, as shown in Figure 29. The volume fractions of primary solid in the three photomicrographs of Figure 29 are 0.53, 0.56, 0.42, from left to right.

The surface and radiographic quality of each casting was also examined. The surface quality of the best castings produced from fully liquid charge was somewhat better than the surface quality of the best castings produced from the semi-solid charge. However, in general, for all castings, the quality of the casting surface was independent of the casting temperature. On the other hand, castings produced from semi-solid charge had significantly less entrapped air and porosity than those castings produced from fully liquid charge. No radiographically sound castings were produced from fully liquid bronze 905 alloy. Two typical casting radiographs (one made from a fully liquid charge and one from a semi-solid charge) are shown in Figure 30 along with photomicrographs of the corresponding microstructures. For castings number 77 through 89, the average radiograph ratings of castings produced from liquid and semi-solid charge were 4 and 2, respectively. A five point rating system was employed; 1 representing good quality and 5 representing poor quality.

3. Die Thermal Analysis

Internal die temperature measurements were made during casting production in the low pressure casting machine using the thermocouples and measurement system described earlier in the apparatus section. Both cast iron and bronze alloy castings were produced. However, thermal measurements on castings made from semi-solid charge material were only made with the bronze alloy. The first group of measurements were made during the casting of both liquid and semi-solid copper base alloy 905, 88%Cu-10%Sn-2%Zn. The results of die temperature measurements at a location 0.0139" from the casting-die interface for two casting temperatures (T = 1100°C, f_s = 0.0; T = 970°C, f_s = 0.52) are shown in Figure 31. The general characteristics of each curve are similar - in both cases the die temperature heats rapidly for 0.2 - 0.3 seconds. At that time, however, the temperature of the die begins to decrease gradually. In comparing the die thermal response for fully liquid and semi-solid bronze 905, we find that the maximum temperatures attained are 574°C and 507°C, respectively. Because the initial die temperature (before casting) is 420°C in each case, the ratio of the temperature rise for the two castings is 1.77. The initial rates of heating for liquid and semi-solid bronze are 2000°C/

sec and 880^{o}C/sec (ratio 2.27), respectively.

The internal die temperatures measured at locations 0.0139" and 0.0278" from the casting-die interface during the casting of semi-solid bronze 905 ($T \approx 970^{o}C$, $f_s \approx 0.52$) are shown in Figure 32. As expected, the location furthest from the casting-die interface heats up more slowly. Initial die heating rates are 880^{o}C/sec and 240^{o}C/sec (ratio 3.67) for locations 0.0139" and 0.0278", respectively. At 0.1 seconds, the thermal gradient between the two thermocouples is 1302^{o}C/cm.

The internal die temperatures measured at a position 0.0139" from the casting-die interface during the casting of superheated eutectic cast iron (Fe-2.6%C-3.2%Sn) at temperatures 1380^{o}C and 1330^{o}C (liquidus temperature is 1303^{o}C) are shown in Figure 13. The general characteristics of each curve are similar to the curves produced during the casting of bronze 905 alloy, Figure 31. In comparing the curves produced during the casting of eutectic cast iron at the casting temperatures of 1380^{o}C and 1330^{o}C, we find that the maximum temperature attained in each case is 527^{o}C and 519^{o}C, respectively. The rates of initial temperature increase are 1200^{o}C/sec and 840^{o}C/sec, respectively.

(b) High Pressure System

Die temperature measurements were made during the production of bronze 905 alloy castings, both liquid and semi-solid charge material, in the high pressure die casting machine. The thermocouple was located 0.0139" from the casting-die interface. Owing to difficulties in electrically grounding the die casting machine and to the presence of stray magnetic fields, the oscilloscope recording of the thermocouple output displayed some noise. However, it was possible during the majority of tests to limit the noise level to less than 3% of the measured signal. To insure that the thermocouple output was unaffected by electrical transients and changes in the level of the electrical ground during the casting cycle, one blank shot was made at room temperature. The thermocouple output during this test was constant.

The raw thermocouple output produced during the casting of superheated liquid, $T_o = 1100^oC$, and semi-solid, $T_o = 960^oC$, $f_s = 0.57$, bronze 905 are shown in Figure 34. The same data, converted to temperature is plotted in Figure 35. For short times ($t < 0.15$ sec), each temperature plot is characterized by a large amount of rapid variation. During this period, the maximum temperatures attained are 645^oC and 315^oC for the casting of liquid and semi-solid bronze 905, respectively. After this period, however, the die temperature for each case rises to a peak and then falls. After approximately 0.5 seconds, the die temperature at the thermocouple location levels and maintains a constant value.

The initial rates of die heating are 2.47×10^{4} °C/sec and 8.25×10^{3} °C/sec (ratio = 2.99) for the fully liquid and semi-solid castings, respectively. The die temperatures at 0.60 seconds are 400°C and 270°C for the same two castings. The ratio of the corresponding temperature rise above ambient is 2.08.

VI. HEAT FLOW SIMULATION

A computer program was developed to simulate heat flow within the die of a die casting machine. The specific objective of this study was to assess and compare the die thermal behavior for a superheated (fully liquid) metal charge and a partially solid metal charge. In addition, die temperature measurements were carried out to verify and modify the numerical analysis when necessary.

The computer program employs a finite one-dimensional heat flow model which is solved using a forward difference technique. The geometry and dimensions of the model are shown in Figure 26. The physical assumptions made to facilitate solution of the problem are:

(1) the die is filled instantaneously,

(2) the die and casting comprise an adiabatic system with no heat losses to the surroundings,

(3) the die is initially at uniform temperature and undergoes no solid state transformations upon heating,

(4) the physical properties of the liquid metal are independent of temperature,

(5) the solidifying casting is sound (has no porosi-

ty).

(6) heat flow at the die-metal interface is characterized by a surface heat transfer coefficient which is a simple function of time.

Heat flow within the liquid portion of the casting has been treated for two different conditions. The first case assumes full convection in the liquid, and therefore, no temperature gradient. In the second, the liquid is stagnant and heat flow occurs by conduction only.

The mathematical problem can be represented by the thermal diffusion equation:

$$\alpha \frac{\partial^2 T}{\partial x^2} = \frac{\partial T}{\partial t} \qquad (15)$$

where $\alpha = k/\rho C_p$. In this identity, the material constants k, ρ, and C_p represent the thermal conductivity, the density, and the heat capacity, respectively. In order to use this equation for flow problems involving solidification, it is necessary to employ an "effective" heat capacity to account for heat liberated during solidification. However, the "effective" heat capacity - the derivative of enthalpy with temperature - is undefined for pure metals and eutectic alloys owing to the discontinuity of the enthalpy function at the solidification temperature. Most investigators have avoided this problem by either ignoring eutectic solidification or by distributing the eutectic heat of solidification over a small temperature range.

A more simple and accurate approach is that developed below. Consider the one-dimensional flow and accumulation of heat in a volume element of dimensions Δx, Δy, Δz. The energy balance on this element produces the following conservation equation:

$$k \left[\left.\frac{\partial T}{\partial x}\right)_{x+\Delta x} - \left.\frac{\partial T}{\partial x}\right)_{x} \right] \Delta y \ \Delta z = \frac{\partial H}{\partial t} \Delta x \ \Delta y \ \Delta z \qquad (16)$$

where H represents the enthalpy content of the volume element. Eliminating terms and invoking the definition of the derivative, we obtain:

$$k \frac{\partial^2 T}{\partial x^2} = \frac{\partial H}{\partial t} \qquad (17)$$

Since temperature is a finite single valued function of enthalpy, no difficulties arise, except additional bookkeeping within the computer program.

The mathematical problem is specified more fully by the following set of boundary and initial conditions:

1) $x = 0 \; ; \; \frac{\partial T}{\partial X} = 0 \; ,$ (from symmetry)

2) $x = L \; ; \; \frac{\partial T}{\partial X} = 0 \; ,$ (insulated outer die surface)

3) $x = D \; ; \; \frac{\dot{Q}}{A} = h \; \Delta T_s$

4) $t = 0 \; , \; D < x < L \; ; \; T = T_D$

5) $t = 0 \; , \; 0 < x < D \; ; \; T = T_o$

where T_D and T_o are the initial die and melt temperatures, respectively, and ΔT_s is the temperature difference across the mold metal interface due to the surface heat transfer coefficient, h. The ratio $\dot{Q}/A$ represents the rate of heat flow through the mold metal interface per unit area. D is the casting half thickness, and L is the distance from the casting centerline to the die exterior. Each of the above parameters is depicted in Figure 36.

Before implementing the computer program, equation (17) and the associated boundary conditions (1 -5) must be rewritten in finite difference form. Employing forward differences and the mesh shown in Figure 36, the following set of equations are obtained:

$$H_i\ (t+\Delta t) = H_i(t) + \frac{k}{\rho(\Delta x)^2}\left[T_{i+1}\ (t) - 2T_i(t) + T_{i-1}(t)\right]\ \Delta t \qquad (18)$$

(1) $T_1(t) = T_2(t)$

(2) $T_{25}(t) = T_{24}(t)$

(3) $H_{10}(t+\Delta t) = H_{10}(t) + \frac{2}{\rho\Delta x}\left[\frac{kT_9(t)}{\Delta x} - \left(\frac{k}{\Delta x} + h\right) T_{10}(t) + hT_{11}(t)\right]$

$H_{11}(t+\Delta t) = H_{11}(t) + \frac{2}{\rho\Delta x}\ \frac{kT_{12}(t)}{\Delta x} - \left(\frac{k}{\Delta x} + h\right) T_{11}(t) + hT_{10}(t)]$

(4) $t = 0,\ 1 \le i \le 10;\ T_i = T_o$

(5) $t = 0, 11 \le i \le 25\ ;\ T_i = T_D$

where T_i represents the temperature at the i^{th} nodal point, Δx is the node spacing, Δt is the time interval between iterations, and ρ and k are the metal density and conductivity, respectively.

In addition to the above set of finite difference equations, the functional relationship between enthalpy and temperature is established:

$$H\ (T) = \int_{273}^{T} C_{eff}\ (T')\ dT' \qquad (19)$$

where

$$C_{eff} = \begin{cases} C_p(\text{Liquid}) & T > T_{Liq} \\ f_L(T)\ (C_p(\text{Liquid}) - C_p(\text{Solid}) + \Delta H_f) + C_p(\text{Solid}); & T_{Sol} < T < T_{Liq} \\ C_p(\text{Solid} & T < T_{Sol} \end{cases} \tag{20}$$

where T_{Sol} and T_{Liq} refer to the solidus and liquidus temperature of the alloy, respectively. Two methods are available for determining the temperature dependence of fraction liquid (f_L). With adequate phase diagram information - as in the Fe-C-Si system - a Scheil analysis can be performed.

Otherwise, system complexity requires the use of simplifying assumptions - the most obvious being that fraction solid is a linear function of temperature in the solidification range.

In summary, the relationship describing variation of fraction liquid with temperature is substituted in the C_{eff} equation (20) which is then integrated and entered into the computer program as a series of linear approximations.

The sequence of steps executed by the computer program are as follows: (i) the initial enthalpy and temperature at each node, as indicated by the initial conditions, are stored within the computer, (ii) for the first iteration, equation (18) or the appropriate boundary condition is applied successively at each node throughout the array, yielding $H_i(\Delta t)$, and (iii) the associated temperature $T_i(\Delta t)$ is then calculated, and both the enthalpy and temperature arrays are stored for the next iteration. After the appropriate number of iterations the temperature distribution throughout the die and the casting is printed. The program and associated flow diagram are presented in Appendix B.

Successful operation of the computer program requires a suitable choice for the increments Δt and Δx. For example, excessively large values of Δt yield oscillation in the output. When these oscillations occurred, trial and error selection of the interval size was used to eliminate the instability. Also, to check the convergence of the program, three nodal meshes were used to calculate the temperature response for one set of simulation conditions. It was found that two meshes with a nodal spacing differing by a factor of two yielded identical outputs to within 0.1%.

1. Computer Results

The thermal computer program was inplemented to simulate heat flow within the dies of the low and high pressure casting systems. The value of the surface heat transfer coefficient, h, was adjusted to provide agreement between the output of the computer program and the experimentally measured die temperatures previously reported in the Results section. This approach was employed for fully liquid and semi-solid copper base alloy 905 castings produced in both casting systems. Also, computer simulation was carried out for fully liquid eutectic cast iron castings (a model ferrous system) in the low pressure casting machine.

The experimentally measured die temperature curves (for both high and low pressure systems) each exhibit similar characteristics, Figures 31-33 and 35, as previously described. Initially, the dies heat up rapidly reaching a maximum temperature between 0.05 and 0.3 seconds. However, at this time the die temperature either levels or drops. In order to replicate these characteristics with the computer program, the value of the surface heat transfer coefficient, h, has been abruptly lowered during the casting cycle.

The experimentally measured and calculated die temperatures at a location 0.0139 inches from the casting - die interface for fully liquid ($T = 1100^{o}C$) and semi-solid (T =

970^{o}C, f_s = 0.53) copper base alloy 905 castings produced in the low pressure casting machine are compared in Figure 31. The initial values of h employed for calculation are 0.30 cal/cm^2 ^{o}C sec and 0.15 cal/cm^2 ^{o}C sec for the liquid and semi-solid castings, respectively. The transition to the final value of h (0.08 cal/cm^2 ^{o}C sec) occurs at 0.25 and 0.15 seconds, respectively. Thus the initial value of the surface heat transfer coefficient is both higher and applicable for longer times when castings are produced from liquid charge material. Using these values of h and the transition times, the measured and calculated curves agree well for both liquid and semi-solid castings, particularly for short times. For longer times, the general behavior of the measured and calculated curves is similar.

To insure that the manipulation of h did not merely provide a fortuitous agreement between measured and calculated die temperatures at one location, the die temperature at two locations (0.0139 and 0.0278 inches from casting-die interface) were measured during the casting of semi-solid bronze 905 ($T \simeq 970^{o}$C, $f_s \simeq 0.53$). The experimental and calculated curves, Figure 32, agree at both locations. However, again there is some quantitative deviation at long times.

The measured and calculated die temperatures produced during the low pressure casting of fully liquid eutectic cast iron (T = 1380^{o}C and T = 1330^{o}C) are shown in Figure 33.

To provide agreement between measured and calculated curves, the initial value of h is 0.15 cal/cm^2 ^{o}C sec and changes to 0.06 cal/cm^2 ^{o}C sec at 0.066 seconds. Again, at long times ($t > 0.25$ seconds) there is some disparity between the calculated and measured curves for both casting temperatures. In general, the calculated temperatures, after this time, rise whereas the measured temperatures either level or decrease.

It is more difficult to simulate heat flow within the dies of the high pressure die casting machine during the casting or fully liquid and semi-solid bronze alloy 905, owing principally to the rapid temperature fluctuations which occur at short times, Figure 35. However, it was possible to study isolated sections of measured temperature curves and simulate heat flow during these sections separately. For example, the initial temperature rise for fully liquid ($T = 1100^oC$) and semi-solid ($T = 960^oC$, $f_s = 0.57$) bronze 905, Figure 35, corresponds to values of h equal to 10.0 cal/cm^2 ^{o}C sec and 3.0 cal/cm^{2}C sec, respectively. These h values are significantly higher than those recorded for the low pressure casting machine. However, examination of the experimentally measured temperatures for times greater than 0.1 seconds (i.e., ignoring the period of rapid temperature fluctuation) indicates that the initial values of the surface heat transfer coefficient are 3.0 cal/cm^2 ^{o}C and 0.15 cal/cm^2 ^{o}C sec for fully liquid and semi-solid bronze alloy 905 castings, respectively. For the fully liquid casting the value of h changes to 0.04 cal/cm^2 ^{o}C sec at 0.15 seconds; whereas for the semi-solid casting the value of h changes to 0.08 cal/cm^2 ^{o}C sec at 0.35 seconds. Using these h values and transition times yields good agreement between the measured and calculated curves through ignoring the period of rapid temperature fluctuation.

(a) Surface Die Temperature

The main objective of the thermal computer program was to predict the die surface temperature and surface thermal gradient. The value of the surface heat transfer coefficient for these computer runs was determined by matching the measured and calculated temperatures within the die as described above. Simulations were conducted for copper base alloy 905 and eutectic cast iron in both the high and low pressure casting systems.

i. Low Pressure System

The predicted die surface temperatures produced during the low pressure casting of fully liquid ($T = 1100^oC$) and semi-solid ($T = 970^oC$, $f_s = 0.53$) bronze alloy 905 are shown in Figure 37. The maximum temperatures attained are 614^{o}C and 513^{o}C, respectively. Yielding a ratio of temperature rise equal to 2.09. The initial rates of die surface temperature increase for the two castings are 2600^{o}C/sec and 1080^{o}C/sec, respectively. The initial die thermal gradients at the casting-die interface are 1300^{o}C/cm and 590^{o}C/cm for fully liquid and semi-solid bronze, respectively.

The simulated die surface temperatures for the low pressure casting of fully liquid (T = 1380^{o}C) and semi-solid (T= 1210^{o}C) eutectic cast iron are shown in Figure 39. Because no semi-solid cast iron was actually cast in the low pressure casting machine, the same values of the surface heat transfer coefficients were employed for both cases. The maximum temperatures attained are 537^{o}C and 513^{c}C for fully liquid and semi-solid castings, respectively. The initial rates of die heating are 2760^{o}C/sec and 2000^{o}C/sec; whereas the initial die thermal gradients at the casting-die interface are 1020^{o}C/cm and 811^{o}C/cm for fully liquid and semi-solid eutectic cast iron, respectively.

ii. High Pressure System

The computer simulated die surface temperatures for fully liquid and semi-solid copper base alloy 905 and eutectic cast iron castings made in the high pressure die casting machine are plotted in Figures 38 and 40. The initial period of rapid temperature fluctuation, Figure 35, has been ignored as described earlier. In both fully liquid simulations, the initial value of h was 3.0 cal/cm^{2} ^{o}C sec and was lowered to 0.04 cal/cm^{2} ^{o}C sec at 0.05 seconds. On the other hand, for the simulation of semi-solid castings, the initial value of h was 0.15 changing to 0.08 at 0.25 seconds.

For both copper base alloy 905 and eutectic cast iron, the computer simulation indicates that the die surface temperature is lowered significantly when semi-solid charge material is die cast in the high pressure casting system. For bronze alloy 905 castings, the maximum die surface temperatures attained are 800°C and 315°C for fully liquid and semi-solid charge material, respectively. The corresponding initial rates of temperature increase are 11,000°C/sec and 1,600°C/sec. The values of the initial die thermal gradient at the casting-die interface are 5,640°C/cm and 718°C/cm. For eutectic cast iron, the maximum die surface temperatures are 990°C and 345°C for fully liquid and semi-solid castings, respectively. For these two cases the die surface heats at rates of 16,800°C/sec and 1,600°C/sec. The initial die thermal gradients attain values of 6,590°C/cm and 896°C/cm for fully liquid castings and semi-solid castings, respectively.

VII. DISCUSSION

1. Introduction:

The purpose of this study has been to investigate the machine casting of semi-solid slurries of high melting temperature alloys. Two machine casting systems (high and low pressure) were employed to produce both ferrous and copper base alloy castings.

The low pressure system was used as a laboratory model system prior to coupling of the process to a commercial high pressure die casting machine. Ultimately, the adoption of any new casting system requires that the castings produced have good surface quality, and low porosity content. Also, the variation of solute concentration throughout the casting should be minimal and the microstructure should be fine to enable the use of efficient homogenization heat-treatment procedures when stringent mechanical property specifications are to be met. Finally, economic considerations demand that the cost to produce each casting be competitive with existing conventional casting and forming processes.

However, the accomplishment of these goals and thus successful operation of the casting system (either operated in the Rheocast or Thixocast mode) requires both understanding and control of the three system components; the continuous slurry producer, the reheat or holding furnace, and the casting machine. Of these, two components, the slurry producer and the casting machine, have been dealt with in this investigation. In addition, because the expense of die casting high melting temperature alloys is strongly dependent upon die life, a thermal analysis was carried out to assess the merits of die casting semi-solid alloys. In what follows the three areas investigated (products obtained from the high temperature slurry producer, the castings made from these slurries, and the resulting die thermal behavior) are discussed separately using a format analogous to that of the results section.

2. The Structure of Semi-Solid Slurries

A number of high melting temperature ferrous and copper base alloys have been successfully Rheocast in the continuous slurry producer. Characteristically, for each alloy, the microstructure of water quenched semi-solid samples is composed of primary solid particles surrounded by a fine dendritic network solidified during the water quench. However, the primary solid particles in each case have a different size and shape and contain varying amounts of entrapped liquid. Because these physical characteristics affect the rheological behavior and heat treatment response of semi-solid alloys, ultimately, the production of partially solid slurries will require control of each microstructural parameter.

In a given forming or casting process one may obtain the desired slurry viscosity by altering either the volume fraction solid and/or the internal structure of the slurry.

In general, the viscosity of a given slurry increases with volume fraction solid, Figures 1 and 2. However, at a given volume fraction the viscosity can also be affected by the size and geometry of the primary solid particles. For example, slurries containing smooth, coarse primary solid particle with negligible entrapped liquid have the lowest viscosities (2). Referring to Figures 2 and 3, we find that at a volume fraction solid of 0.5, the apparent viscosities of samples with particle sizes of ~50 microns and ~180 microns are ~22.0 poise and ~3.5 poise, respectively. However, in samples cast from a partially solid charge material, microsegregation manifests itself over distances comparable to the primary solid particle size, Figures 20 - 22. Therefore, a reduction in the size of primary solid particles will reduce the distances separating microstructural heterogeneities. The latter should improve the properties of the resulting castings and accellerate the response to homogenization heat treatment. The relative importance of each of these factors (viscosity and microstructure) will be determined by the specific casting process and the size, geometry, and physical property specifications of the parts to be fabricated.

However, once determined, there are three machine variables which may be altered to obtain the desired microstructure in a partially solidified slurry. These are: the exit temperature (volume fraction solid) of the slurry, the rotation speed (shear rate) of the mixing rotor, and the cooling rate of the slurry during solidification. The average shear rate within the mixing chamber during the production of semi-solid slurries is given by the following equation:

$$\dot{\gamma} = \frac{2\Omega K}{1-K^2} \qquad (21)$$

where $\dot{\gamma}$ is the average shear rate between the walls of the mixing chamber and Ω represents the rotational speed of the rotor in radians per second. The term K is the ratio of the diameter of the mixing rotor and the inside diameter of the mixing chamber.

Use of the above equation predicts that at a rotation speed of 750 RPM, the mixing rotor produces a shear rate of 350 $\sec^{-1}$. Earlier work on a Sn-15%Pb alloy has shown that at this high level of shear rate, changes in shear rate within the available range of the present machine produce only minor changes in particle size, Figure 3(2). Extrapolation of this finding to the high temperature system used in the present study permits the deduction that for a given exit temperature (volume fraction solid) variation of the cooling rate during primary solidification is the only practical method available to appreciable alter the size of the primary solid particles. On the other hand, variation in the shear rate can affect the geometry of the primary solid particles, hence, the viscosity of the slurries. For example, high shear rates are reported to produce smoother primary solid particles with less entrapped liquid (lower effective volume fraction solid) and lower viscosities at a given temperature.

The relationship between the size of primary solid particles and cooling rate, at a given rate of shear, is similar to that observed in conventional dendritic solidification. In conventional solidification of fully liquid alloys, the spacing between dendrite arms decreases as the cooling rate increases. Similarly, earlier work by Joly(2) on partially solid slurries of a Sn-15%Pb alloy, Figure 3, shows that an increase in cooling rate from 0.33°C/min to 25°C/min produces a corresponding decrease in the size of primary solid particles from ~180 microns to ~50 microns. These measurements were made at a shear rate of 750 sec^{-1}. A comparison of the microstructures in Figure 12 shows that the size of primary solid particles in a slurry of 440A stainless steel is between the primary and secondary dendrite arm spacing of a conventionally solidified sample. A definite explanation of this experimental observation is premature at this time due to our lack of understanding of the complex mechanisms of dendrite fragmentation, coarsening, and coalescence occuring in the mixing chamber.

Heretofore, the principal goal in the development of the high temperature rheocaster has been to produce semi-solid slurries of various high temperature alloys - as described in the results section. During this study it was not yet possible to vary the machine variables in a predictable and controlled manner to affect the slurry microstructures. For example, because the monitoring thermocouples of the mixing chamber are located along the outside periphery of the Vesuvius Cruciable; severe thermal lags exist in the temperature measurement system. Thus, it was not possible to determine either the exact temperature or thermal gradient within the mixing chamber proper. Also accurate control of the flow rate through the small exit port was not possible owing to the dependence of the flow rate upon the viscosity of the slurry. Hence, no concerted attempt was made to undertake a systematic investigation of the role of process variables on the structure of a given alloy slurry.

On the other hand, some general trends can be established by comparing the size and geometry of the primary solid particles in semi-solid slurries of the different alloy systems, Figures 12 - 18. The measured primary solid particle size for all the alloys was in the range of ~100 to ~350 microns. However, the ferrous base alloys exhibited a bimodal size distribution with smaller particles of ~100 microns and larger particles of ~200 microns. Entrapped liquid - manifesting itself as carbide veins - in the 440 stainless steel alloys was present only in the larger martensitic particles. Finally, there is a definite similarity between the structure of the bronze and the cobalt base superalloy. While the sizes of the primary solid particles are different (~150 microns for the bronze alloy and ~350 microns for the superalloy) the particles of the two alloys are similar in geometry and appearance of entrapped liquid, Figures 15 and 17.

In conclusion, a refinement of the continuous high temperature slurry producer to permit accurate control of process variables (in slurry exit temperature and cooling rate) should form an important part of future work in the machine casting program.

3. Castings

In this section the radiographic quality and structure (primary particle size and distribution) of castings produced in this study will be discussed. Furthermore, since the Thixocast process was used, the added processing step of reheating the slugs to an accurate reproducable temperature in the liquid-solid range will also be discussed.

The most significant finding of this portion of the investigation was that the castings produced from semi-solid charge material had significantly less entrapped air and shrinkage porosity than those produced from fully liquid charge. An example of this is shown in Figure 30. This finding can be attributed to two factors. First, a semi-solid charge is already partially solid before it enters the die cavity, hence there is less shrinkage porosity in the casting. Second, the more viscous slurry convects less in the shot sleeve and during die filling resulting in reduced air entrappment. This latter statement has been verified in earlier work by Schottman(9) on die filling behavior of completely liquid and semi-solid slurries carried out with transparent dies.

In that work, high speed motion pictures taken through the transparent die half showed that a semi-solid slurry can be made to enter a die cavity with essentially a solid front fill. Figure 41 shows sequences of frames taken from the high speed motion picture. The all liquid charge material entering the die cavity, shown in Figures 41a and 41b, breaks up and splashes off the opposite die wall. Whereas, the partially solid, viscous, charge material flows smoothly with an essentially solid front at similar stages of the die fill. The smoother, less turbulent flow results in lower amounts of entrapped air.

Most of the castings made in this study, including those from a semi-solid charge material, contain some porosity as do conventionally produced low temperature metal (e.g., zinc, aluminum) die castings. Pores with entrapped gas are reduced in size due to the high pressures, up to ~20,000 psi, acting on the solidifying casting. Therefore, subsequent heat treatment of these castings can lead to blistering. If ferrous alloy die castings are to be properly heat treated, then porosity in these castings, especially gas porosity, should be minimized.

The solid front fill condition observed with semi-solid slurries is certainly an advantage that should be exploited. The exact conditions (flow velocity, size, and geometry of the gate, etc.) for its occurance have not yet been established. Thus, a comprehensive program aimed at establishing the ideal die filling conditions for semi-solid slurries should be undertaken.

The distribution of primary solid particles in the castings made were homogeneous, Figures 24, 25, and 29. This type of study should continue - especially work should be carried out to determine minimum section thickness through which a slurry can flow without segregation of the solid and the liquid. Furthermore, the effect of abrupt cross-sectional changes on the flow behavior of semi-solid slurries should be studied.

Finally, in order to produce castings of uniform quality, the viscosity of the reheated charge material must be consistantly controlled. The two factors affecting viscosity are volume fraction solid (reheat temperature) and internal structure (size and geometry of primary solid particles) of the slugs. It is thus imperative to first be able to continuously produce slurries of desired structure in the rheocaster. Second, the reheat and slug transfer operation should be mechanized to insure reproducibility. In the present apparatus, reheat temperature is manually controlled and the slugs are initially produced from semi-solid slurries having variable structures and volume fraction solid. Future plans call for a small constant load piercing probe device to be incorporated in the reheat furnace assembly to permit measurement of the relative viscosity of each slug prior to casting.

4. Die Thermal Analysis

Die deterioration is a major limitation confronted when attempts are made to die cast fully liquid high melting temperature alloys. Two prevalent modes of degradation are die cracking and chemical and mechanical erosion; each phenomena being governed by the behavior of heat flow within the die during filling. Basically, severe thermal gradients within the die near the casting-die interface cause thermal cracking whereas high surface temperatures lead to surface erosion.

In this study, both experimental measurements and computer simulation indicate that during the die casting of semi-solid alloys the die temperatures and thermal gradients are dramatically lower than when fully liquid alloys are die cast. For example, in the low pressure system measured temperature rise, above the initial die temperature, for the all liquid charge (superheated 100°C) and the semi-solid charge (volume fraction solid ~0.5) were 150°C versus 90°C, respectively, Figure 31. Similar measurements in the high temperature system yielded values of 475°C and 150°C, respectively, Figure 35.

Internal die temperatures measured in both the high and low pressure casting systems show similar characteristics. Plots of temperature versus time generated during the casting of semi-solid and liquid copper base alloy 905 in both systems exhibit an initial fast rise in temperature followed by a period of relatively constant temperature.

The initial rate of temperature change with time in the die are significantly larger when an all liquid metal charge is used. This is true for both the low pressure (laboratory) and the high pressure commercial casting machine. The latter shows much more pronounced differences between an all liquid charge and a semi-solid charge. For example, slopes calculated from Figures 31 and 35 are 2000°C/sec versus 880°C/sec, and 2.5×10^{4} °C/sec and 8×10^{3} °C/sec, respectively.

The experimentally measured die temperatures in the commercial die casting machine show rapid oscillations in temperature, up and down, at short times, $t < 0.1$ seconds, Figure 35. High speed movies taken to determine plunger velocity during casting showed that the fill time of the casting is approximately equal to the duration of these temperature disturbances. Furthermore, when the pressure intensifier was shut down (resulting in a reduction of pressure on the gate area from 17,000 psi to 6800 psi) the magnitude of these disturbances was significantly dampened.

Thus all evidence indicates that these initial temperature disturbances are related to physical phenomena occurring during die fill. Examination of the high speed photographs (9) shown in Figure 41, taken on the transparent low temperature system, indicates that metal splashing occurs in die. Under ideal conditions this should not occur with a semi-solid charge. However, the different die and gate geometries and higher flow velocities used in the commercial machine could induce some splashing in the semi-solid charge. Solidification or deflection of these high velocity droplets in the die causes the rapid variation in temperature prior to complete filling of the die.

As was pointed out in the literature survey, the heat transfer coefficient at the casting-die interface is an important variable controlling the flow of heat within both the casting and the die. In this study, correlation of experimentally measured die temperatures with computer simulation enabled prediction of the value of the surface heat transfer coefficient in the different casting machines used. In lieu of direct temperature measurements at the die surface porper (first thermocouple was located 0.014" below the die surface) these values are essential in predicting the die surface temperature and temperature gradient.

In this study, in order to provide good agreement between the measured and calculated die temperatures it was necessary to change the values of the surface heat transfer coefficient, h, during computer simulations. The abrupt change in this value corresponded approximately to the die fill time, t ~0.1 seconds, determined by measuring the plunger velocity, Figure 31. The two values of the surface heat transfer coefficient, h_I and h_f, denote the initial and final heat transfer coefficients.

In the low pressure (laboratory) casting apparatus the calculated h_I and h_f values were in the range of 0.01 to 0.03 and 0.06 to 0.08 cal/^{o}C sec cm^2, respectively, for both the liquid (superheated 100^{o}C) and semi-solid (volume fraction solid ~0.5) bronze charge, Figures 31 to 33. The variation in the values of h_I and h_f between the castings produced with the all liquid and semi-solid charge was much more pronounced in the high pressure commercial die casting machine. For fully liquid bronze $h_I = 3.0$, $h_f = 0.04$; for semi-solid bronze $h_I = 0.15$ and $h_f = 0.08$ cal/^{o}C sec cm^2.

Using these values of h provides excellent agreement between the measured and calculated internal die temperatures at short times, $t < 0.2$ seconds, Figures 31 to 33. The discrepancy between measured and calculated die temperature for long times is probably due to limitations of the computer model used.

During the development of the computer model it was assumed that the castings produced contained no porosity. This was not the case particularly when fully liquid metal was die cast, Figure 30. Porosity affects heat flow by reducing both the effective heat of fusion and the effective thermal conductivity of the casting. Also, the casting-die assembly did not constitute an adiabatic system as assumed. Instead, heat loss from the exterior die surface - particularly the side walls - reduces the internal die temperature. Finally, heat flow within the die is not one dimensional as assumed. For example, the thermocouple in the low pressure casting system was located near the corner of the die cavity, thus heat flow from this region of the casting was actually three dimensional. Each of these factors contributes to the reduction of die temperature for long times below that predicted by the computer simulation.

Nevertheless, it is expected that for short times the computer program may be employed successfully to predict the die surface temperature and surface temperature gradient. Computer calculations using heat transfer coefficient values reported above show that when a semi-solid charge material is used both the die surface temperature and temperature gradient are drastically reduced. This was shown to be true in both the low and the high pressure casting machines, with the latter showing a more pronounced effect. For example, in the high pressure commercial die casting machine predicted maximum die surface temperatures for castings made from a fully liquid (superheated 100°C) and semi-solid (volume fraction solid ~0.05) charge materials are 800°C and 315°C, respectively. The corresponding surface temperature gradients are 5640°C/cm and 718°C/cm, respectively.

As pointed out earlier these reductions in die surface temperature and surface temperature gradient should be reflected in improved die life. Though this expectation is supported by earlier work carried out by other investigators (13, 26), it should ultimately be demonstrated experimentally.

VIII. CONCLUSIONS

A. General

1. The advantages of applying the Rheocasting process to machine (die) casting of high temperature alloys was demonstrated. When a partially- solid metal slurry is cast in a die casting machine both die life and quality of the cast part should be improved. Experimental and theoretical heat flow studies showed that a significant lowering of both die surface temperature and surface temperature gradient is achieved by casting a bronze in the semi-solid state. Castings produced from semi-solid charge material had significantly less entrapped air and shrinkage porosity than those produced from a fully liquid charge.

B. Structures of Semi-Solid Slurries

2. A variety of high temperature alloys including copper base alloy 905, cast iron (2.6 wt % C 3.2 wt % Si), 440 and 304 stainless steel, and cobalt-base alloy H.S. 31 can be continuously rheocast in the high temperature slurry producer.

3. The average cooling rates experienced during primary solidification in the mixing chamber is of the order of ~$40^{o}C$/min. The resulting primary solid particles in the slurries of all the alloys studied are in the 100 to 300 micron

size range.

4. The cast iron and 440 stainless steel alloy slurries exhibited a bimodal size distribution of primary solid particles, ~100 and ~200 microns, with little entrapped liquid. The structure of the copper and cobalt base alloy slurries are similar with spheroidal primary solid particles of 150 and 350 microns, respectively.

5. The solid particles formed during primary solidification have essentially flat concentration profiles with abrupt concentration variations at particle boundaries and veins of entrapped liquid.

C. Castings

6. Castings produced in a commercial die casting machine from semi-solid copper-base alloy 905 charge material have significantly less entrapped air and shrinkage porosity than those produced from the fully liquid alloy. The more viscous semi-solid slurry convects less in the shot sleeve and during die filling resulting in reduced air entrapment.

7. The distribution of primary solid particles in all the die castings produced (from the copper-base alloy 905, the cast iron and the 440 stainless steel) was uniform throughout the cross-section of the castings.

D. Die Thermal Analysis

8. Both experimental measurements and computer simulation indicate that during the die casting of semi-solid alloys the die temperatures and temperature gradients are dramatically lower than when fully liquid superheated alloys are cast.

9. In the low pressure laboratory casting machine, measured temperature rise, above the initial die temperature for the all liquid (superheated 100°C) copper-base 905 alloy charge material and the semi-solid charge (volume fraction solid ~0.5) were 150°C versus 90°C, respectively.

10. The initial rate of temperature change with time in the die are significantly larger when an all liquid charge is used. For example, in the high pressure commercial die casting machine values of 2.5×10^4 °C/sec and 8×10^3 °C/sec were obtained for a superheated liquid copper-base alloy 905 and the 0.5 volume fraction solid charge materials, respectively.

11. Correlation of experimentally measured die temperatures with computer simulation enabled prediction of the value of the surface heat transfer coefficient. An abrupt change in the surface heat transfer coefficient occurs at approximately the same time that the die cavity is completely filled.

12. In the low pressure (laboratory) casting apparatus the calculated initial and final heat transfer coefficients were in the range of 0. 1 to 0.30 and 0.06 to 0.08 cal/°C sec cm^2, respectively, for both the liquid and semi-solid charge copper-base alloy 905.

13. In the high pressure commercial die casting machine initial and final heat transfer coefficients for the superheated (100°C) copper-base 905 alloy were 3.0 and 0.04 cal/°C sec cm^2, respectively. The corresponding values for the semi-solid (volume fraction solid ~0.5) were 0.15 and 0.08 cal/°C sec cm^2, respectively.

14. Computer calculations show that when a semi-solid charge material of copper-base alloy 905 is used both die surface temperature and temperature gradient are drastically reduced. In the high pressure commercial die casting machine the predicted maximum die surface temperatures are 800°C and 315°C, respectively. The corresponding surface temperature gradients are 5640°C/cm and 718°C/cm, respectively.

IX. SUGGESTIONS FOR FUTURE WORK

1. A comprehensive model of heat and fluid flow should be developed for the continuous rheocaster. This model should be tested experimentally. It can subsequently be used in design modifications needed for more efficient operation of the rheocaster.
2. The continuous rheocaster should be further developed and mechanized to produce semi-solid slurries with predictable structures and controlled volume fraction solid.
3. The solid front fill condition observed during mold filling of viscous semi-solid slurries should be fully exploited. Conditions (flow velocity, size, geometry and location of the gates, etc.) leading to this type of die filling should be developed via a comprehensive program using transparent dies and high speed motion pictures.
4. Further study is needed to determine minimum section thickness through which a slurry can flow without segregation of the solid and the liquid. The flow behavior of semi-solid slurries through complex geometries, with abrupt cross-sectional changes, should also be studied.
5. The thixocast reheating furnace and the transfer mechanism should be automated such that semi-solid charge material of desired viscosity is consistently injected into the shot sleeve. The constant load piercing device being developed is a step in this direction.

6. The die casting machine should be equipped with visicorder devices to permit measurement of displacement, velocity, and pressure during casting. This will permit a better correlation of casting conditions to casting quality.

7. A more comprehensive model of heat flow during solidification of the metal in the die should be developed. This model should be tested experimentally using temperature measurement techniques developed in this study.

8. The homogenization heat treatment response of rheocast structures should be studied using microprobe techniques presented in this study.

9. A coherent program should be undertaken to determine the mechanical properties of rheocast alloys. These properties should be compared to conventionally all liquid, cast specimens.

10. A comprehensive study should be undertaken to determine the economic feasibility of machine casting high temperature alloys. The fabrication costs should be based on expected die lives and compared to competitive alternate manufacturing techniques.

11. Finally, the casting system described should be automated and developed to a commercial scale operation. The technical predictions of improved die life and its effect on economic factors involved can only be proven out in the competitive environment of the marketplace.

REFERENCES

1. Nyhat Kinikoglu, MIT Solidification Group, unpublished work.

2. P.A. Joly, R. Mehrabian, "Rheology of Metals", to be published.

3. D.B. Spencer, R. Mehrabian, M.C. Flemings, "Rheological Behavior of Sn-15%Pb in the Crystallization Range", Met. Trans., Vol. 3, 1972, pp. 1925-1932.

4. R. Mehrabian, M.C. Flemings, "Die Casting of Partially Solidified Alloys", Trans. AFS, Vol. 80, 1972, pp. 173-182. (Also, Die Casting Engineer, July-August 1973, pp. 49-59).

5. M.C. Flemings, R. Mehrabian, "Casting Semi-Solid Metals", Transactions, International Foundry Congress, Moscow, 1973, AFS Trans., Vol. 81, pp. 81-88.

6. E.F. Fascetta, R.G. Riek, R. Mehrabian, M.C. Flemings, "Die Casting Partially Solidified High Copper Content Alloys", Die Casting Engineer, Spet.-Oct. 1973, pp. 44-45. (Also, AFS Cast Metals Research Journal, Vol. 9, No. 4, Dec. 1973, pp. 167-171).

7. R.G. Riek, A. Vrachnos, K.P. Young, N. Matsumoto, R. Mehrabian, "Machine Casting of a Partially Solidified High Copper Content Alloy", Trans. AFS, Vol. , 1975, p. 25.

8. M.C. Flemings et al., "Machine Casting of Ferrous Alloys", Interim Technical Report, ARPA Contract DAAG46-C-0110,

1 January - 30 December 1973, prepared for Army Materials and Mechanics Research Center, Watertown, Mass.

9. M.C. Flemings et al., "Machine Casting of Ferrous Alloys", Interim Technical Report, ARPA Contract DAAG46-73-C-0110, 1 January - 30 June 1974, prepared for Army Materials & Mechanics Research Center, Watertown, Mass.

10. R. G. Riek et al., "Machine Casting of Ferrous Alloys", to be published.

11. C. Schwartz, "Mathematics of Solidification Processes in the Casting of Metals", Zeitschrift fur angewandte Mathematik und Mechanik, Vol. 13, 1933, p. 202.

12. H. Carslaw and J. Jaeger, Conduction of Heat in Solids, Oxford University Press, Oxford, 2nd Edition, 1960.

13. S.J. Noesen and H.A. Williams, "The Thermal Fatigue of Die Casting Dies", Transactions, Society of Die Casting Engineers, 1966, paper 801.

14. C.M. Adams, Jr., "Thermal Considerations in Freezing", Liquid Metals and Solidification, ASM, Cleveland, 1958.

15. C.C. Reynolds, Solidification in Die and Permanent Mold Castings, Ph.D. Thesis, Departmetn of Metallurgy, Massachusetts Institute of Technology, 1963.

16. P. Thukkaram, "Heat Transfer in Die Casting Dies", paper no. 61, Transactions, Sixth S.D.C.E. Die Casting Congress, Cleveland, Ohio, 1970.

26. J.M. Samuels, A.B. Draper, "An Analysis of Thermally Induced Stresses in Die Casting Dies", paper no. G-T75-052, Transactions, 8th S.D.C.E. Congress, Detroit, Michigan, 1975.

27. G.W. Scholl, "Hybrid Computer Simulation of Transient Heat Transfer in Die Casting", S.M. Thesis, Department of Industrial Engineering, Pennsylvania State University, 1973.

28. D. Ragone, C.M. Adams, H.F. Taylor, "Some Factors Affecting Fluidity of Metals", Transactions AFS, Vol. 67, 1959, 640-652.

29. M.C. Flemings et al., "Fluidity of Aluminum Alloys", Transactions AFS, Vol 69, 1961, 625-635.

30. L.F. Coffin, Jr., Trans. ASME, Vol. 76, p. 923, 1954.

31. H.B. Elman et al., "Comparative Evaluation of Die Materials for Bras Die Casting", paper no. 803, Transactions, Society of Die Casting Engineers, 1966.

32. J.C. Benedyk, D.J. Moracz and J.F. Wallace, "Thermal Fatigue Behavior of Die Materials for Aluminum Die Casting", paper no. 111, Transactions, Society of Die Casting Engineers, 1970.

33. A. Kasak, G. Steven, "Microstructural Considerations in Heat Checking of Die Steels", paper no. 112, Transactions, 6th S.D.C.E. Congress, Cleveland, Ohio, 1970.

34. W.R. Wollering and L.C. Oertle, "Thermal Fatigue as a Cause of Die Failure", Transactions, Society of Die Casting Engineers, 1966, Vol. 4, paper no. 804.

17. C.W. Nelson, "A Study of Die Casting Water Line Variables", paper no. 53, Transactions, Fifth S.D.C.E. Die Casting Congress, Detroit, Michigan, 1968.

18. D. Lindsay and J.F. Wallace, "Heat and Fluid Flow in the Die Casting Process", paper no. 12, Transactions, Fifth S.D.C.E. Die Casting Congress, Detroit, Michigan, 1968.

19. C.W. Nelson, "Nature of Heat Transfer at the Die Face", paper no. 63, Transactions, Sixth S.D.C.E. Die Casting Congress, Cleveland, Ohio, 1970.

20. G.M. Dusinberre, "Heat Transfer Calculations by Finite Differences", 2nd Edition, International Textbook, Scranton, Penna., 1961.

21. E.R.G. Eckert and R.M. Drake, Jr., Analysis of Heat and Mass Transfer, McGraw-Hill, New York, 1972.

22. A.J. Campagna, Ph.D. Thesis, Department of Metallurgy, Massachusetts Institute of Technology, 1970.

23. M. Basaran, Ph.D. Thesis, Department of Metallurgy, Massachusetts Institute of Technology, 1974.

24. W.D. Murry and F. Landis, "Numerical and Machine Solutions of Transient Heat Conduction Problems Involving Melting and Freezing", Transactions ASME, Vol. 81, May 1959.

25. W.D. Kaiser et al., "A Computer Model for Studying Transient Heat Transfer Conditions During Die Filling", paper no. 5472, Transactions, 7th S.D.C.E. Congress, Chicago, Illinois, 1972.

35. M. Suzuki, "Residual Stress and Heat Checking in Die Casting Dies", paper no. 6472, Transactions, S.D.C.E. Detroit, Michigan, 1972.

36. J.M. Samuels and A.B. Draper, "Mechanisms of Initial Die Failure When Poured with Stainless Steel", Transactions, Society of Die Casting Engineers, 1972, paper 6572.

37. A.B. Draper, J.M. Samuels, "Ablative Coatings and Die Materials for Ferrous Die Casting", Transactions, S.D.C.E. Congress, paper no. G-775-152, Detroit, Michigan, 1975.

TABLE I

Life of Core and Die Materials(31)

Cast Metal: Brass

Cerro Core Study	TZM 6800	Mallory 3950 3855	Gyromet 1100 3600	Mar M 200 2881	
Cerro Die Study	TZM (as cast) 27,000	TZM (nitrided) 18,000	TZM (sol. treated) 15,000	H-20 12,000	
American Standard Die Study	TZM 33,757	Mo (Sintered) 28,000	Mallory 3950 20,000	Inconel 713 10,000	H-13 6,000

Compositions

TZM	Mo - 0.8%Zr - 0.46%Ti
Mallory 3950	W - 3.5%Ni - 1.5%Fe
Gyromet 1100	W - 4%Ni - 8%Co - 4.5%Mo - 0.3%C
Mar M 200	Fe - 18%Ni - 8%Co - 4.5%Mo - 0.3%C
H 20	Fe - 9%W - 2%Cr - 0.35%C
H 13	Fe - 5%Cr - 1.35%Mo - 1.0%V - 1.0%Si - 0.3%Mn - 0.4%C
Inconel 713	Ni - 13%Cr - 6%Al - 4%Mo - 2%Cb - 0.5%Ti

TABLE II

Number of Cycles for Crack Initiation(32)
Water Cooled Specimen Dipped into Aluminum

H-13	H-19	TZM	Alloy #25	Maraging (250)
5000	4000	no cracks	no cracks	1200-1800

TABLE III

Summary of Microprobe Results

Alloy	Solute Concentration Within Primary Solid Particle	Solute Concentration of Entrapped Liquid	Solute Concentration of Quenched Liquid
Bronze 905	2.25 wt% Sn	16.60 wt% Sn	16.88 wt% Sn
440C Stainless Steel	19.0 wt% Cr 0.56 wt% Mn 0.23 wt% Mo 0.12 wt% Si	none	~27.5 wt% Cr ~o.7 wt% Mn ~0.4 wt% Mo ~0.12 wt% Si

TABLE IV

Casting Conditions for Castings No. 72- No. 89

Casting Number	Ingot Number	Ingot Reheat Temp. (°C)	Die Temp. (°C)	Intensifier Position	Speed Valve Position
72	10-3	1086	186	off	3 turns
73	10-3	1096	178	off	3 turns
74	10-4	1101	175	off	3 turns
75	10-7	1099	158	on-1800psi	3 turns
76	10-8	1096	153	on-1800psi	3 turns
77	10-27	971	152	on-1800psi	3 turns
78	10-28	971	158	on-1800psi	3 turns
79	10-28	971	161	on-1800psi	3 turns
80	10-29	969	155	on-1800psi	3 turns
81	9-4	960	157	on-1800psi	3 turns
82	10-20	1096	156	on-1800psi	3 turns
83	10-1	960	164	on-1800psi	3 turns
84	10-16	960	153	on-1800psi	3 turns
85	10-16	960	143	on-1800psi	3 turns
86	10-20	1096	135	on-1800psi	3 turns
87	11-1	1095	153	on-1800psi	3 turns
88	10-23	960	153	on-1800psi	3 turns
89	10-23	960	151	on-1800psi	3 turns

TABLE V

Composition of High Melting Temperature Alloys Used in This Investigation

Copper Base Alloy 905	88%Cu - 10%Sn - 2%Zn
Eutectic Cast Iron	Fe - 2.6%C - 3.2%Si
440C Stainless Steel	Fe - 17%Cr - 1%Si - 1%Mn - 1%C
304 Stainless Steel	Fe - 19%Cr - 9%Ni - 0.08%C
HS 31 Cobalt base Superalloy	Co - 25.5%Cr - 11%Ni - 7.5%W - 0.5%C
M-2 Tool Steel	Fe - 6.25%W - 5%Mo - 4%Cr - 2%V - 0.85%C

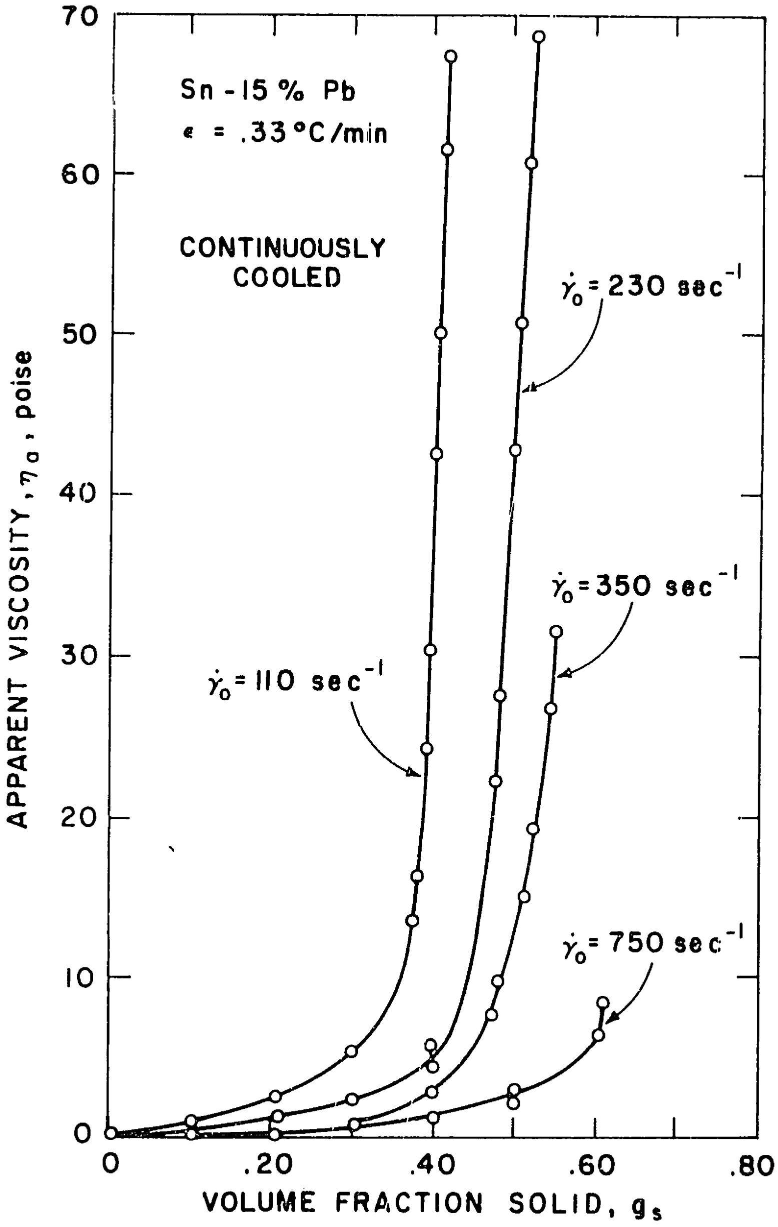

Figure 1. Measured apparent viscosity versus volume fraction solid of four Sn-15%Pb alloy samples sheared continuously and cooled from above the liquidus temperature at a constant cooling rate of $\varepsilon = 0.33\ ^{\circ}C$/min.

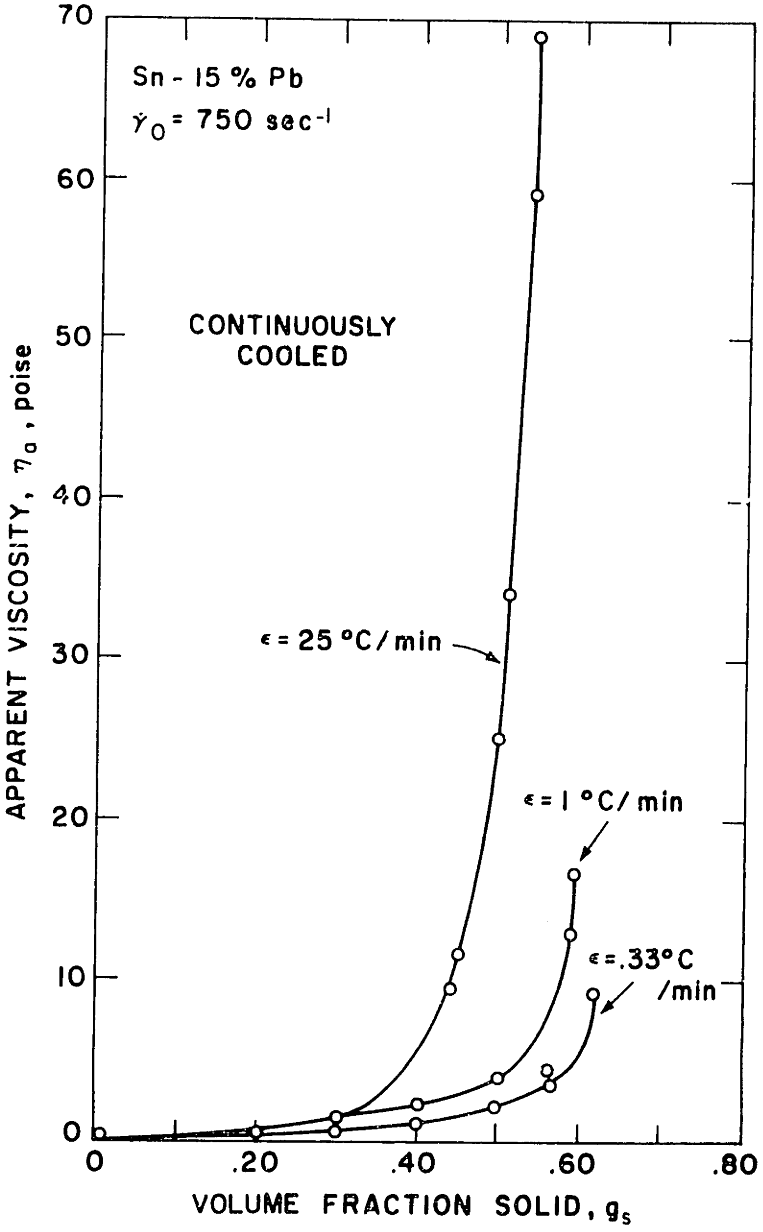

Figure 2. Measured apparent viscosity versus volume fraction solid of three Sn-15%Pb samples sheared continuously at a rate of $\dot{\gamma}$ = 750 sec^{-1} and cooled from above the liquidus temperature at constant cooling rates.

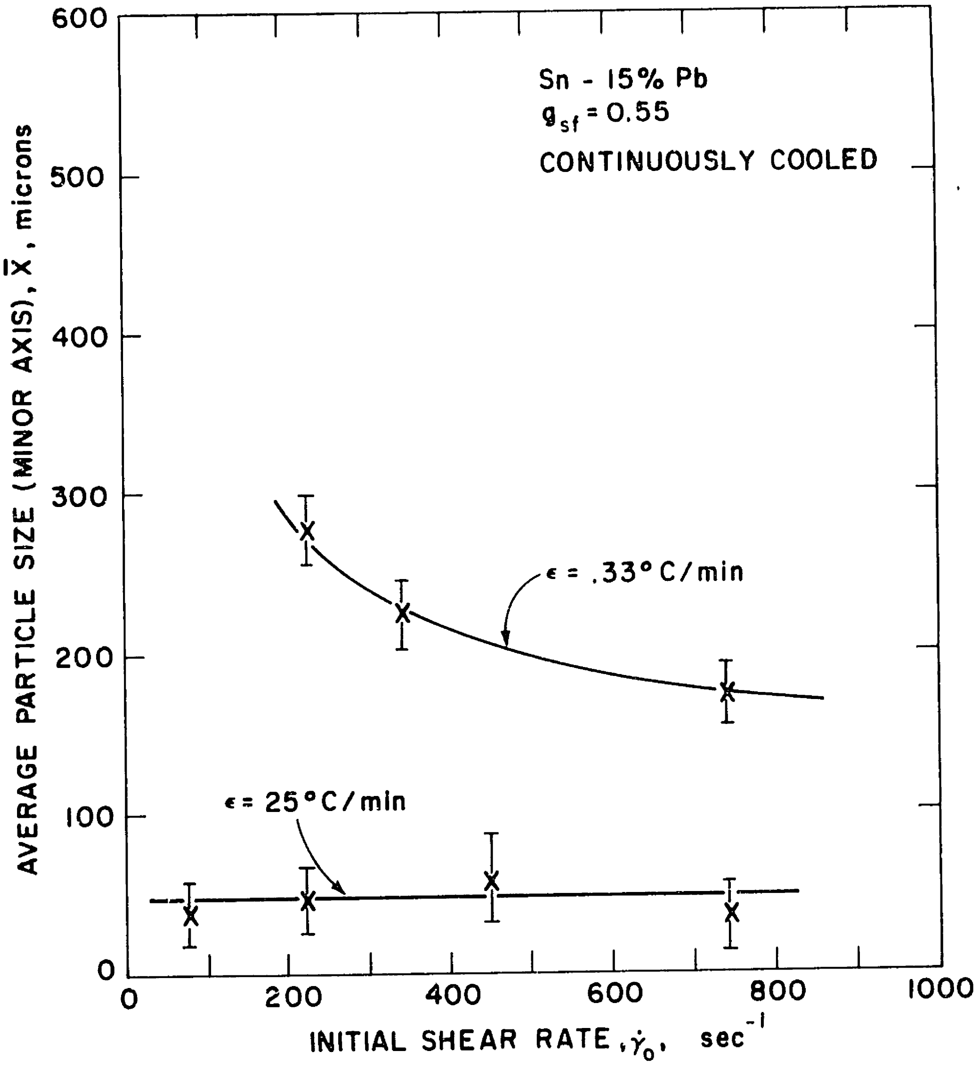

Figure 3. Average size of primary solid particles versus shear rate in Sn-15%Pb alloy samples sheared continuously and cooled from above the liquidus at constant cooling rates.

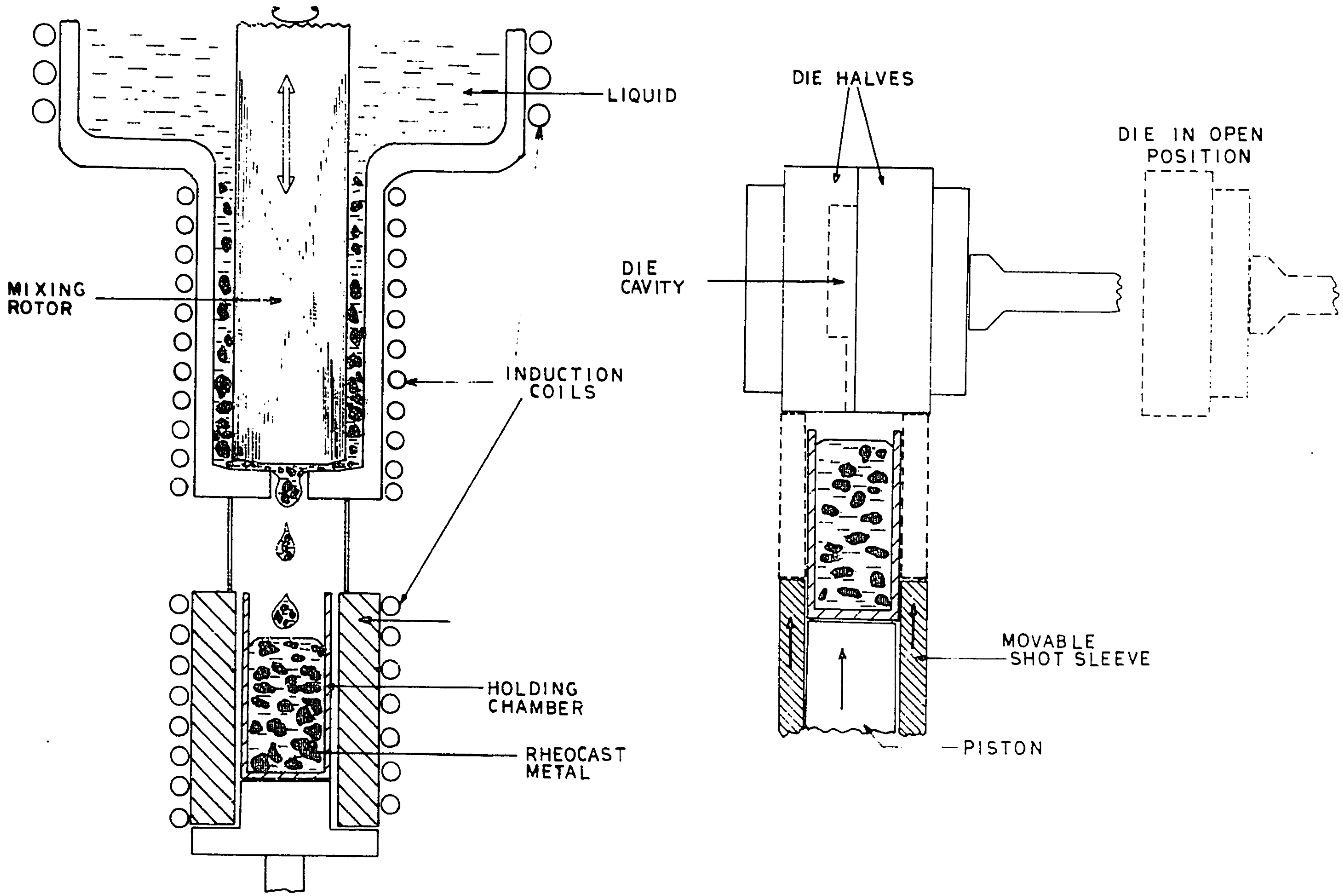
LIQUID
MIXING ROTOR
INDUCTION COILS
HOLDING CHAMBER
RHEOCAST METAL
DIE HALVES
DIE IN OPEN POSITION
DIE CAVITY
MOVABLE SHOT SLEEVE
PISTON

Figure 4. Schematic of the low pressure casting system showing the continuous slurry producer, the collection chamber, and the casting machine.

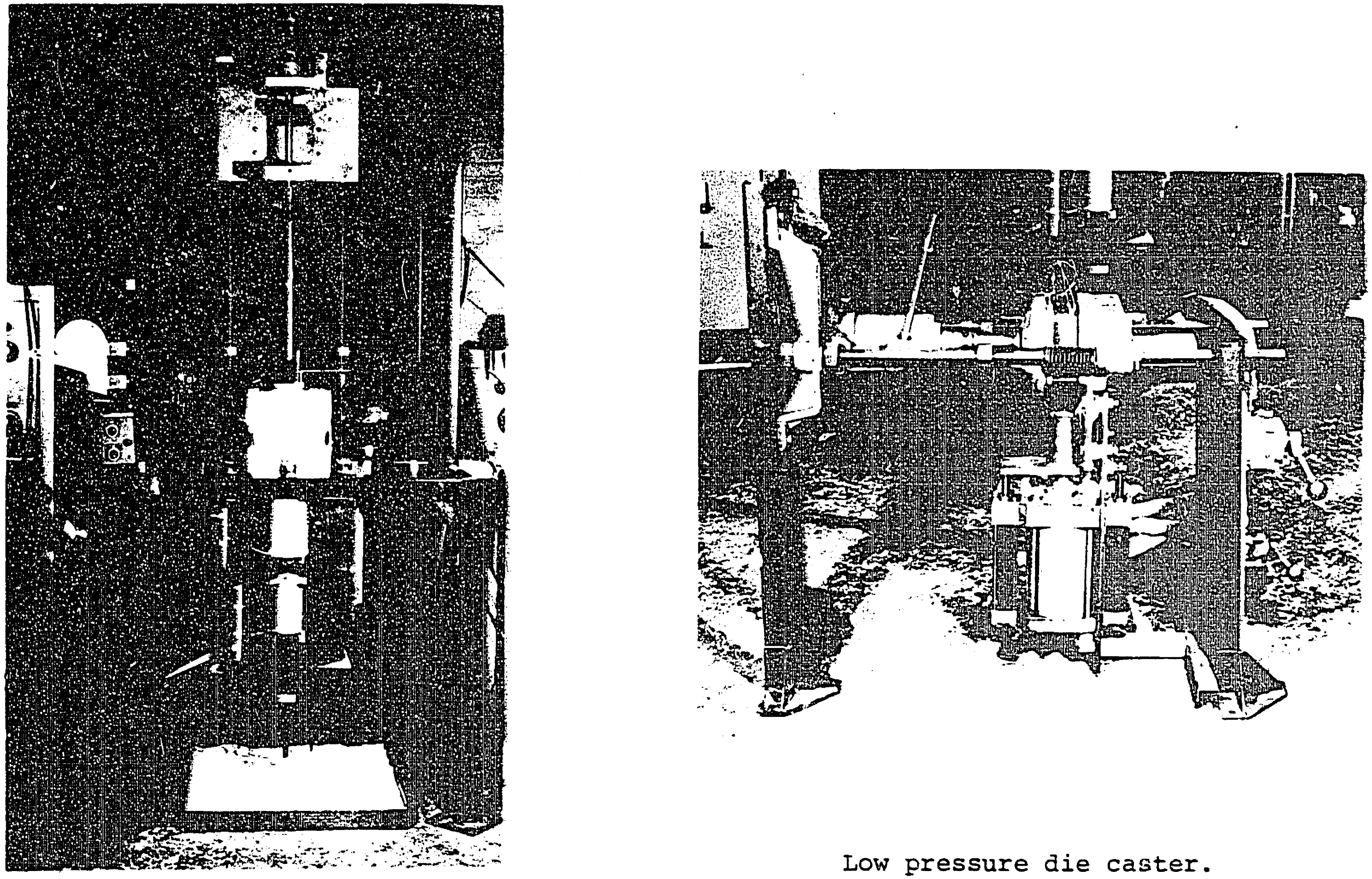

Continuous semi-solid slurry producer and collection chamber beneath.

Low pressure die caster.

Figure 5. Photograph of the low pressure casting system for high temperature alloys.

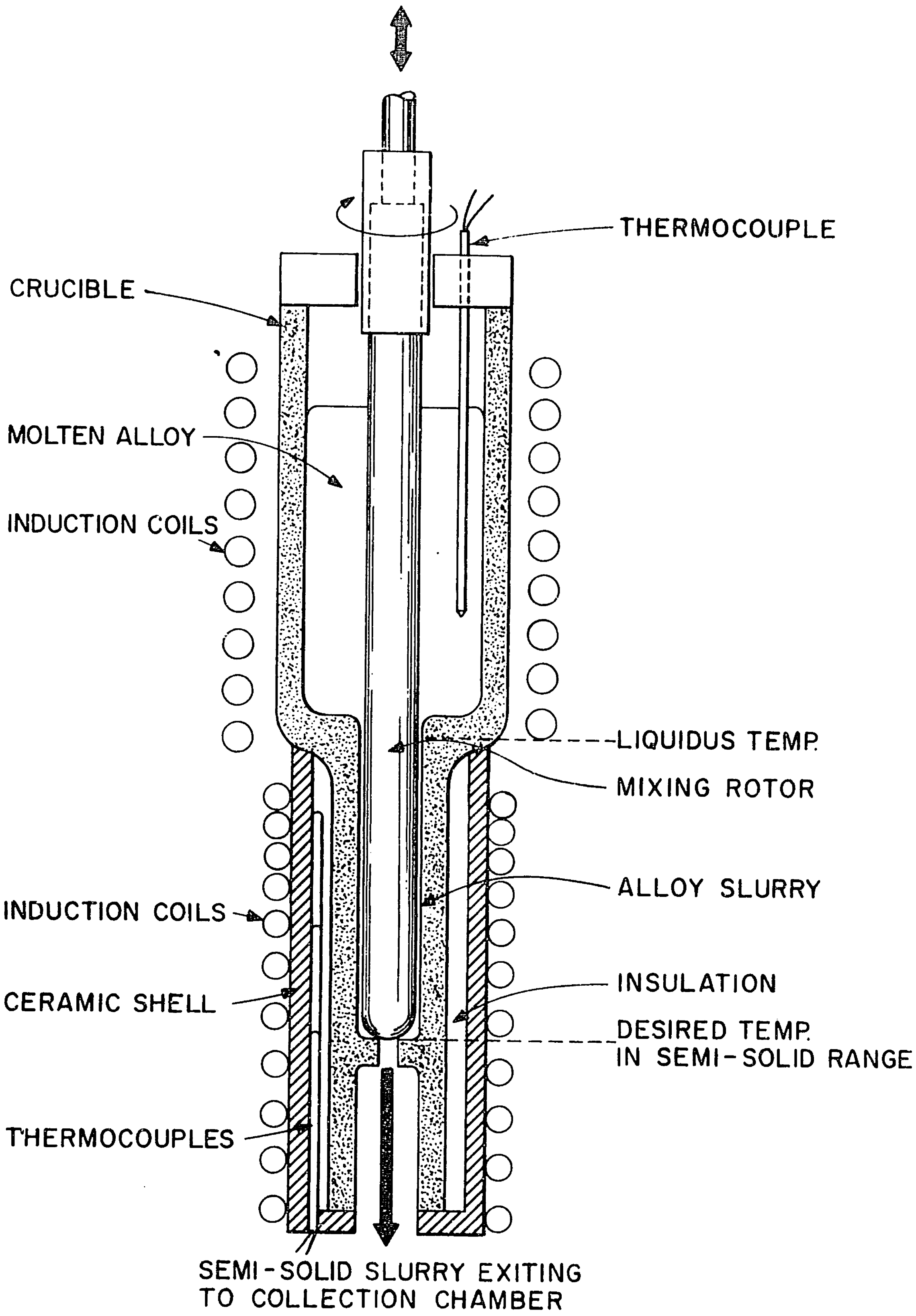
THERMOCOUPLE
CRUCIBLE
MOLTEN ALLOY
INDUCTION COILS
LIQUIDUS TEMP.
MIXING ROTOR
ALLOY SLURRY
INDUCTION COILS
INSULATION
CERAMIC SHELL
DESIRED TEMP.
IN SEMI-SOLID RANGE
THERMOCOUPLES
SEMI-SOLID SLURRY EXITING
TO COLLECTION CHAMBER

Figure 6. Schematic of the apparatus for producing partially solid slurries of high temperature alloys.

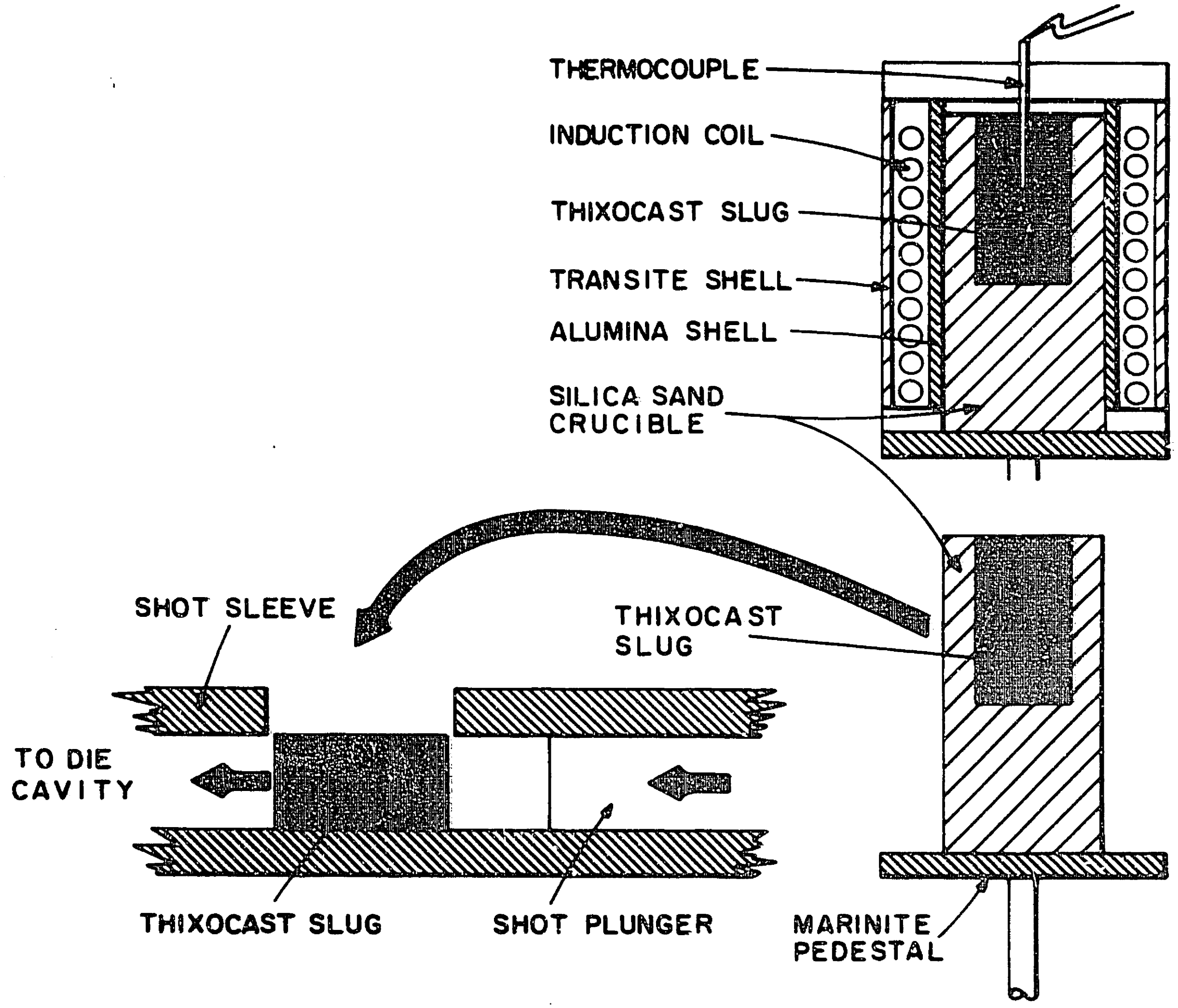
THERMOCOUPLE
INDUCTION COIL
THIXOCAST SLUG
TRANSITE SHELL
ALUMINA SHELL
SILICA SAND CRUCIBLE
THIXOCAST SLUG
MARINITE PEDESTAL
SHOT SLEEVE
TO DIE CAVITY
THIXOCAST SLUG
SHOT PLUNGER

Figure 7. Schematic of the high pressure casting system including the reheat furnace and the shot chamber.

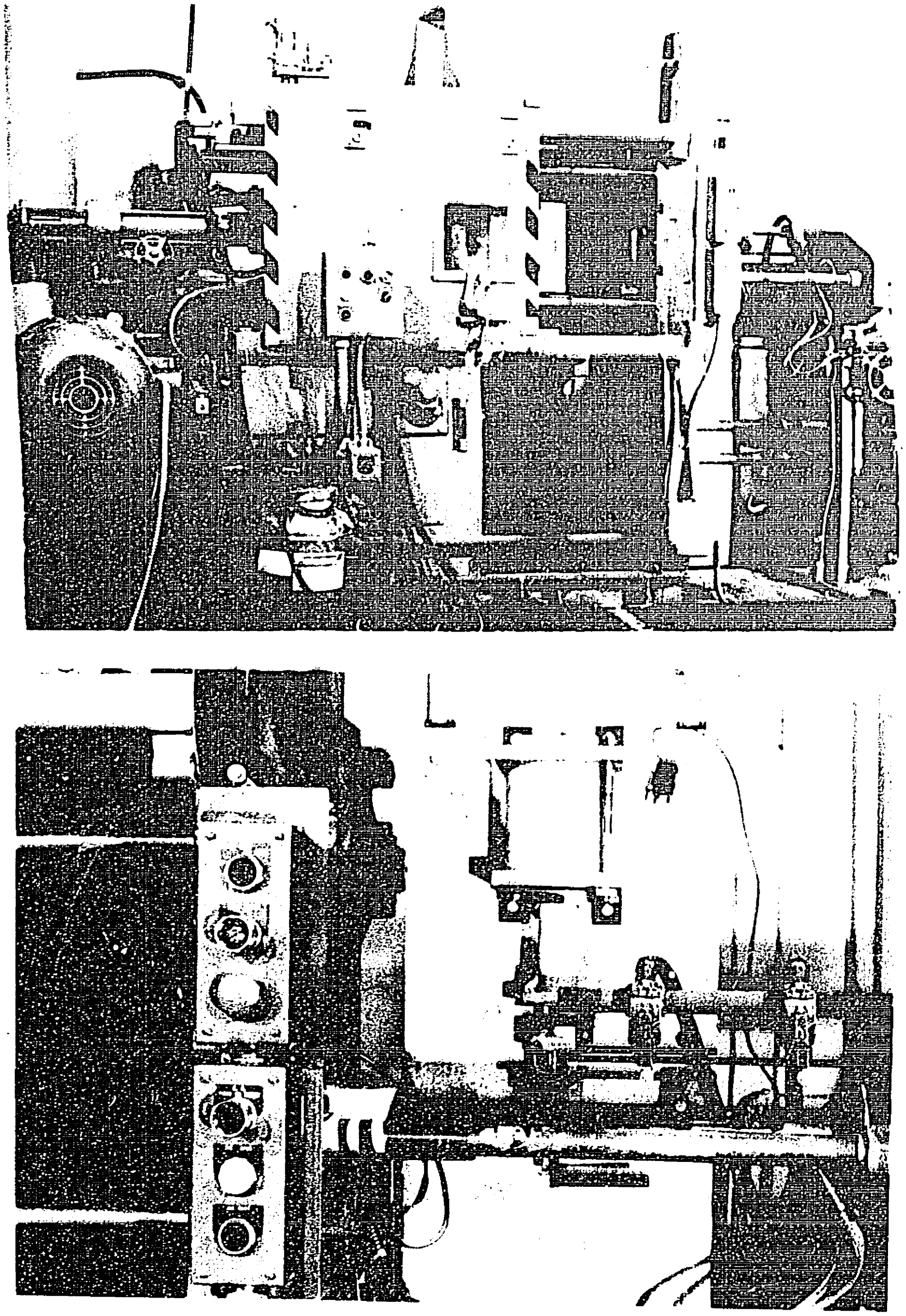

Figure 8. Photograph of the high pressure casting system. Top: overall view of B&T die casting machine. Bottom: close view of shot chamber and reheat furnace.

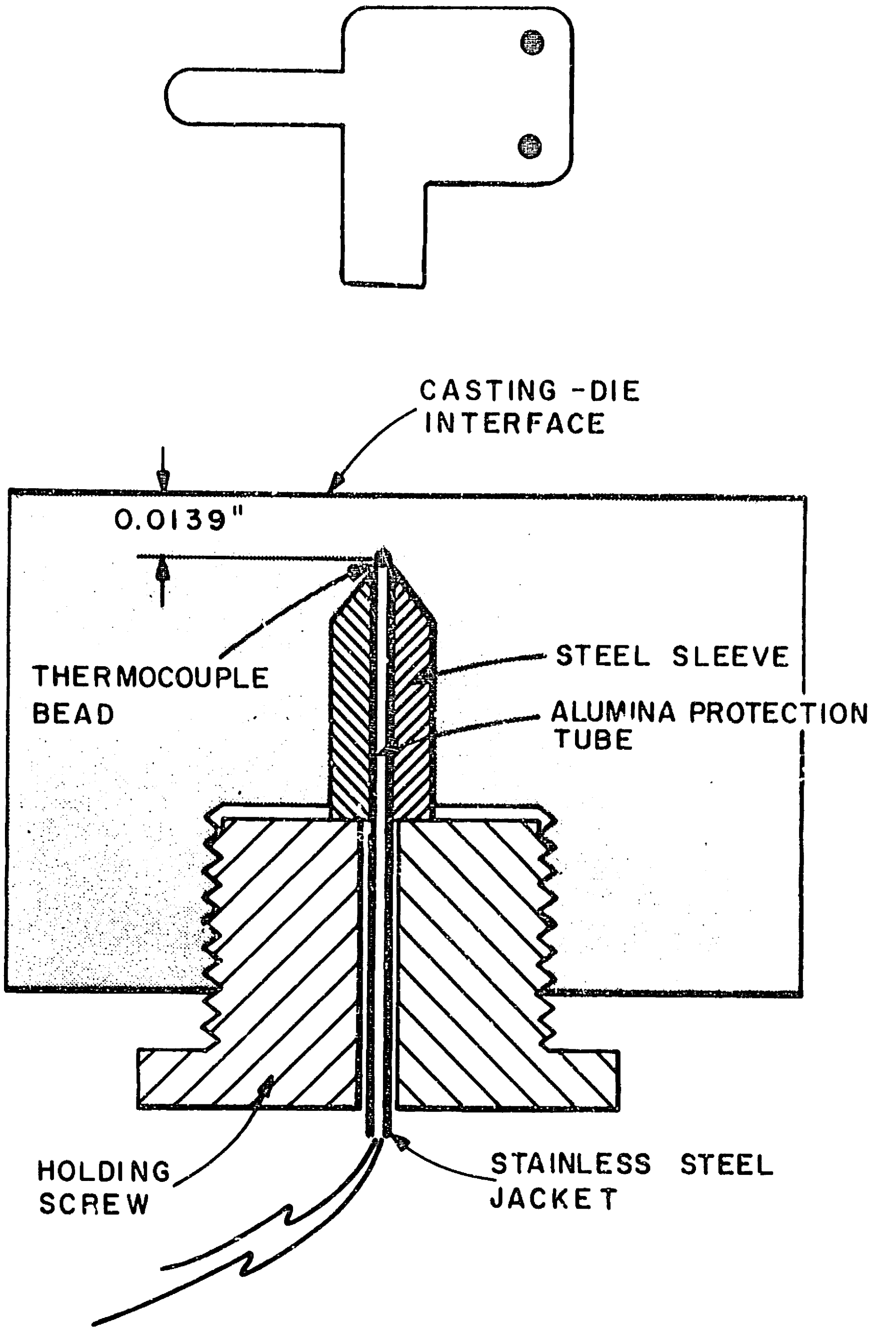
CASTING -DIE INTERFACE
0.0139"
THERMOCOUPLE BEAD
STEEL SLEEVE
ALUMINA PROTECTION TUBE
HOLDING SCREW
STAINLESS STEEL JACKET

Figure 9. Schematic of thermocouple assembly in the low pressure die casting machine. Figure on top shows position of the thermocouple in the die cavity.

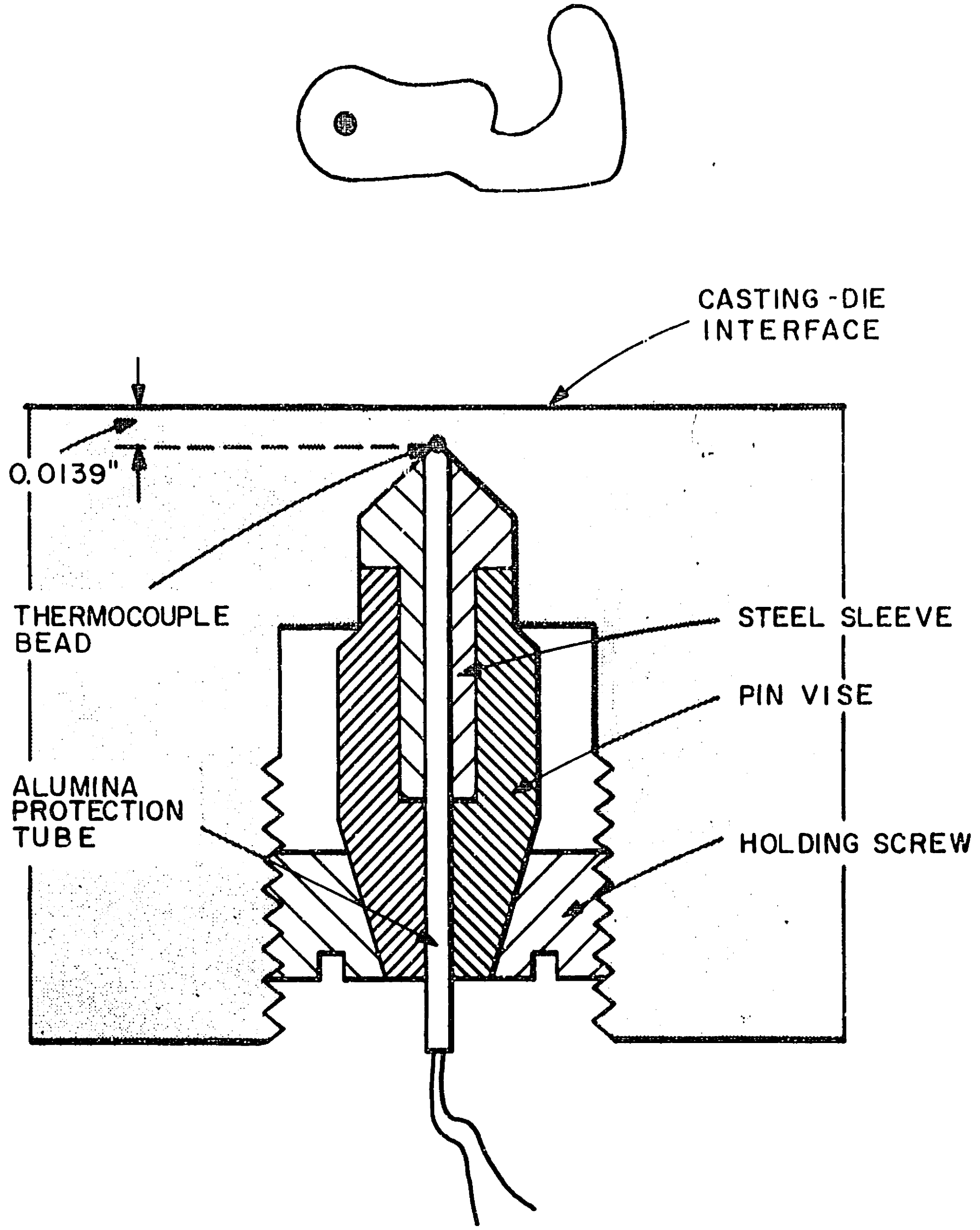
CASTING-DIE INTERFACE
0.0139"
THERMOCOUPLE BEAD
STEEL SLEEVE
PIN VISE
ALUMINA PROTECTION TUBE
HOLDING SCREW

Figure 10. Schematic of thermocouple assembly in the high pressure die casting machine. Figure on top shows position of the thermocouple in the die cavity.

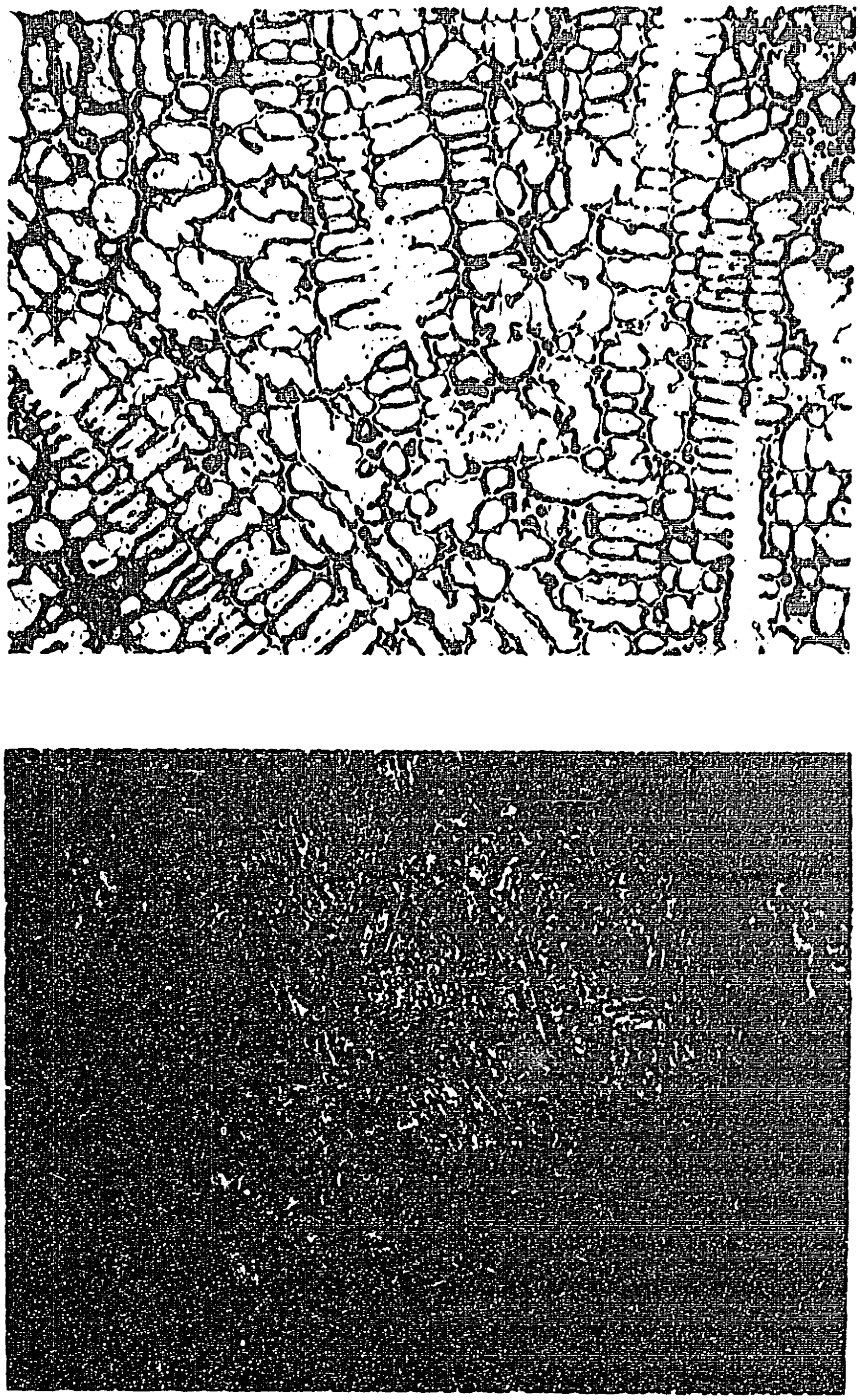

Figure 11. Microstructures of conventionally solidified 440C stainless steel alloy. Top: slow furnace cooled ingot, 50X. Bottom: rapidly cooled, water quenched sample, 50X. Cupric Chloride etch.

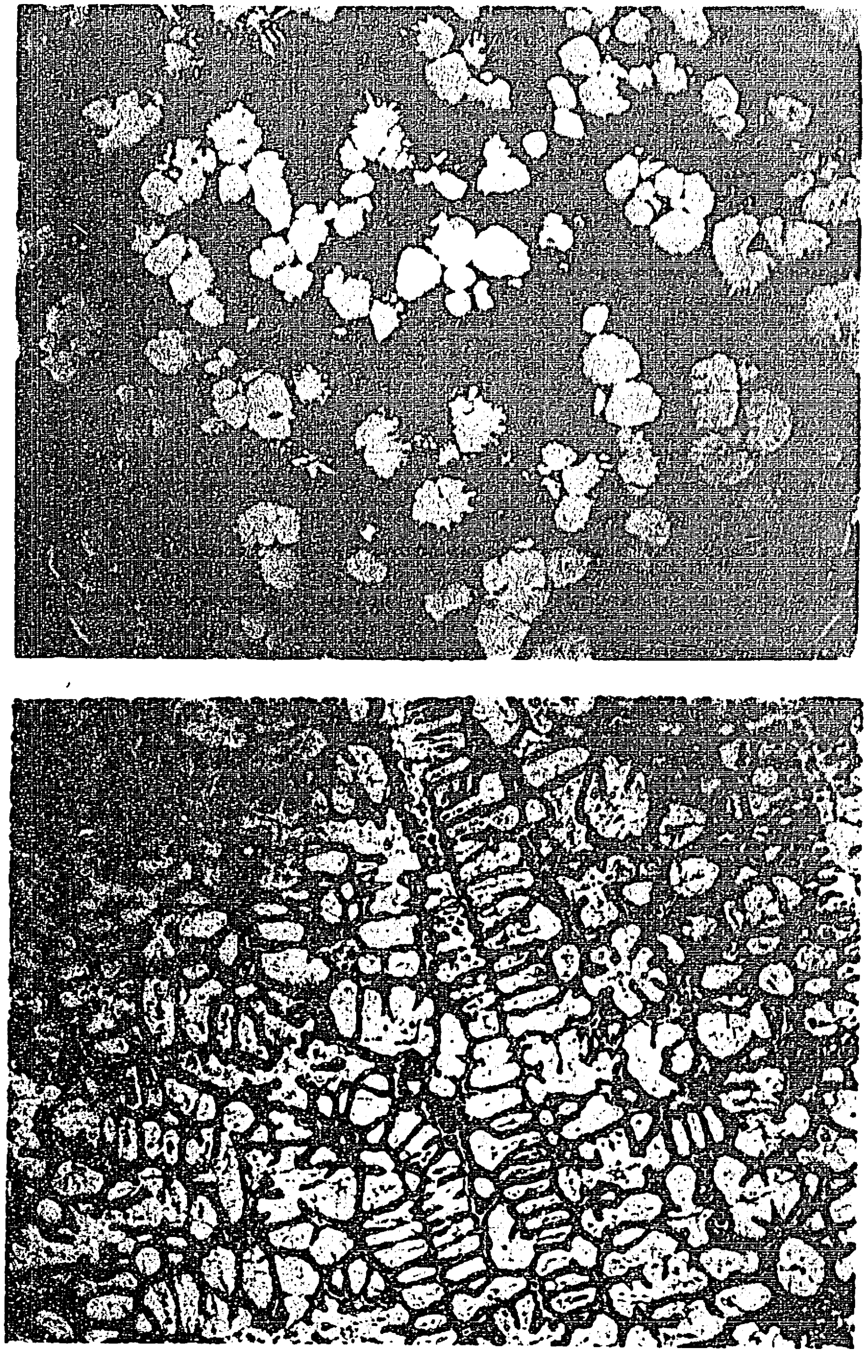

Figure 12. Comparison of microstructures for Rheocast and conventionally cast 440A stainless steel alloy. Top: Rheocast water quenched droplet, 50X. Bottom: conventional slowly cooled liquid ingot, 50X. Cupric Chloride etch.

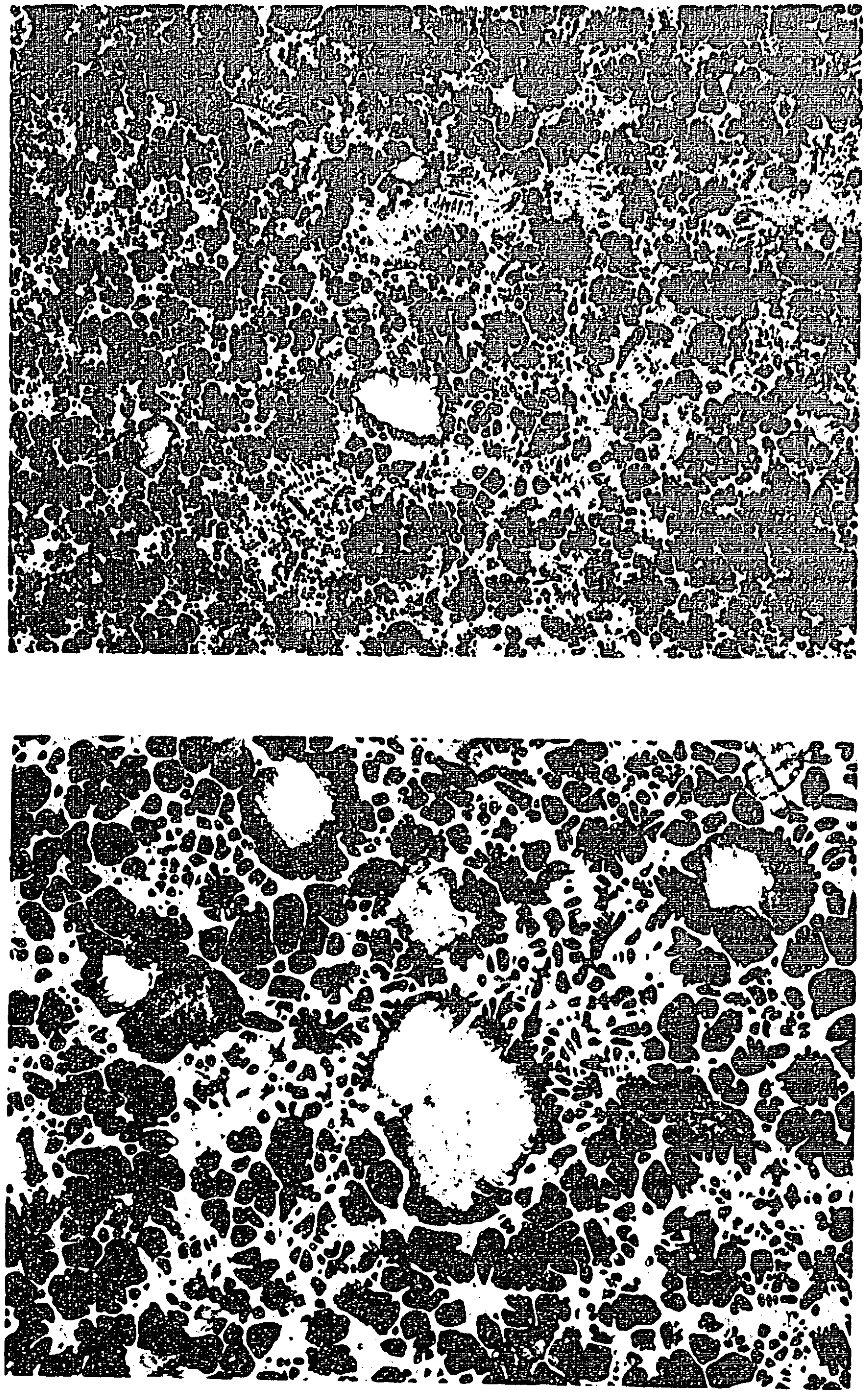

Figure 13. Microstructure of a water quenched semi-solid 440C stainless steel sample made in the high temperature slurry producer. Top: 50X. Bottom: 100X. Cupric Chloride etch.

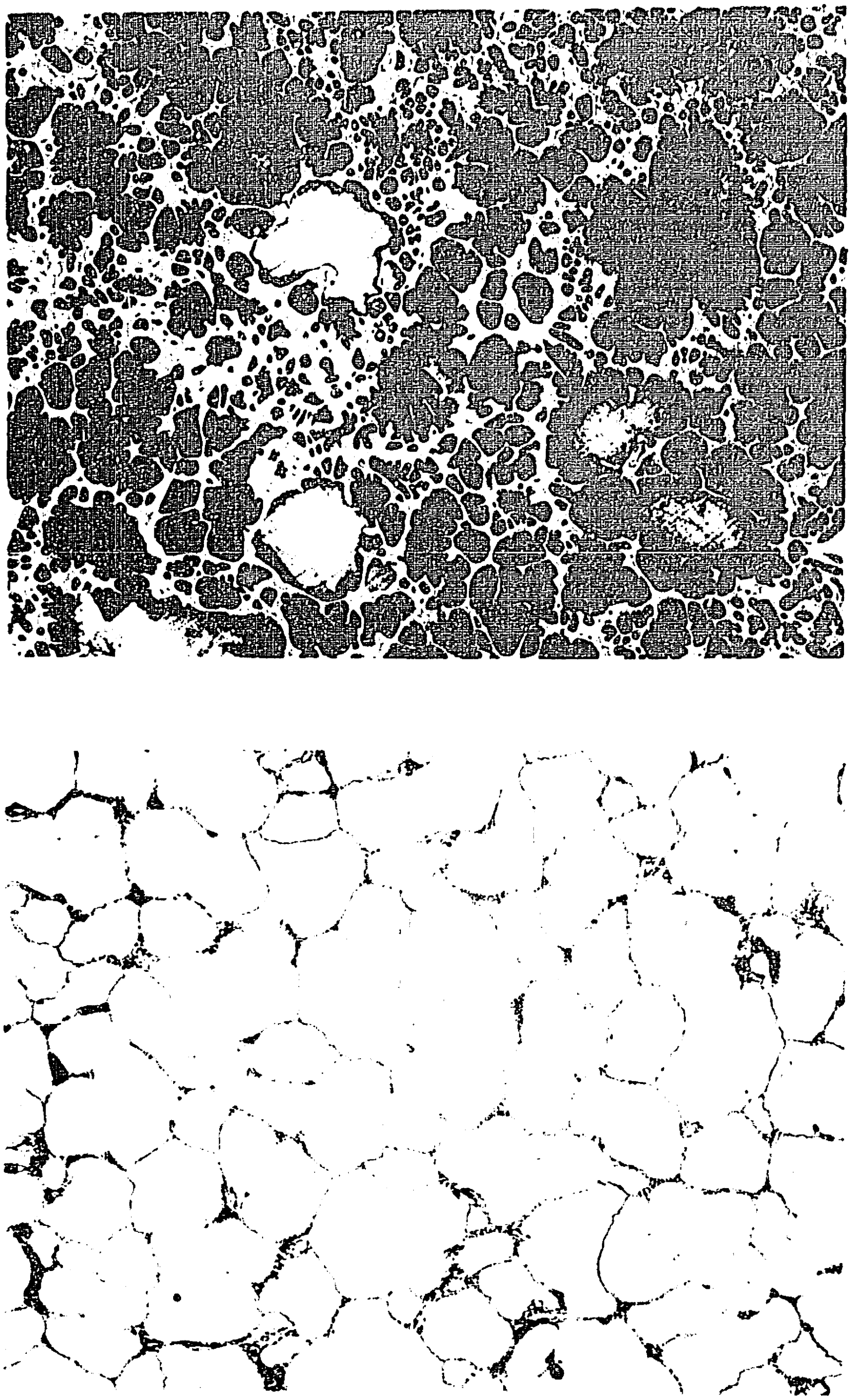

Figure 14. Microstructures of continuously produced semi-solid 440C stainless steel alloy slurries. Top: rapidly cooled, water quenched sample. Bottom: slowly cooled ingot, 100X.

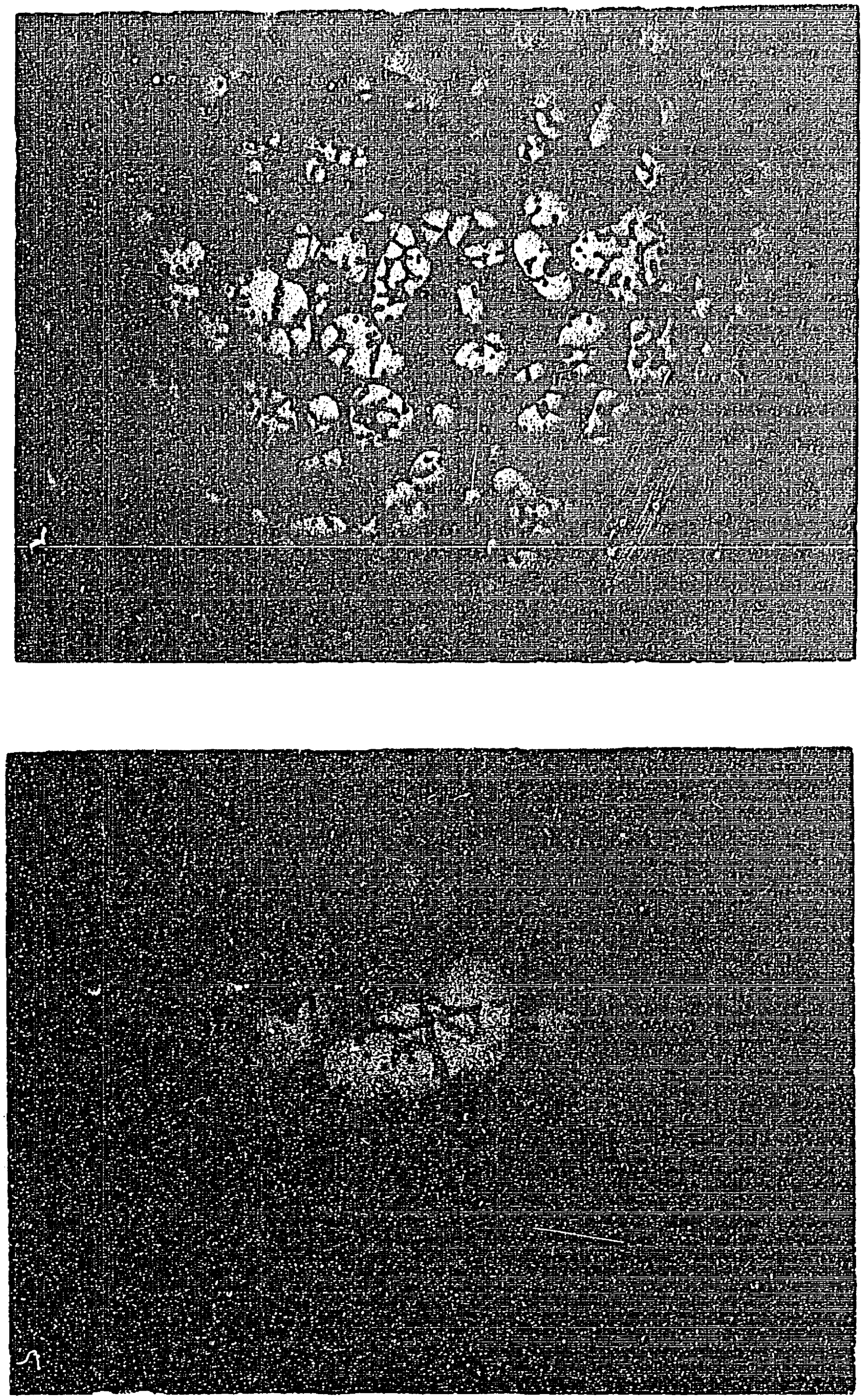

Figure 15. Microstructure of continuously produced semi-solid copper base alloy 905, 88%Cu-10%Sn-2%Zn. Samples were directly water quenched. Top: 50X. Bottom: 100X.

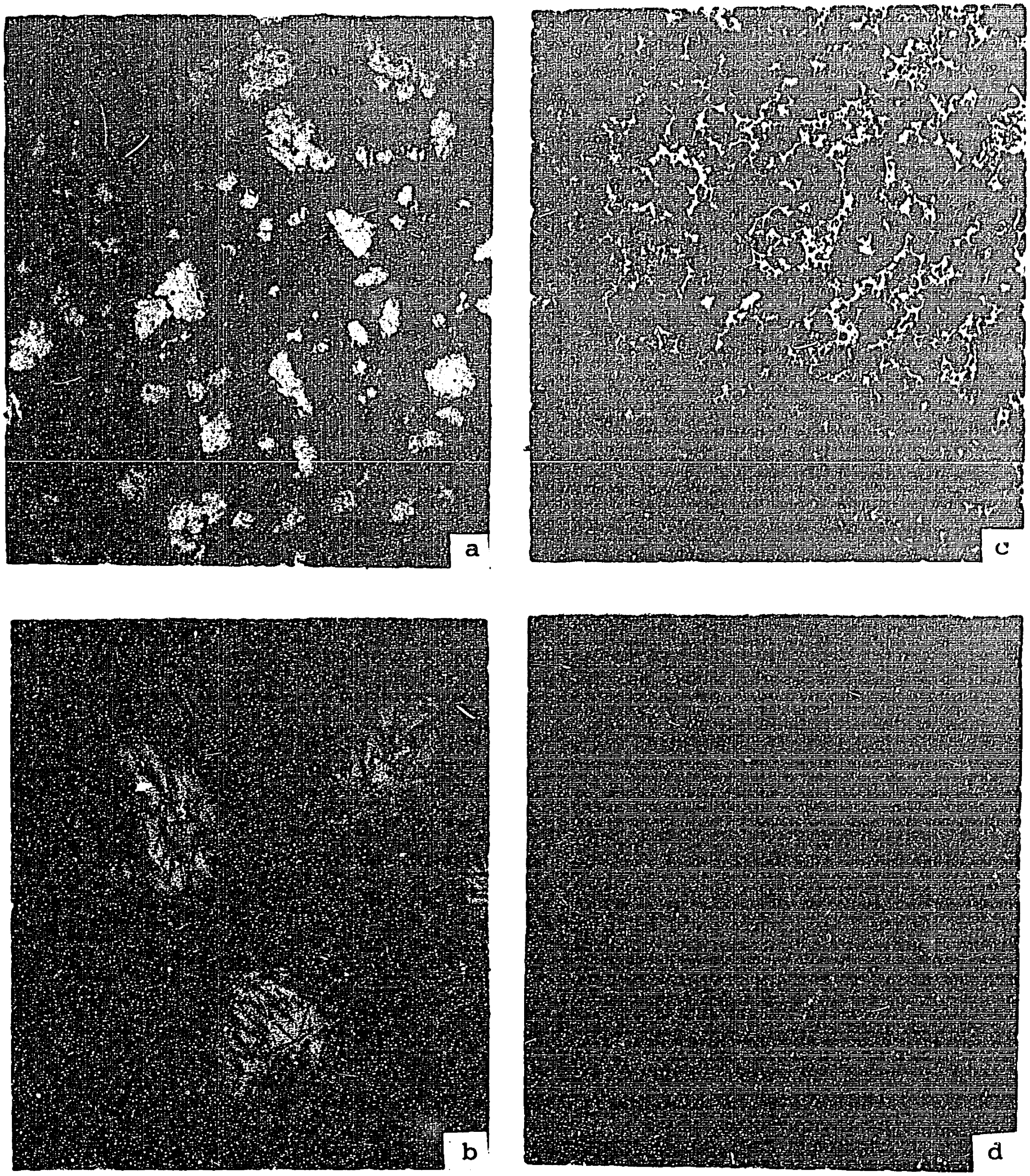

Figure 16. Microstructure of continuously produced semi-solid eutectic cast iron, Fe-2.6%C-3.2%Si. Samples were directly water quenched. (a) and (b) structure showing martensite plates in primary solid particles, 50X, 200X; (c) and (d) structures showing cementite plates, 50X, 100X.

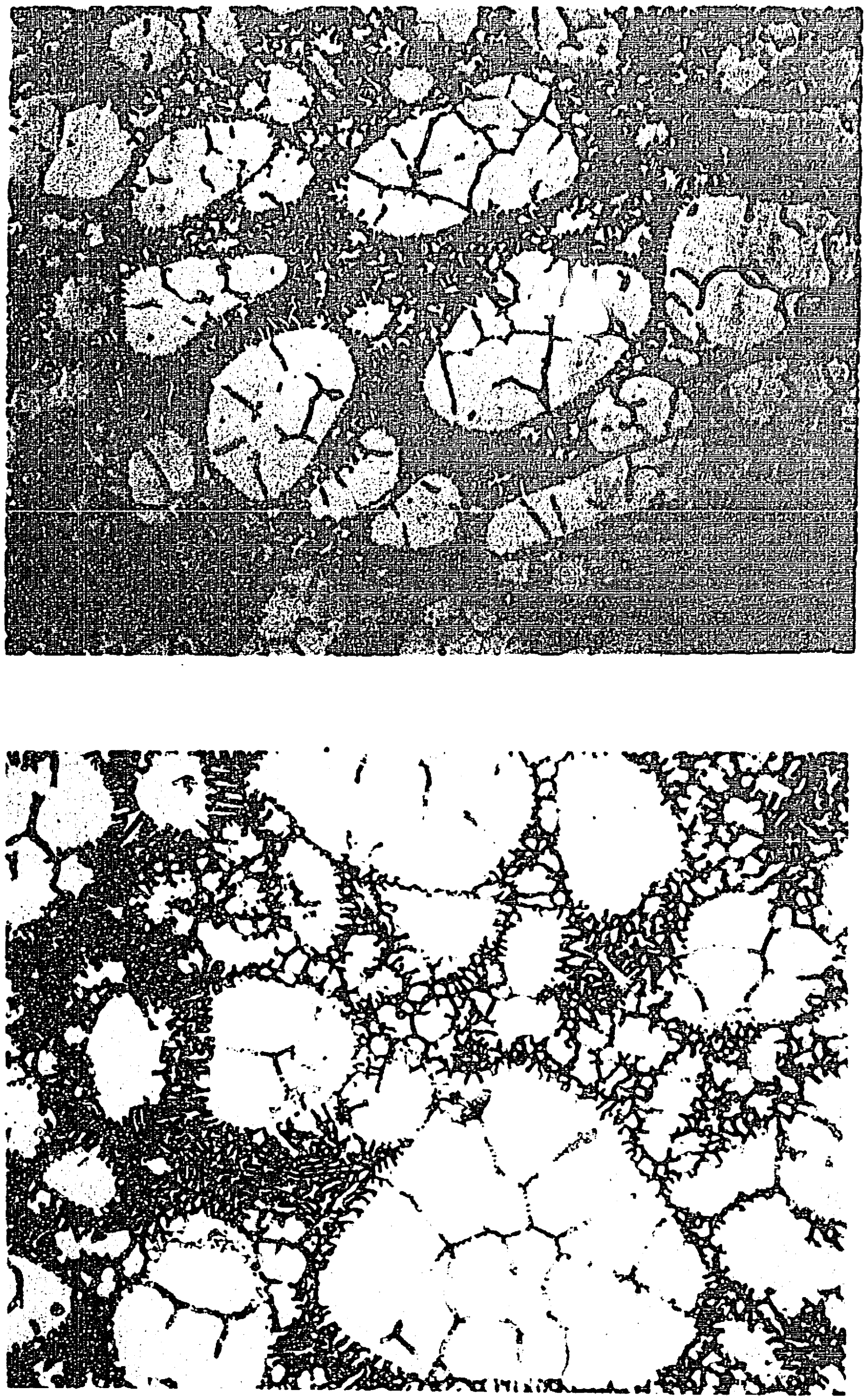

Figure 17. Microstructures of continuously produced semi-solid HS-31 superalloy. Samples were directly water quenched. Top, 50X; Bottom, 100X.

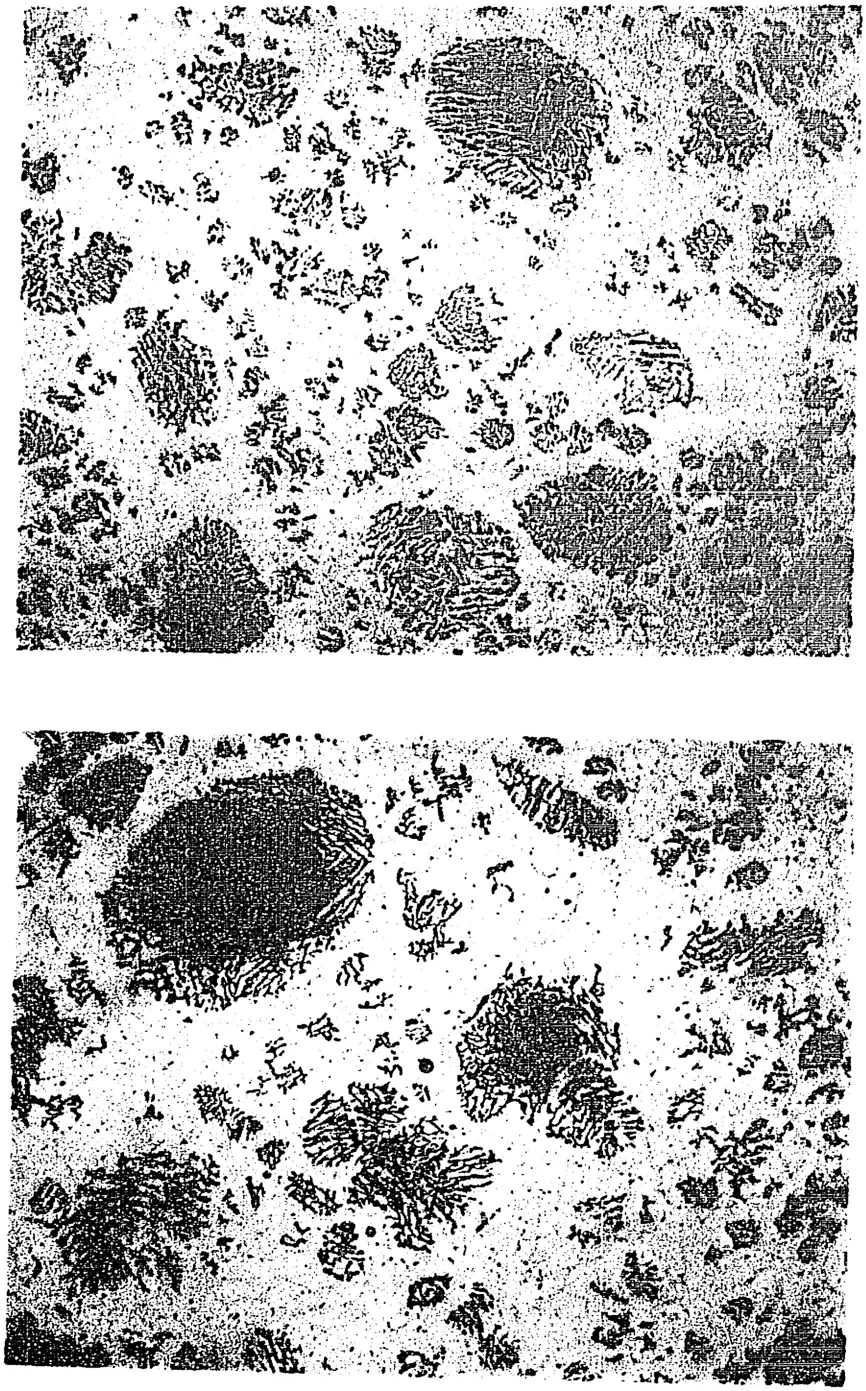

Figure 18. Microstructures of continuously produced semi-solid 304 stainless steel. Samples were directly water quenched. Top, 50X; Bottom, 100X.

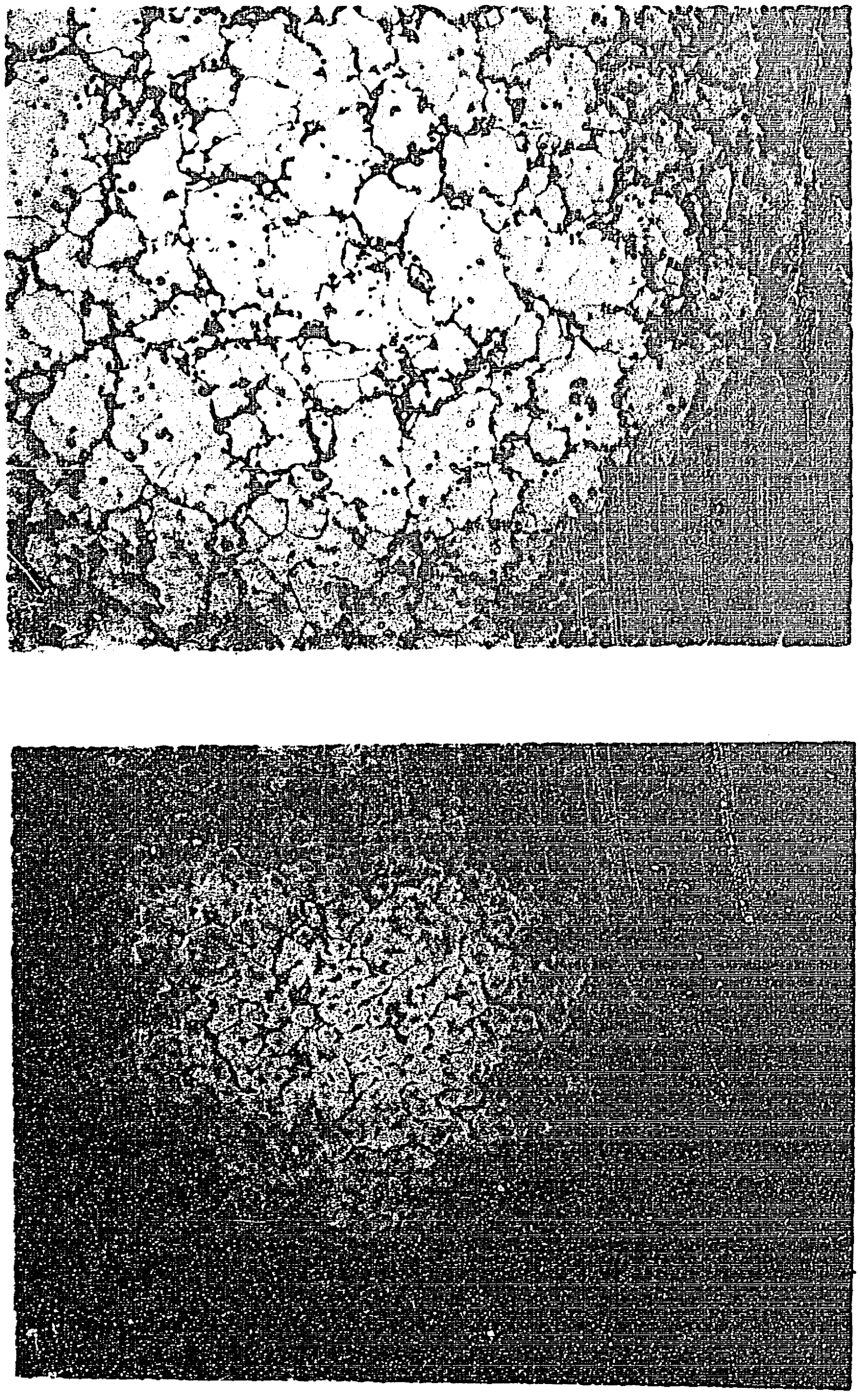

Figure 19. Microstructures of continuously produced semi-solid alloy. Samples were slowly cooled. Top: microstructure of HS 31 superalloy. Bottom: microstructure of M-2 tool steel. 50X.

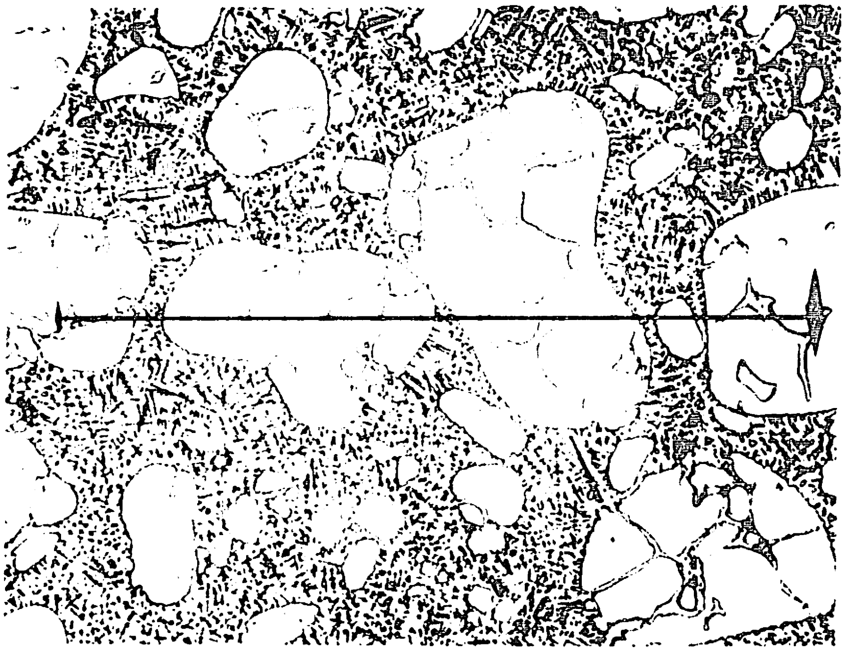

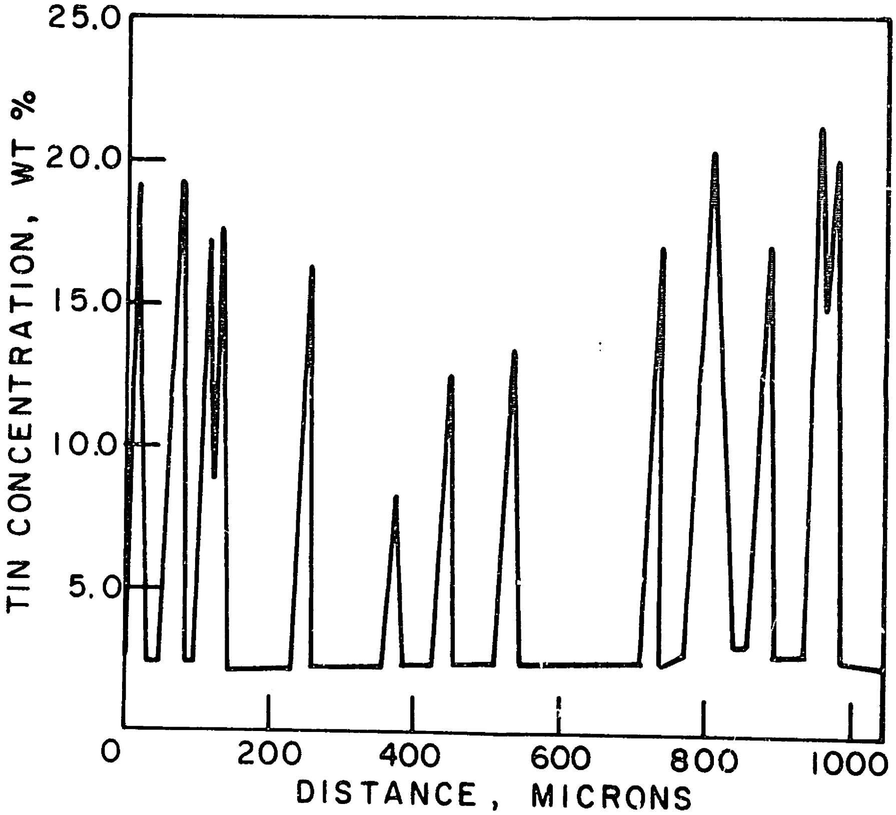

Figure 20. Microprobe data showing composition variation in semi-solid copper base alloy 905, 88%Cu-10%Sn-2%Zn. Sample was directly water quenched. The black line represents the path of the microprobe beam.

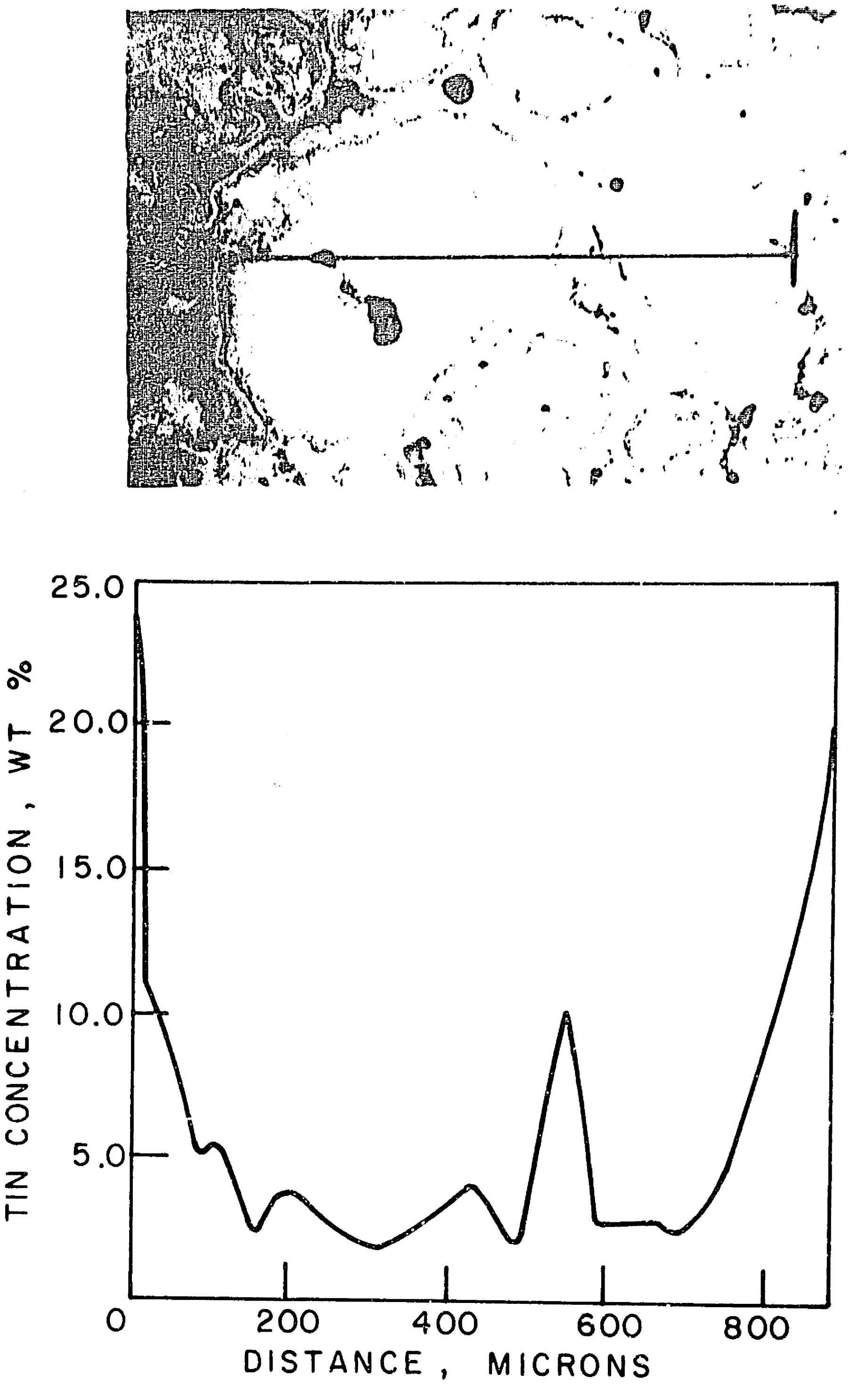

Figure 21. Microprobe data showing composition variation in semi-solid copper base alloy 905, 88%Cu-10%Sn-2%Zn. Sample was slowly cooled. The black line represents the path of the microprobe beam.

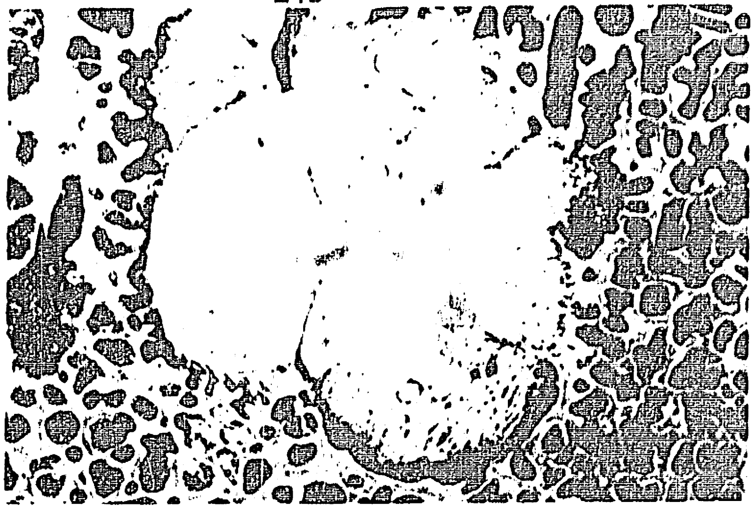

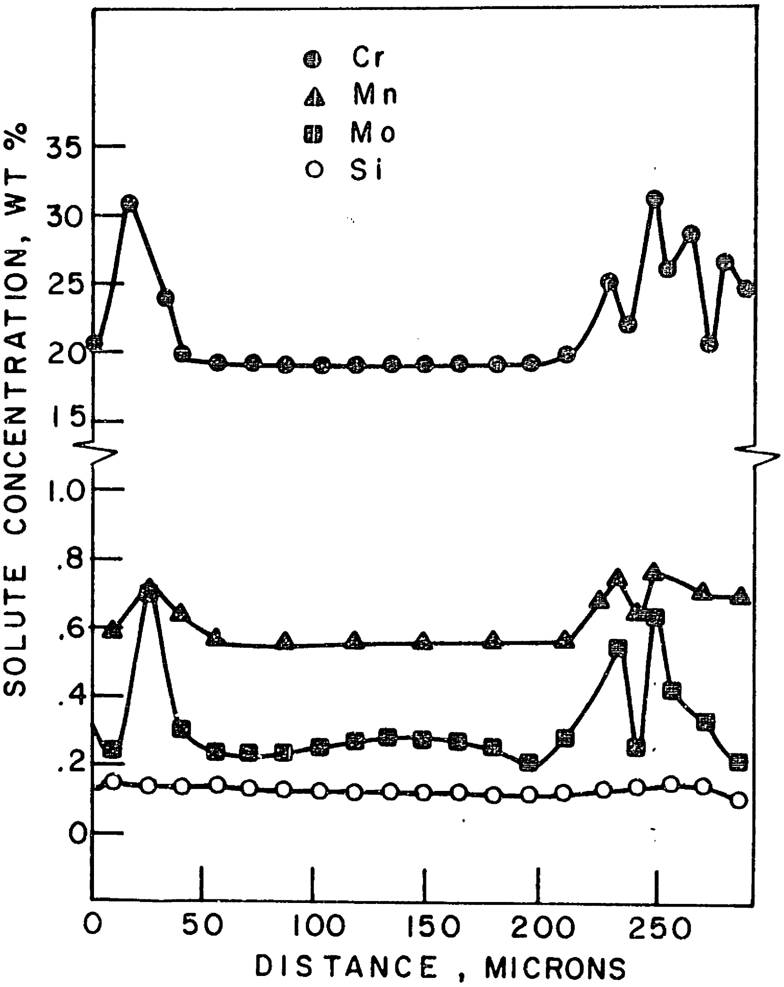

Figure 22. Microprobe data showing composition variation in semi-solid 440C stainless steel. Sample was directly water quenched. The black line represents the path of the microprobe beam.

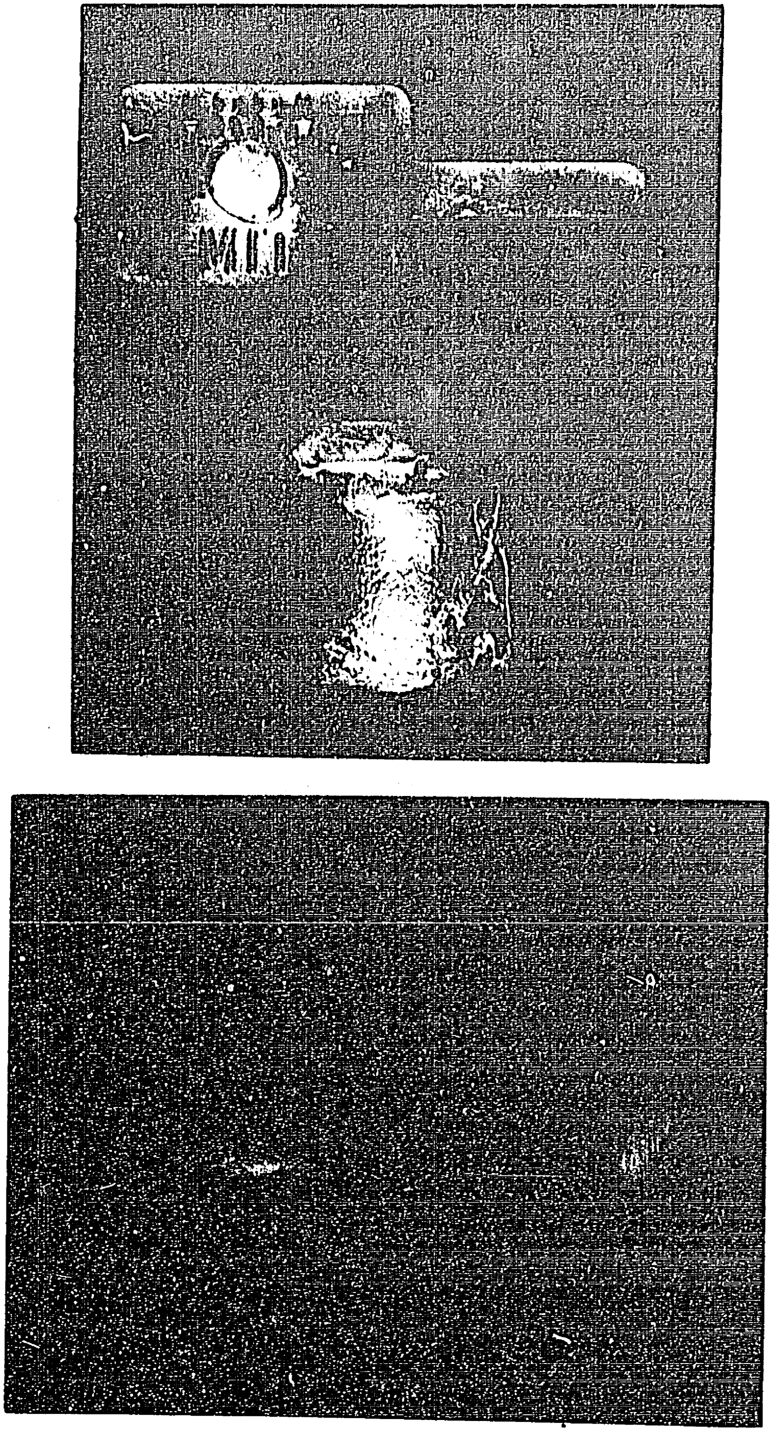

Figure 23. Castings produced in the low and high pressure casting systems. Top: 440C stainless steel casting produced in the low pressure casting machine, 1X. Bottom: copper base alloy 905, 88%Cu-10%Sn-2%Zn, casting produced in the high pressure die casting machine, ~2X.

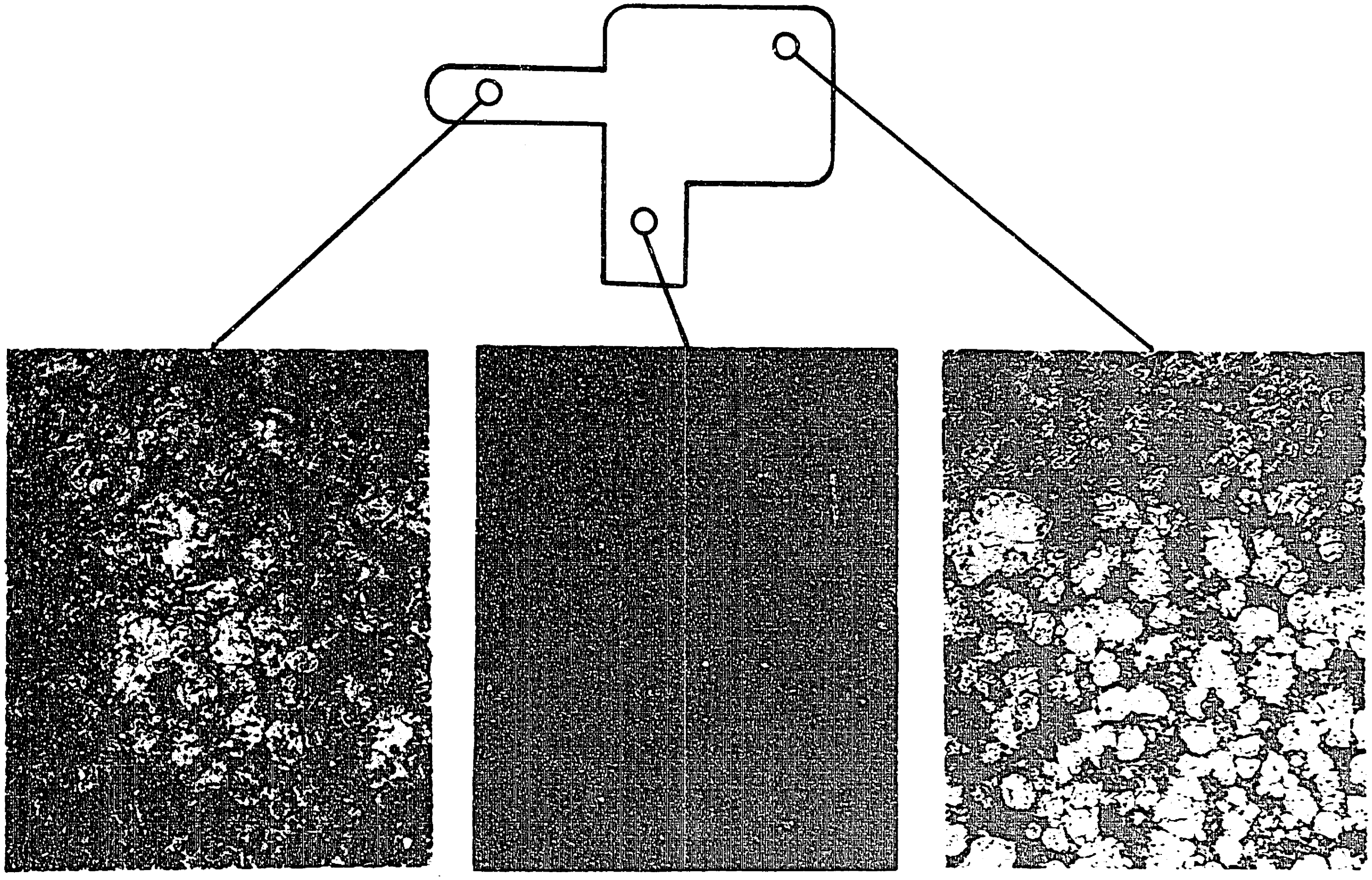

Figure 24. Photomicrographs showing homogeneous distribution of primary solid particles in various regions of a eutectic cast iron, Fe-2.6%C-3.2%Si, casting produced in the low pressure casting machine, 50X.

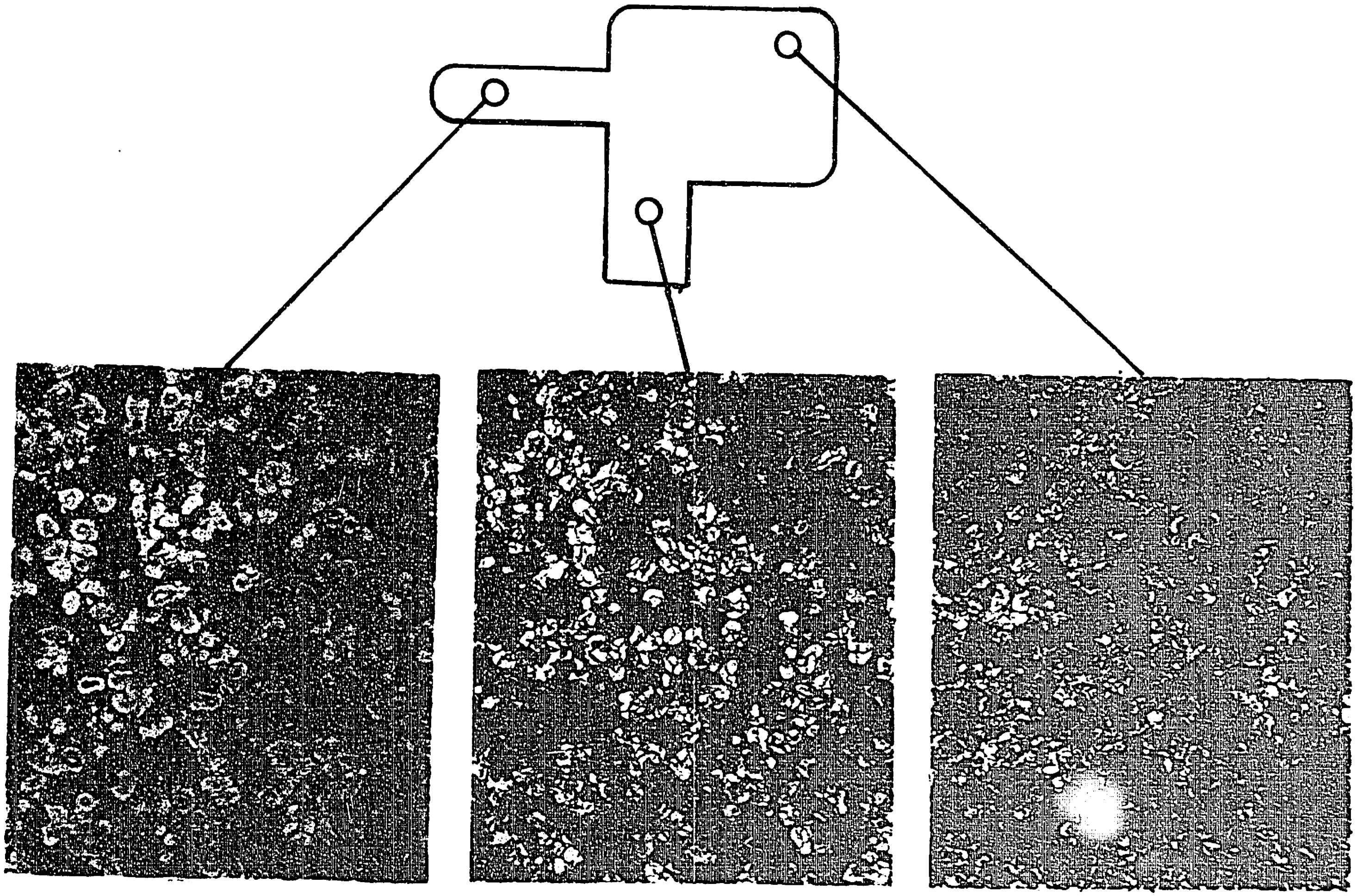

Figure 25. Photomicrographs showing homogeneous distribution of primary solid particles in various regions of a 440C stainless steel casting produced in the low pressure casting machine, 50X.

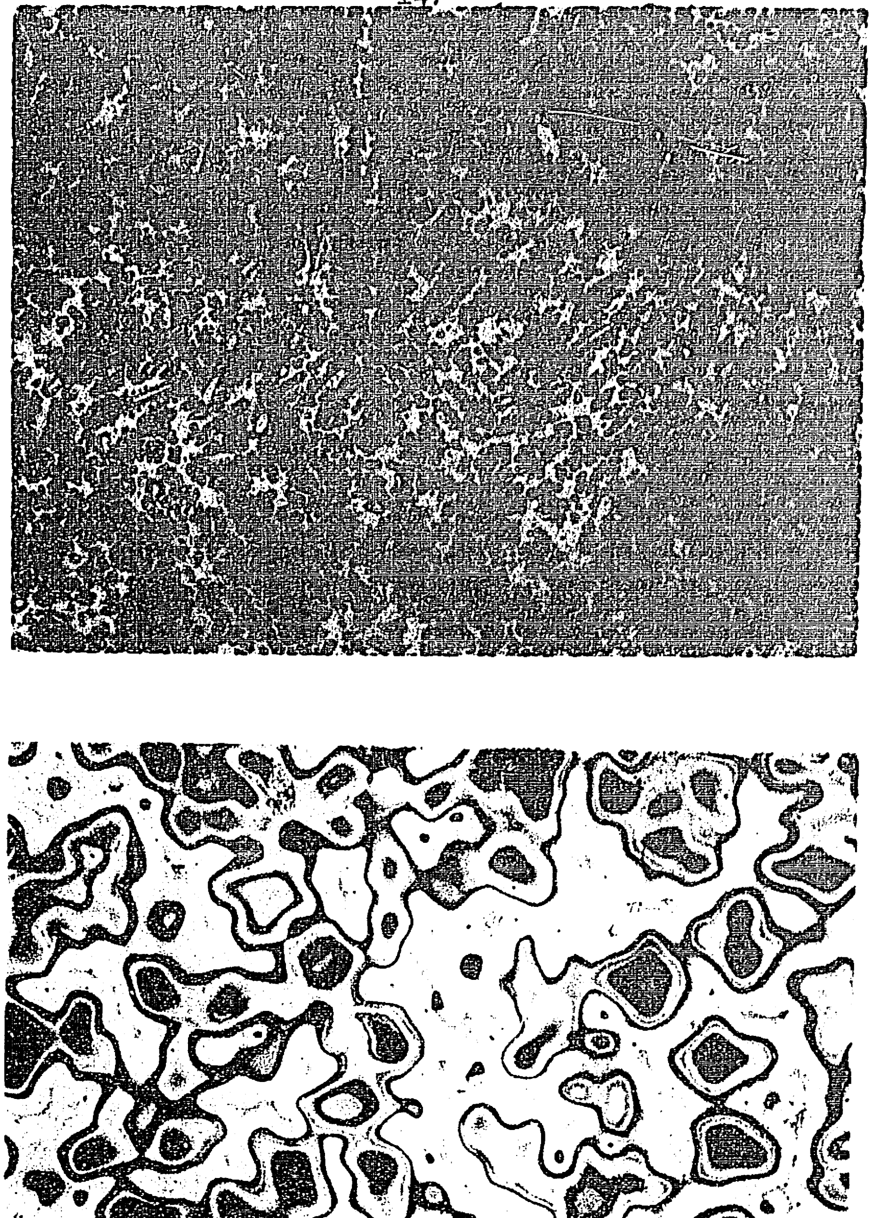

Figure 26. Microstructures of conventionally solidified (from the liquid state) copper base alloy 905, 88%Cu-10%Sn-2%Zn. Top: sample directly water quenched. Bottom: sample slowly cooled. 100X.

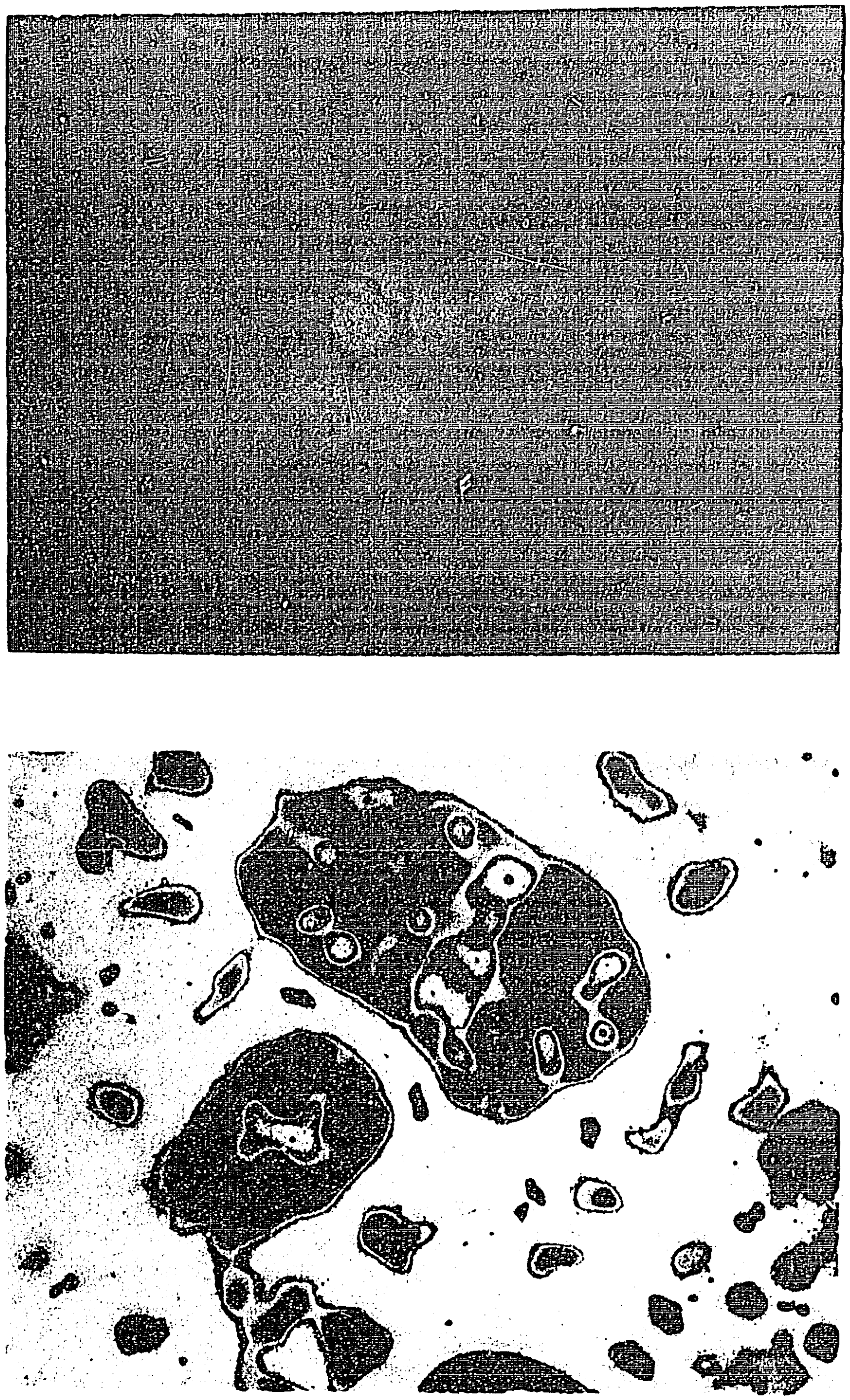

Figure 27. Microstructure of continuously produced semi-solid copper base alloy 905, 88%Cu-10%Sn-2%Zn. Top: sample directly water quenched, 100X. Bottom: sample slowly cooled.

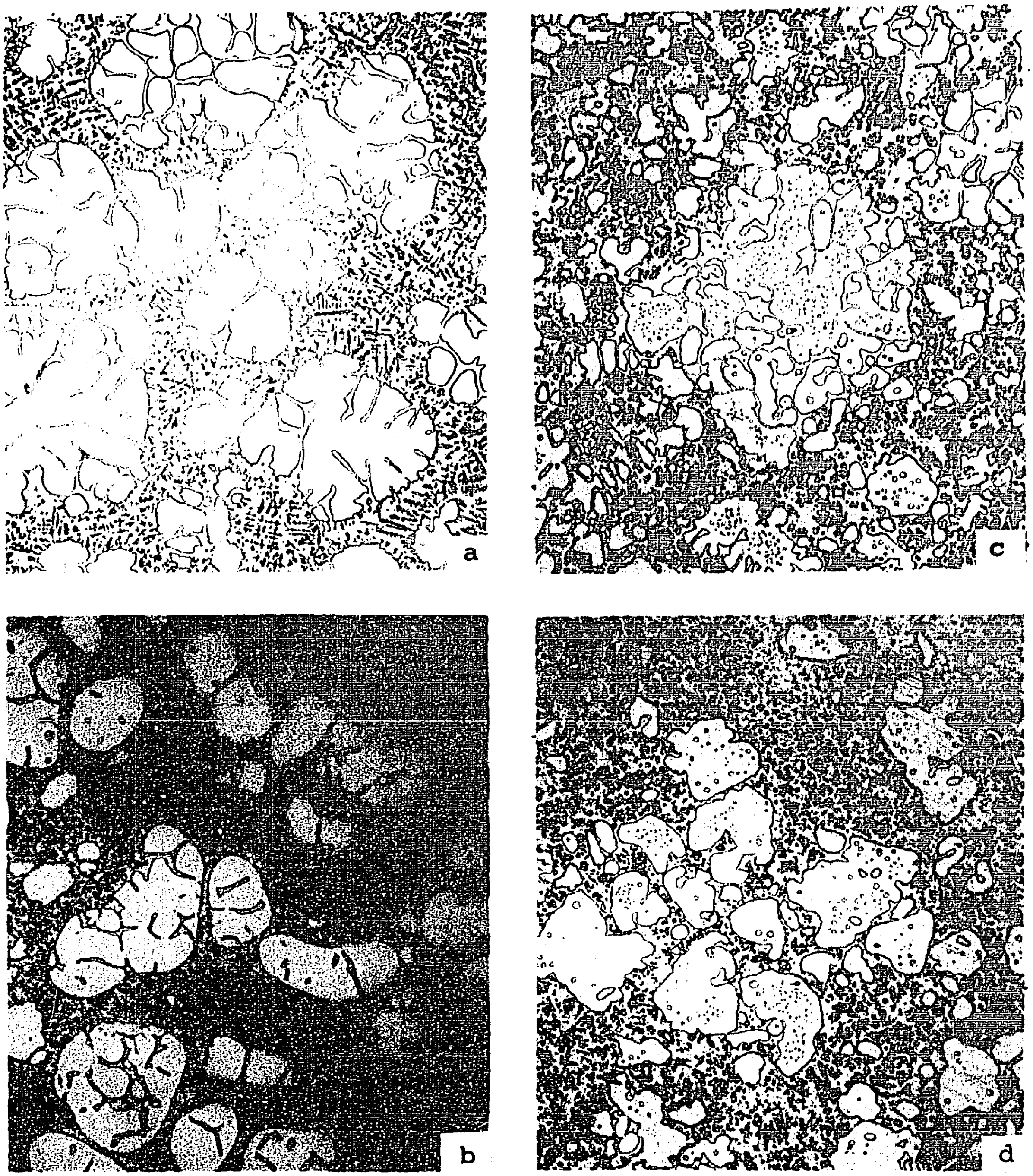

Figure 28. Comparison of the microstructures of semi-solid copper base alloy 905, 88%Cu-10%Sn-2%Zn showing correlation between water quenched samples and castings. (a) and (b) are water quenched samples, (c) and (d) are the corresponding castings, 100X.

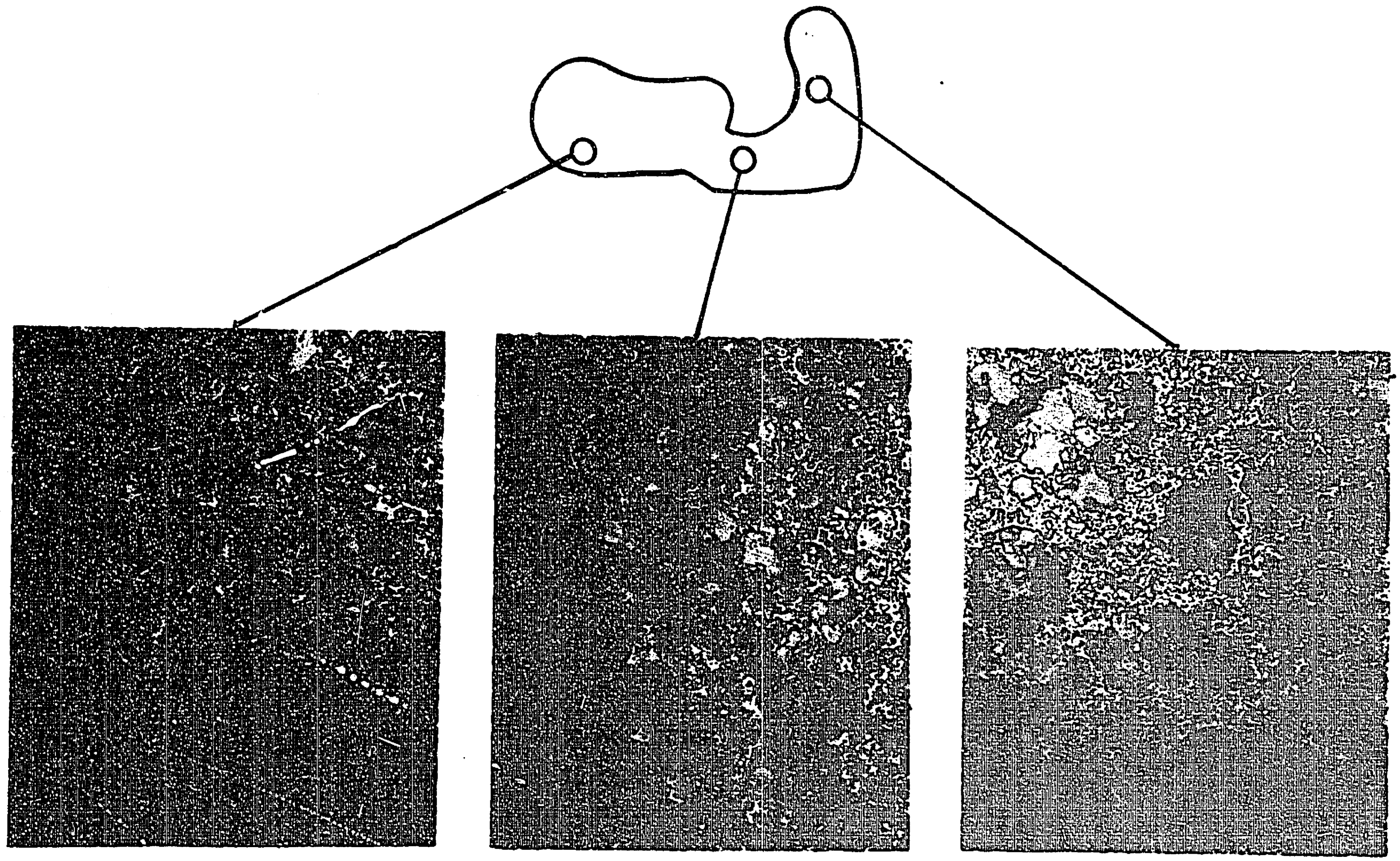

Figure 29. Photomicrographs showing homogeneous distribution of primary solid particles in various regions of a copper base alloy 905, 88%Cu-10%Sn-2%Zn, casting produced in the high pressure die casting machine, 50X.

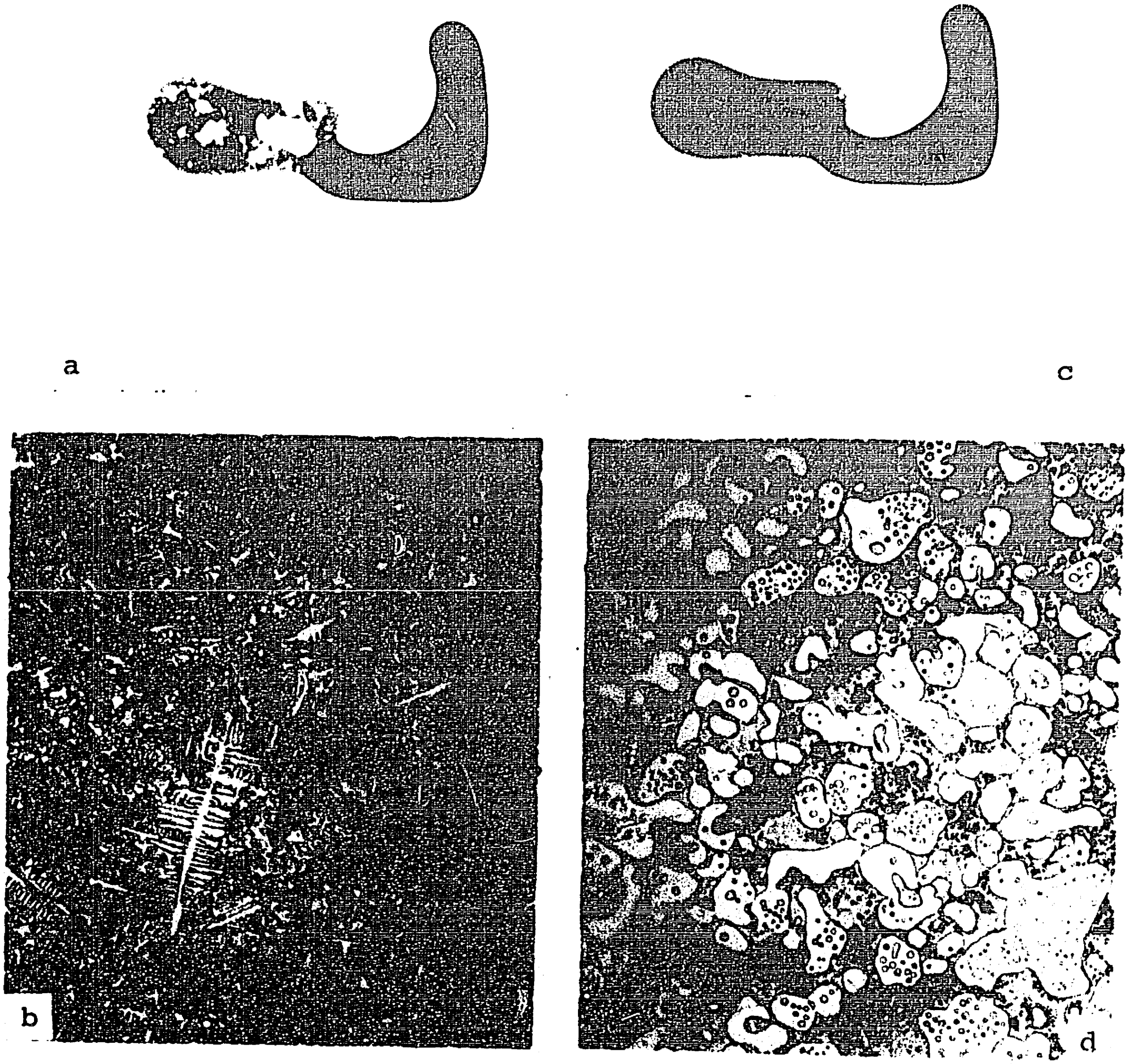

Figure 30. Radiographs and microstructures of conventionally cast and Rheocast copper base alloy 905, 88%Cu-10%Sn-2%Zn, made in the high pressure casting system. (a) and (c) show the radiographs of castings made from superheated liquid and semi-solid metal, respectively, (b) and (d) show the corresponding microstructures at 100X.

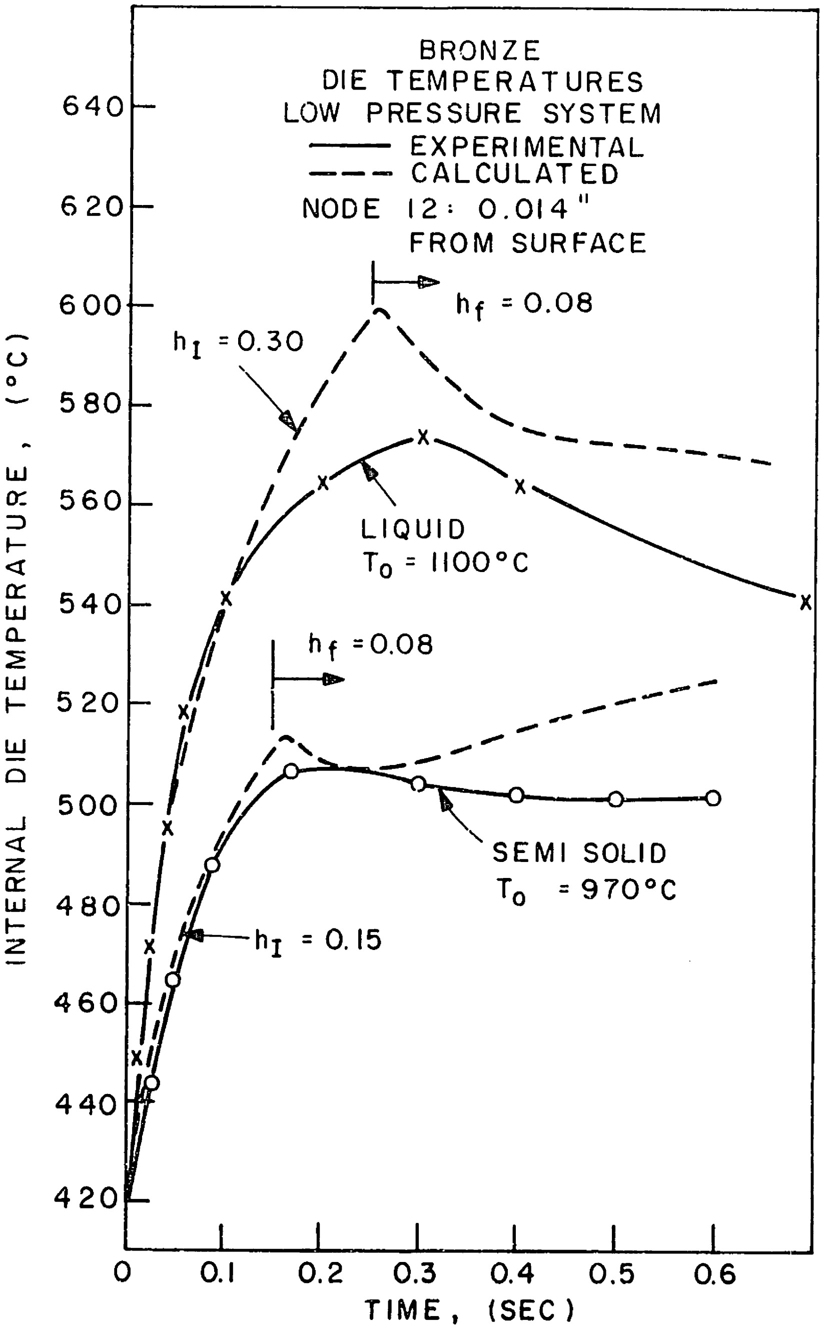

Figure 31. Measured die temperature during the casting of liquid and semi-solid copper base alloy 905, 88%Cu-10%Sn-2%Zn, in the low pressure die casting machine. Thermocouple was located at node 12, 0.0139" from casting-die interface. Dotted lines represent the calculated temperature variation produced by computer simulation.

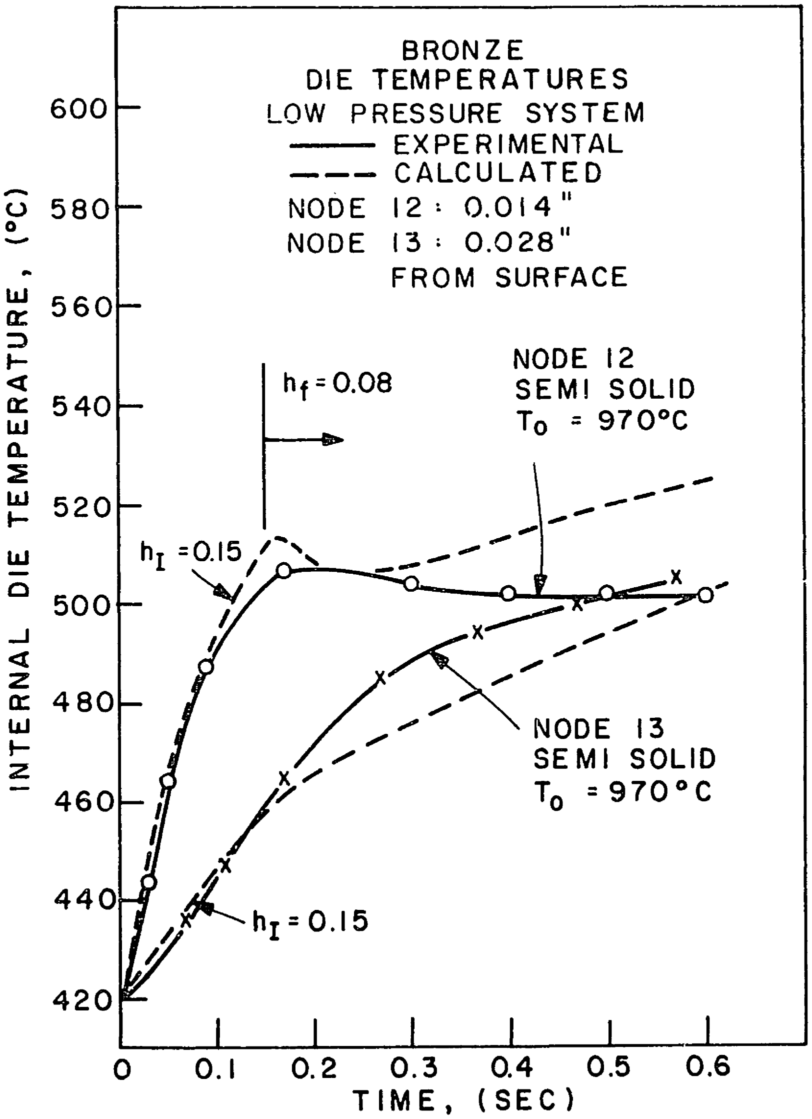

Figure 32. Measured internal die temperatures during the casting of semi-solid copper base alloy 905, 88%Cu-10%Sn-2%Zn, in the low pressure die casting machine. Dotted line represents the calculated temperature variation produced by computer simulation. Thermocouples located at nodes 12 and 13, 0.0139" and .0278" from the casting-die interface, respectively.

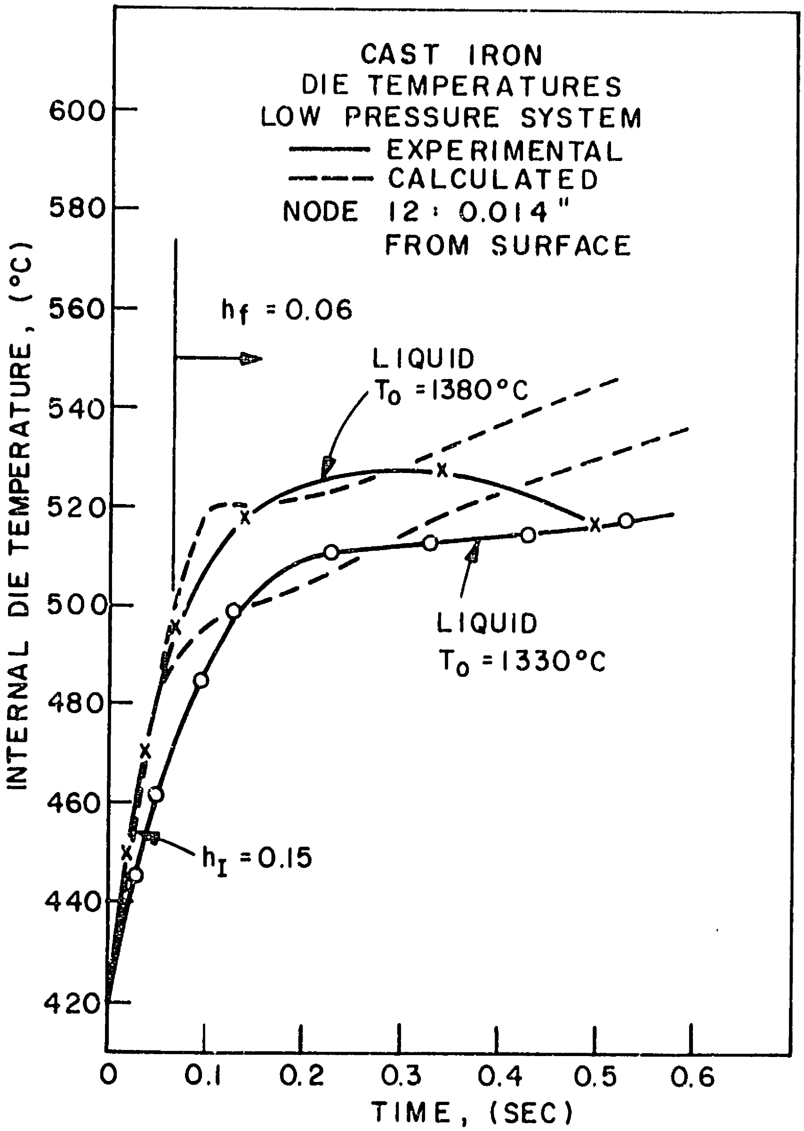

Figure 33. Measured internal die temperatures during the casting of liquid eutectic cast iron, Fe-2.6%C-3.2%Si, in the low pressure die casting machine. Thermocouple located at node 12, 0.0139" from the casting-die interface. Dotted line represents the calculated temperature variation produced by computer simulation.

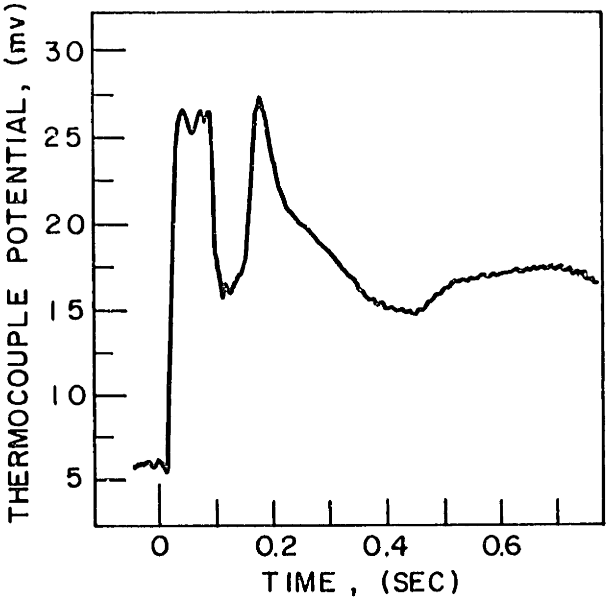

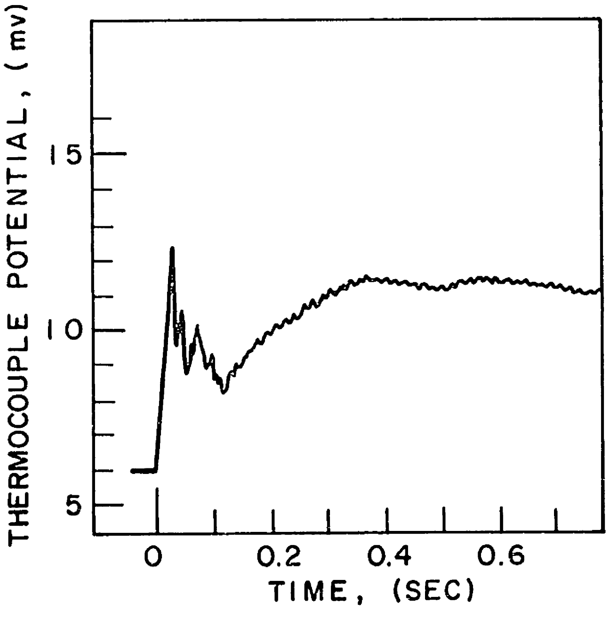

Figure 34. Oscilloscope display showing the actual thermocouple millivoltage measured during the casting of liquid (top) and semi-solid (bottom) copper base alloy 905, 88%Cu-10%Sn-2%Zn, in the high pressure die casting machine. Thermocouple located at node 12, 0.0139" from the casting-die interface.

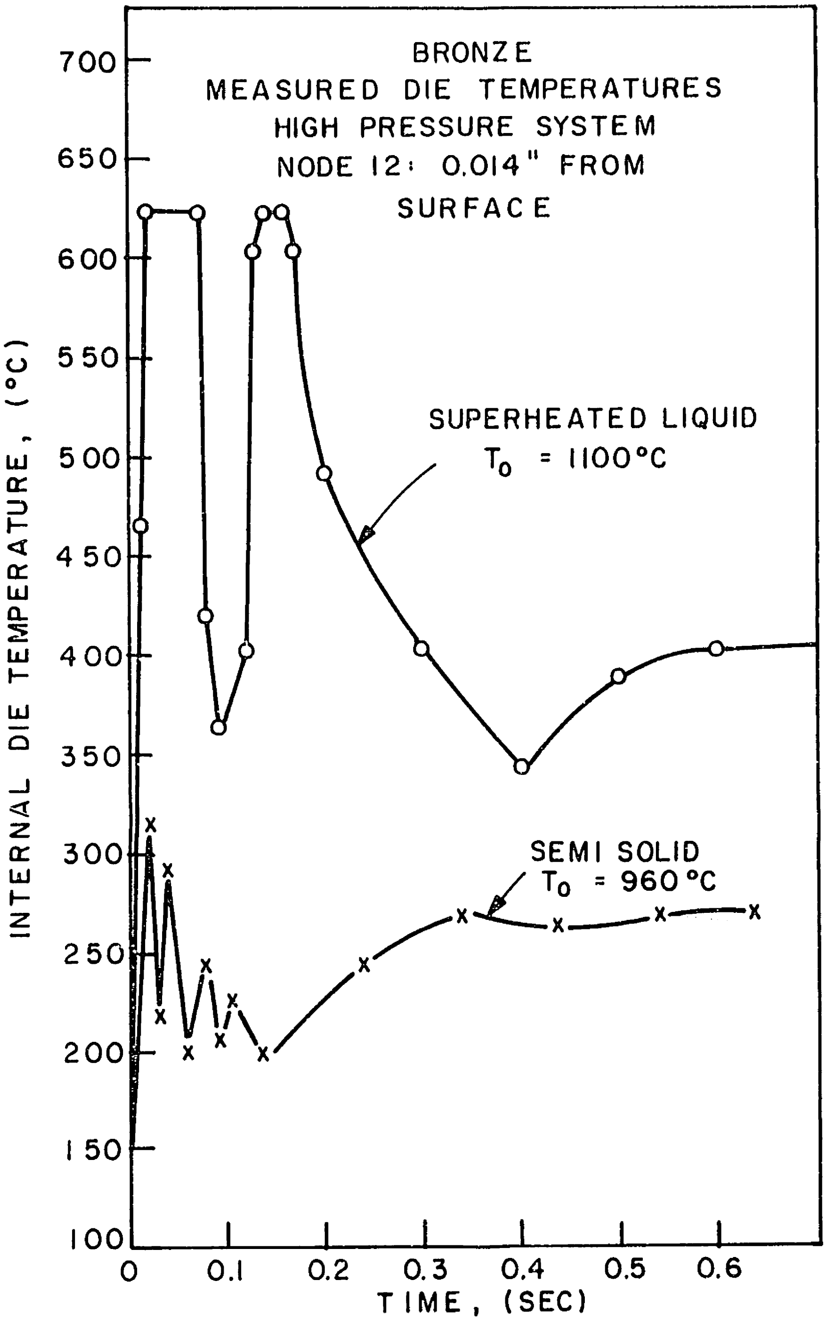

Figure 35. Measured internal die temperatures during the casting of liquid and semi-solid copper base alloy 905, 88%Cu-10%Sn-2%Zn, in the high pressure die casting machine. Thermocouple located at node 12, 0.0139" from the casting-die interface.

INFINITE FLAT MOLD: ONE DIMENSIONAL HEAT FLOW

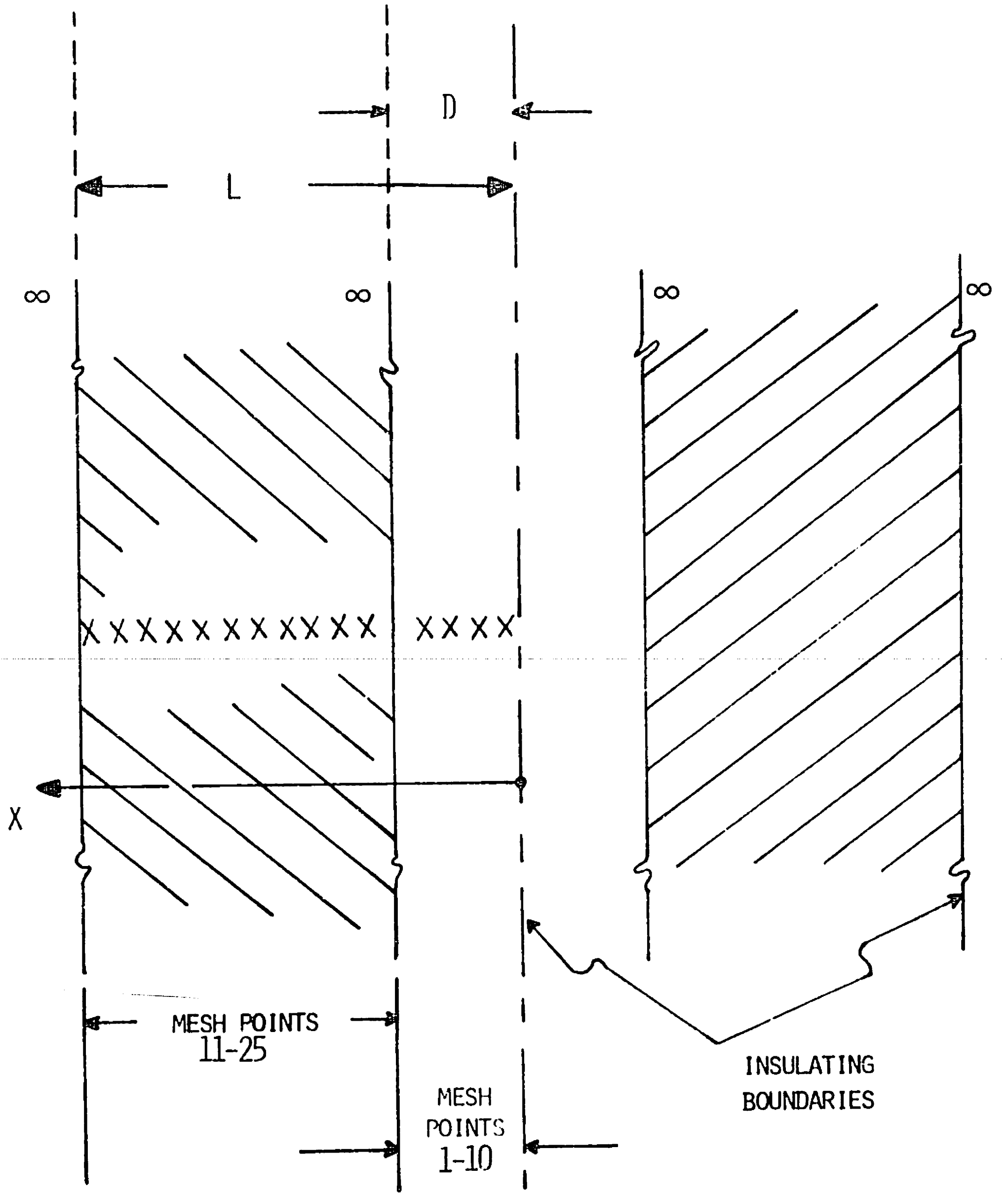
D
L
∞
∞
∞
∞
XXXXXXXXXXXX
XXXX
X
MESH POINTS 11-25
MESH POINTS 1-10
INSULATING BOUNDARIES

Figure 36. Schematic diagram showing the one dimensional computer model.

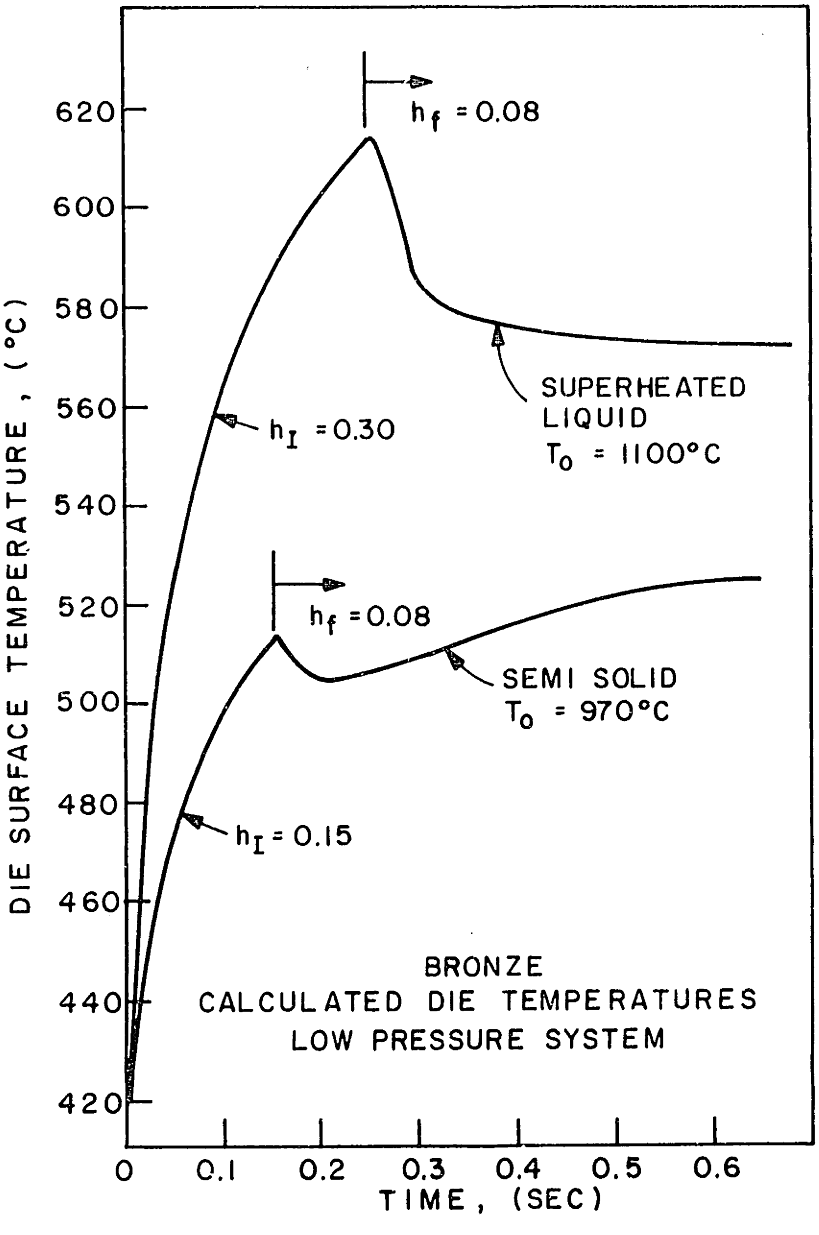

Figure 37. Computer simulated die surface temperatures as a function of time for the liquid and semi-solid copper base alloy 905, 88%Cu-10%Sn-2%Zn, cast in the low pressure system.

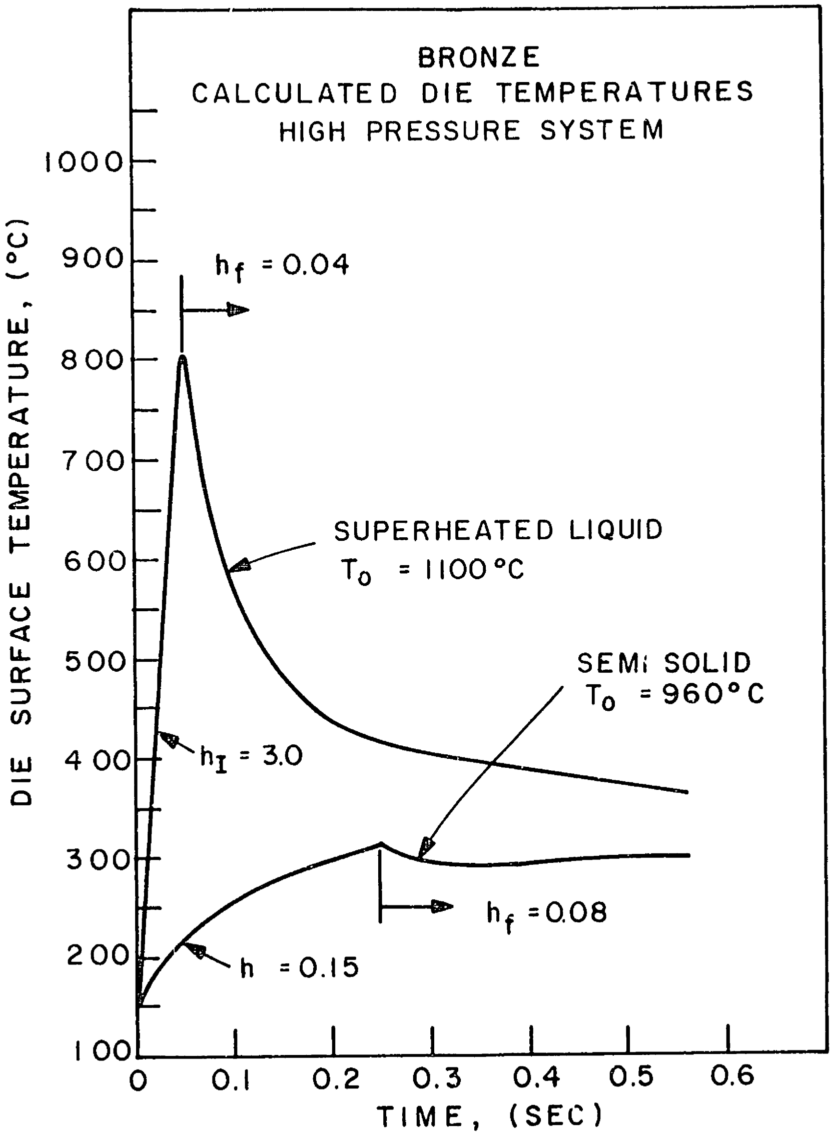

Figure 38. Die surface temperatures as a function of time for liquid and semi-solid copper base alloy 905, 88%Cu-10%Sn-2%Zn, cast in the high pressure die casting machine.

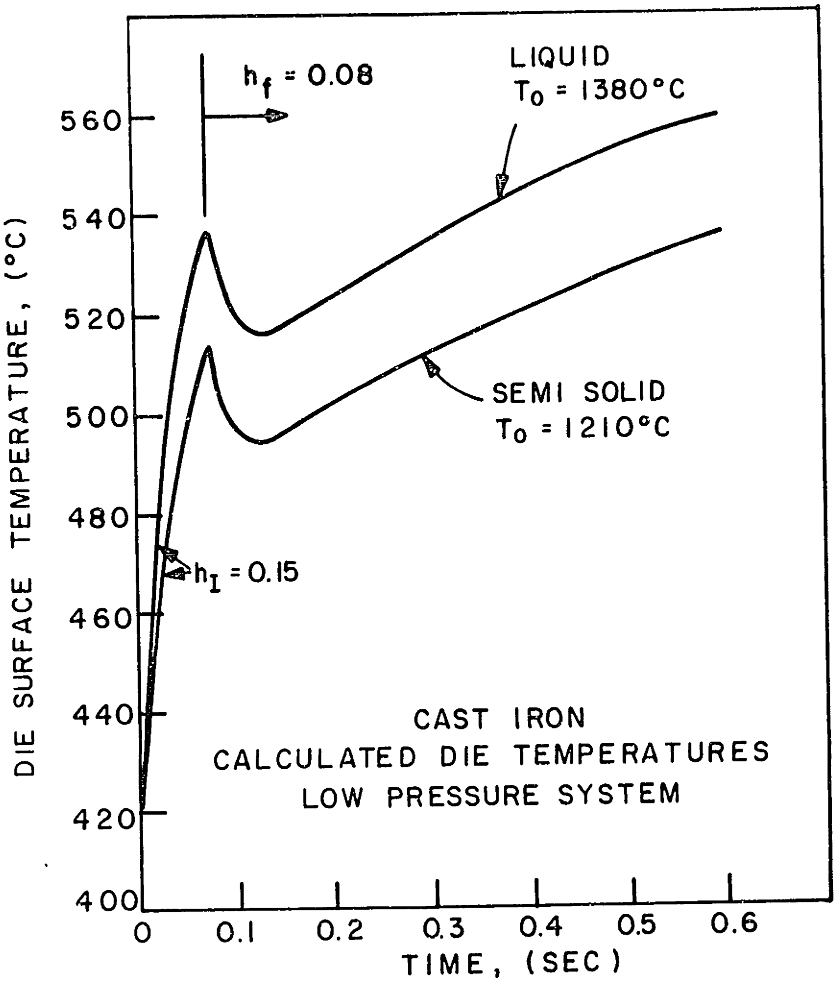

Figure 39. Die surface temperatures as a function of time for liquid and semi-solid eutectic cast iron, Fe-2.6%C-3.2%Si, cast in the low pressure die casting machine.

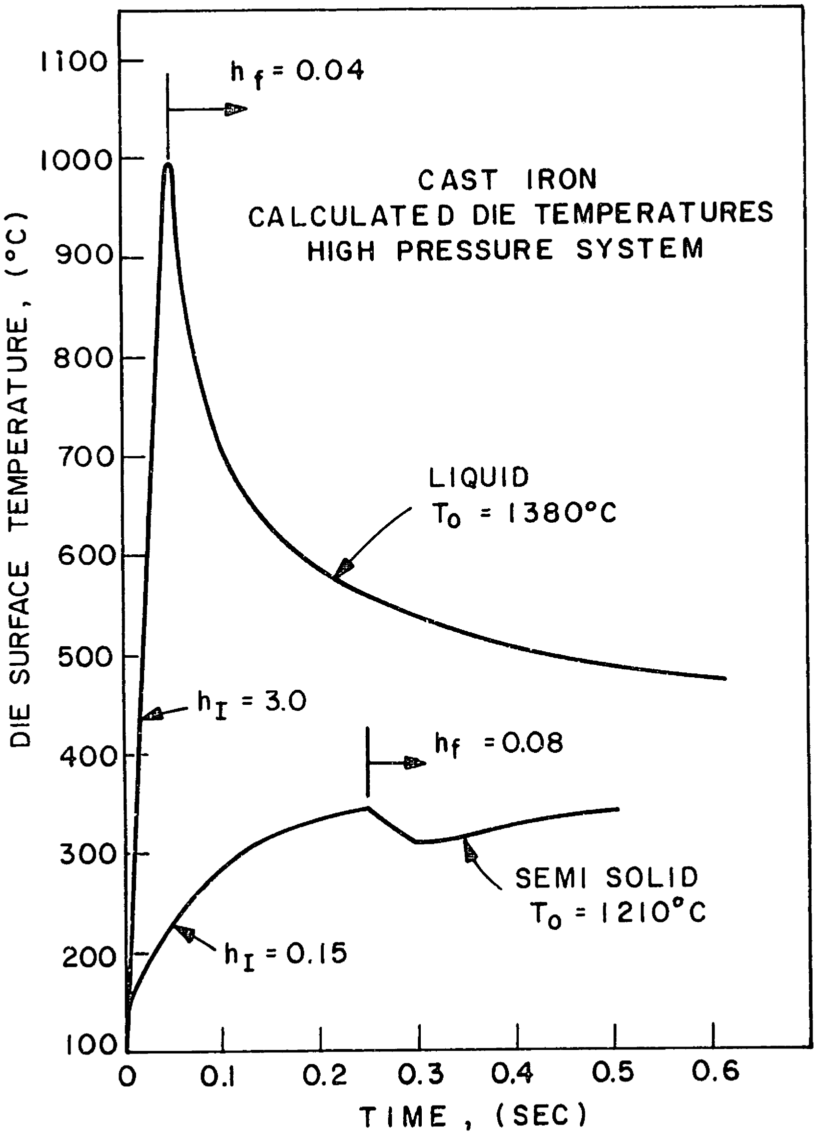

Figure 40. Die surface temperatures as a function of time for liquid and semi-solid eutectic cast iron, Fe-2.6%C-3.2%Si, cast in the high pressure die casting machine.

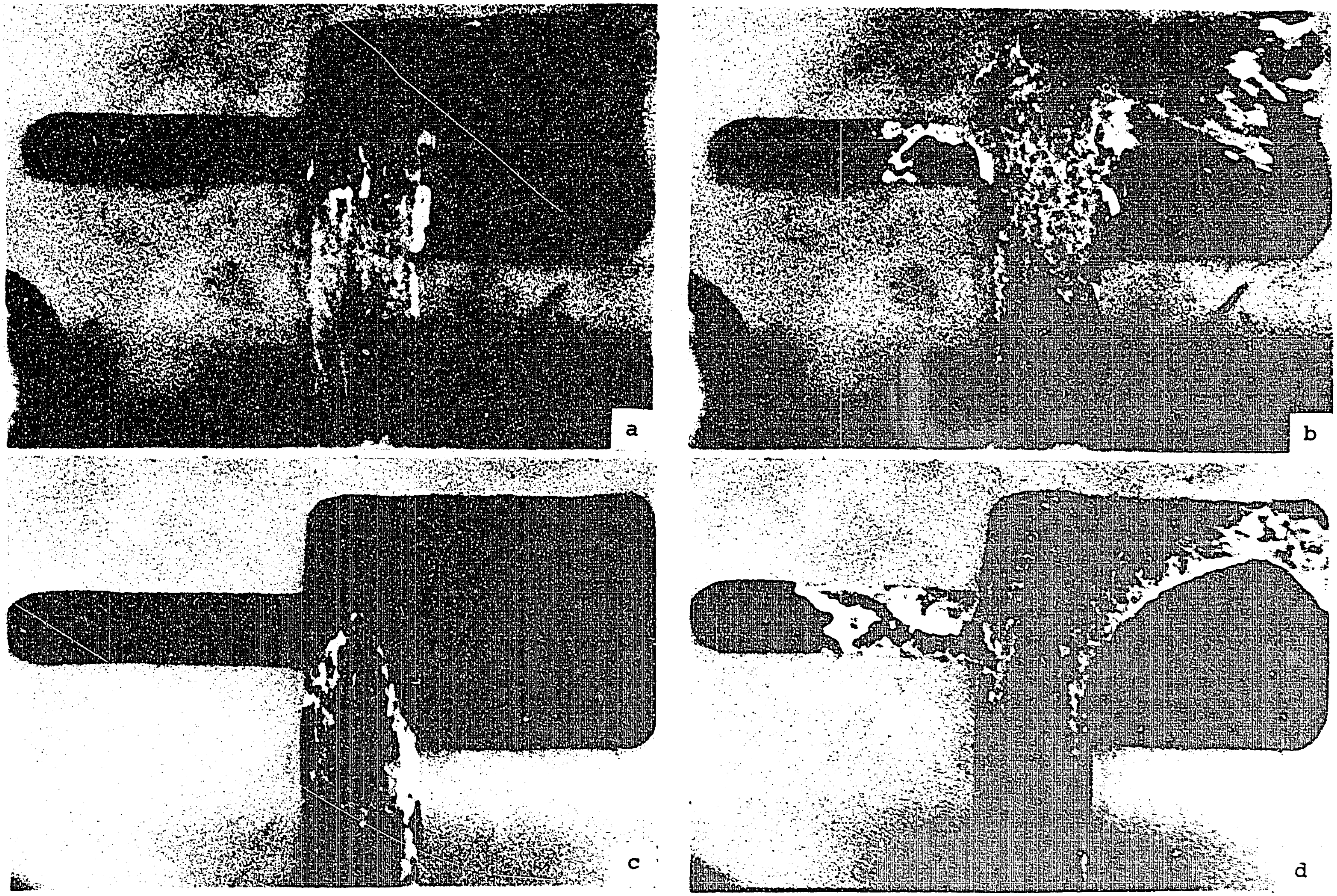

Figure 41: Sequence of frames from a high speed motion picture of a die filling with liquid.

APPENDIX A.

1. Electron Beam Microanalyzer

Continuous scans were done on a Norelco AMR/3 using an L.F crystal with a take-off angle of 15.5^{o}. The work was performed at Man Labs, Inc., Cambridge, Massachusetts.

The raw microprobe data was converted to weight percent solute using Casting's approximation:

$$C_i = \frac{I_i - I_b}{I_i^{o} - I_i^{b}}$$

where C_i is the concentration of component i, wt%, and I_i, I_i^{b}, and I_i^{o} are the intensity, background intensity, and pure standard intensity, respectively, of component i.

APPENDIX B

COMPUTER PROGRAM AND FLOW DIAGRAM

COMPUTER FLOW DIAGRAM

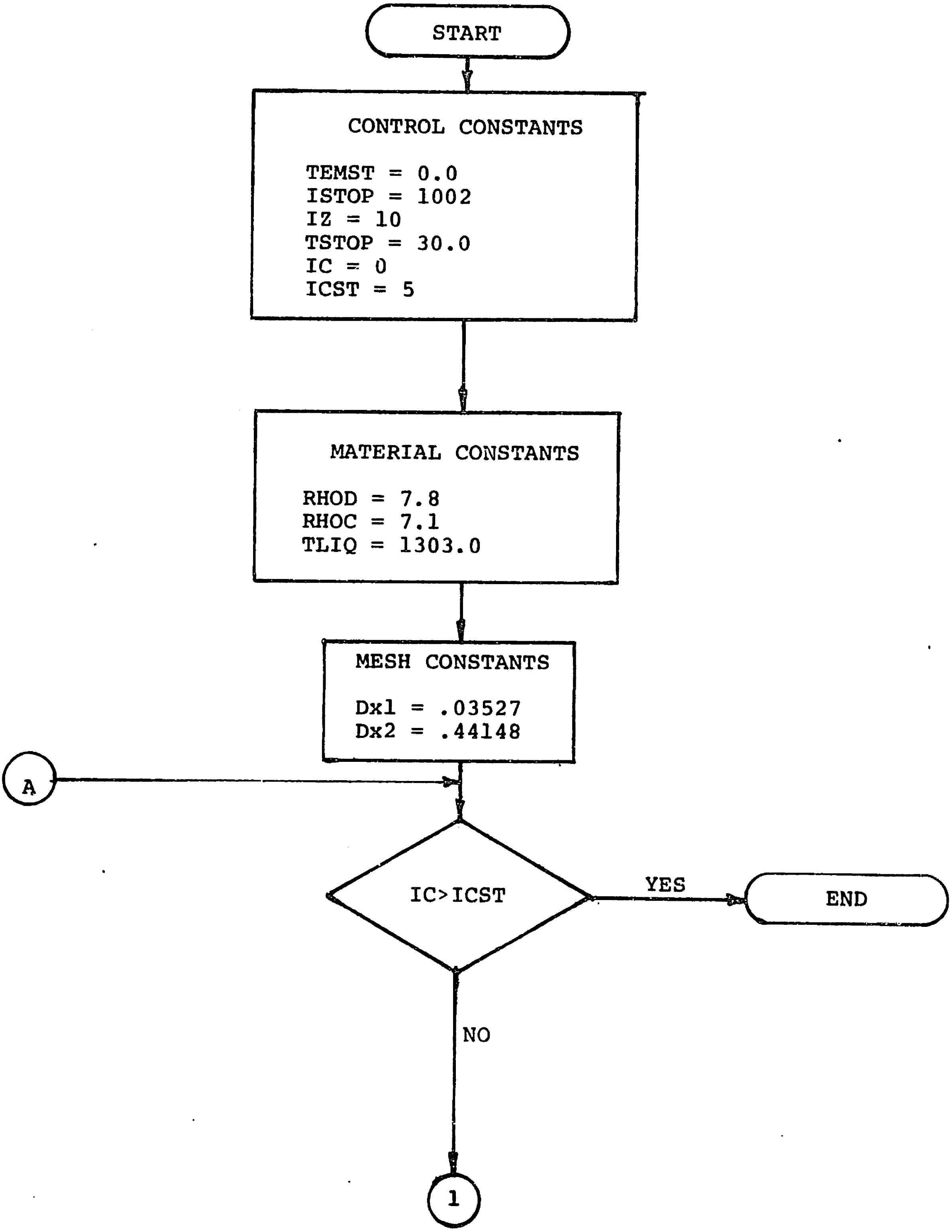
START
CONTROL CONSTANTS
TEMST = 0.0
ISTOP = 1002
IZ = 10
TSTOP = 30.0
IC = 0
ICST = 5
MATERIAL CONSTANTS
RHOD = 7.8
RHOC = 7.1
TLIQ = 1303.0
MESH CONSTANTS
Dx1 = .03527
Dx2 = .44148
A
IC>ICST
YES
END
NO
1

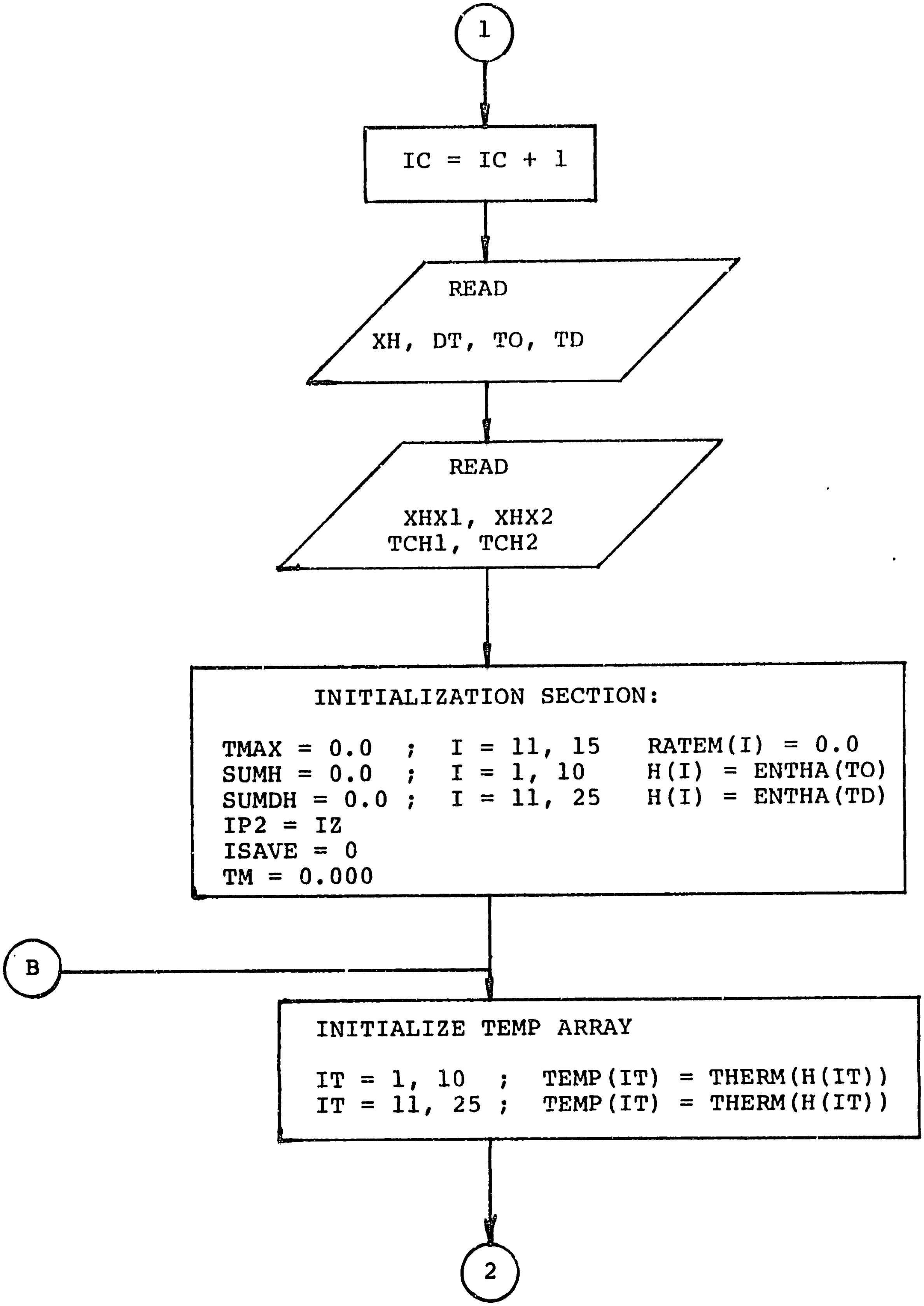
1
IC = IC + 1
READ
XH, DT, TO, TD
READ
XHX1, XHX2
TCH1, TCH2
INITIALIZATION SECTION:
TMAX = 0.0 ; I = 11, 15 RATEM(I) = 0.0
SUMH = 0.0 ; I = 1, 10 H(I) = ENTHA(TO)
SUMDH = 0.0 ; I = 11, 25 H(I) = ENTHA(TD)
IP2 = IZ
ISAVE = 0
TM = 0.000
B
INITIALIZE TEMP ARRAY
IT = 1, 10 ; TEMP(IT) = THERM(H(IT))
IT = 11, 25 ; TEMP(IT) = THERM(H(IT))
2

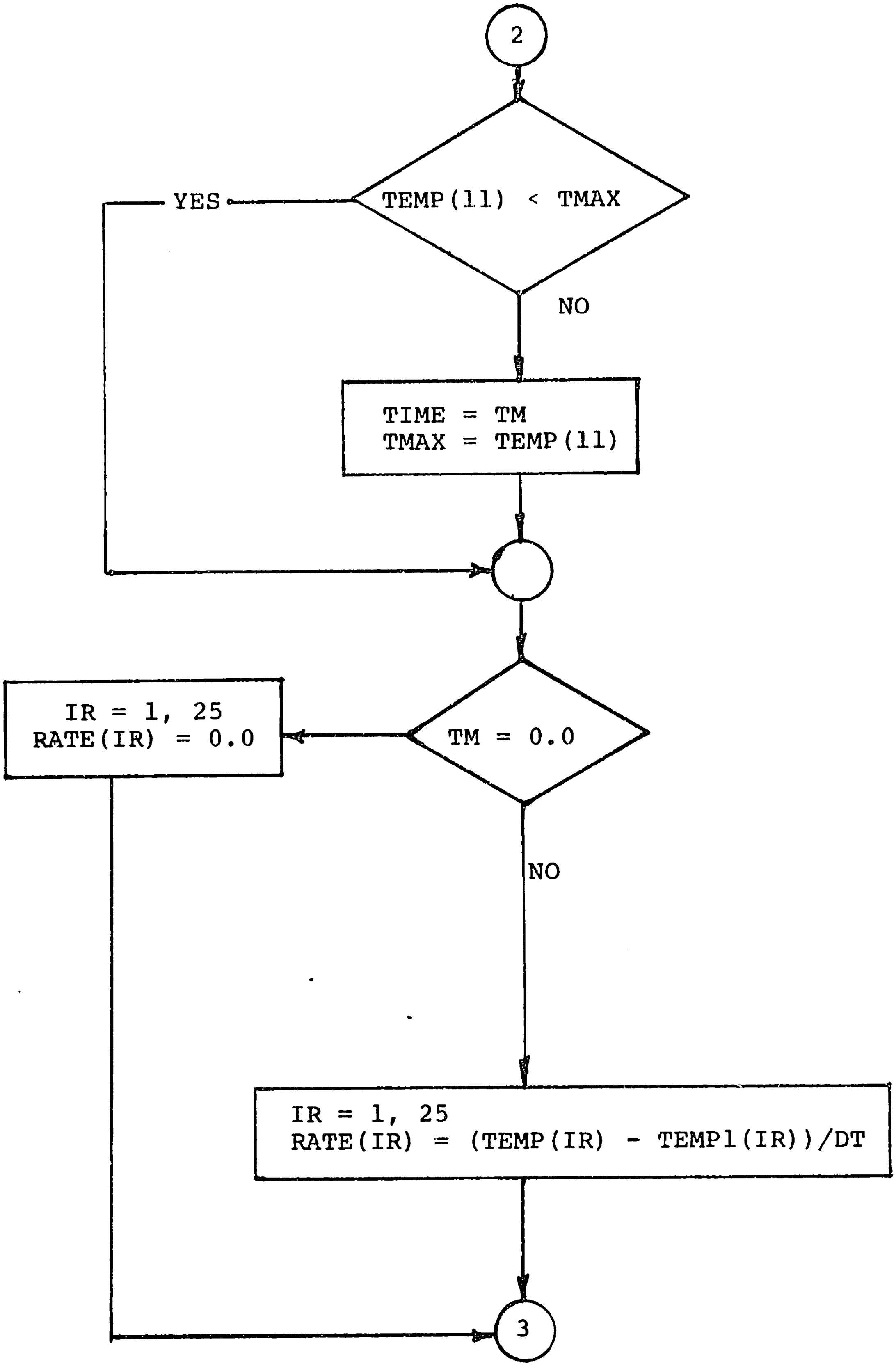
2
TEMP(11) < TMAX
YES
NO
TIME = TM
TMAX = TEMP(11)
TM = 0.0
IR = 1, 25
RATE(IR) = 0.0
NO
IR = 1, 25
RATE(IR) = (TEMP(IR) - TEMP1(IR))/DT
3

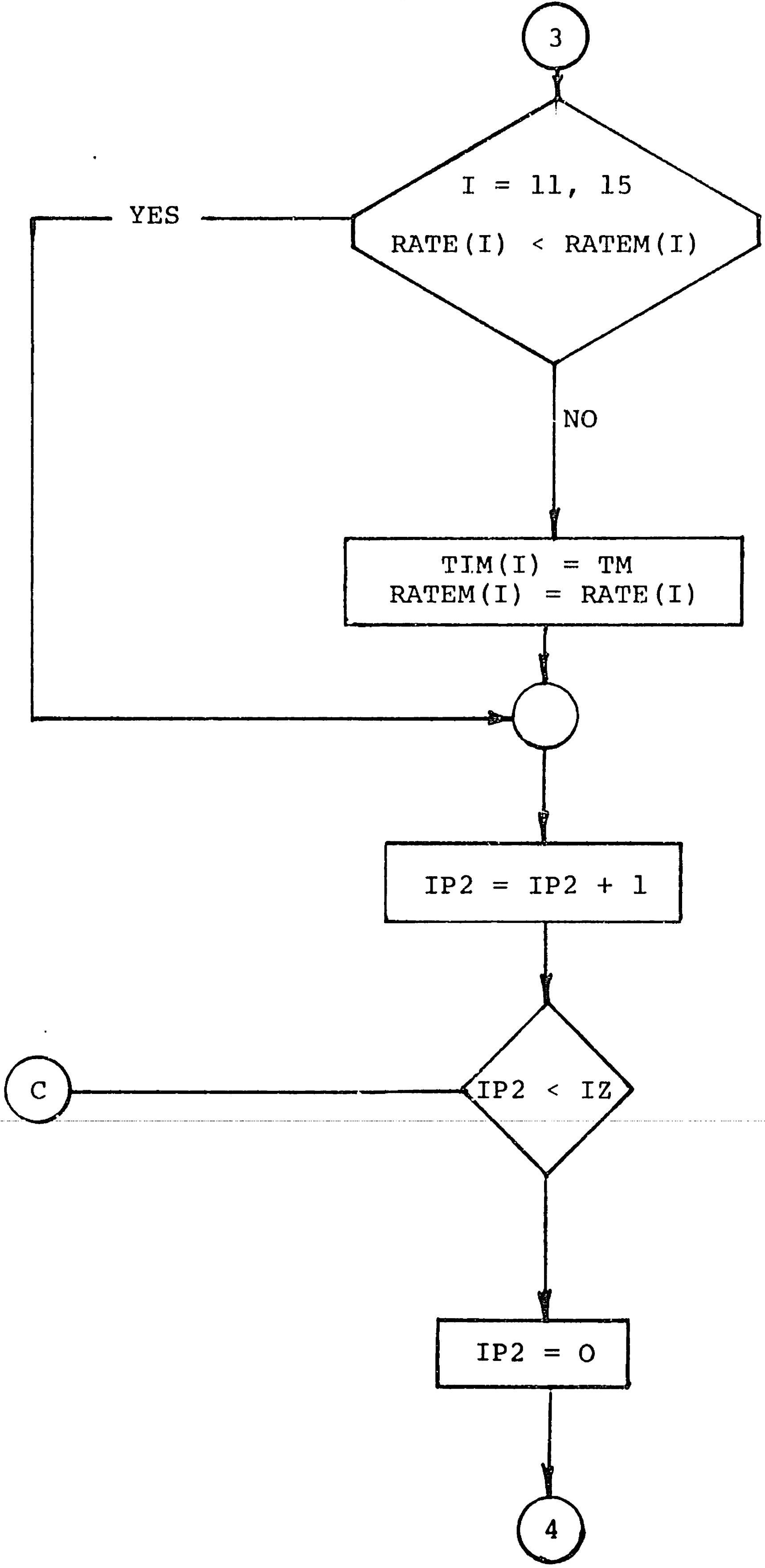
3
I = 11, 15
RATE(I) < RATEM(I)
YES
NO
TIM(I) = TM
RATEM(I) = RATE(I)
IP2 = IP2 + 1
IP2 < IZ
C
IP2 = 0
4

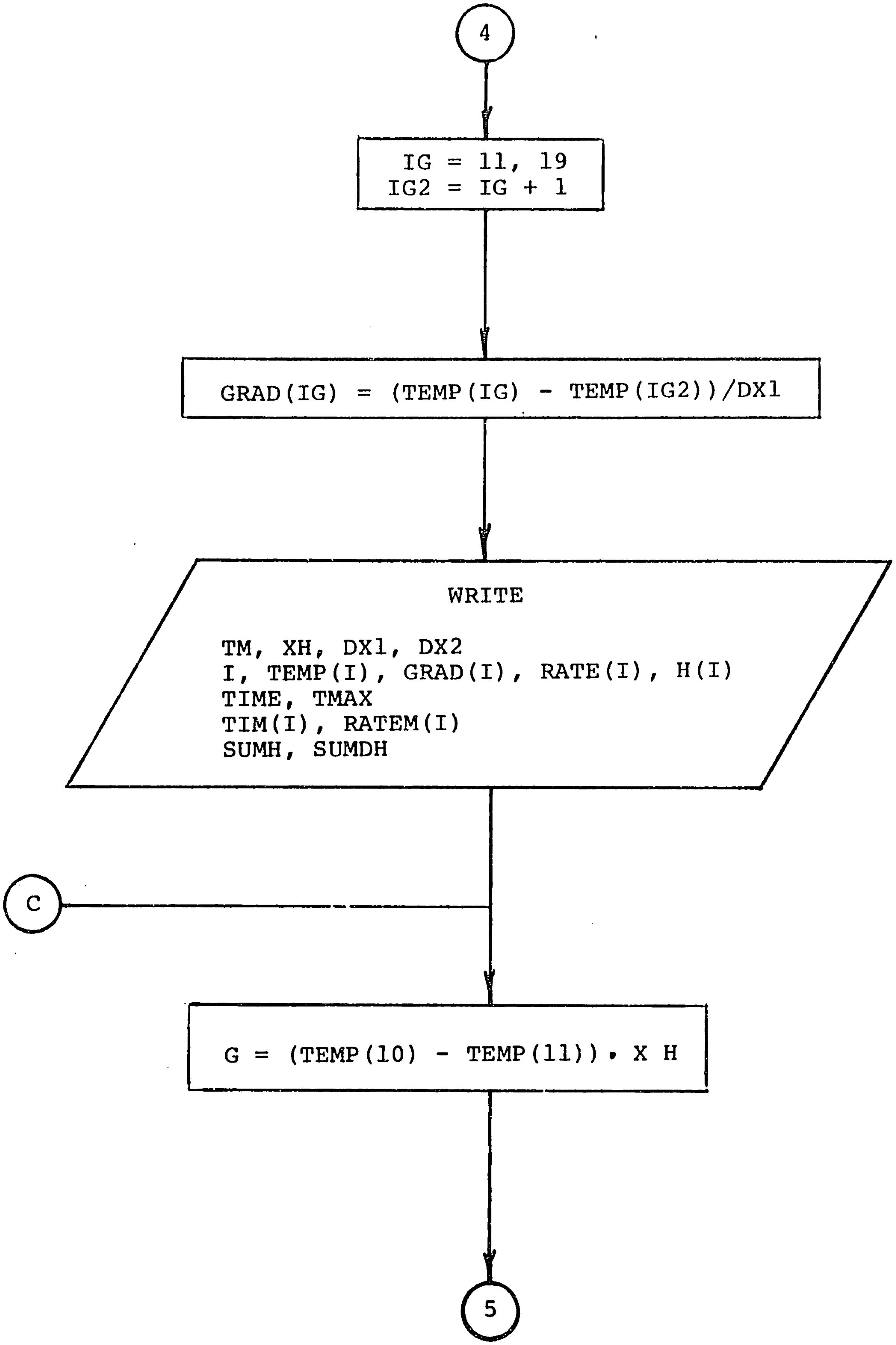
4
IG = 11, 19
IG2 = IG + 1
GRAD(IG) = (TEMP(IG) - TEMP(IG2))/DX1
WRITE
TM, XH, DX1, DX2
I, TEMP(I), GRAD(I), RATE(I), H(I)
TIME, TMAX
TIM(I), RATEM(I)
SUMH, SUMDH
C
G = (TEMP(10) - TEMP(11)) • X H
5

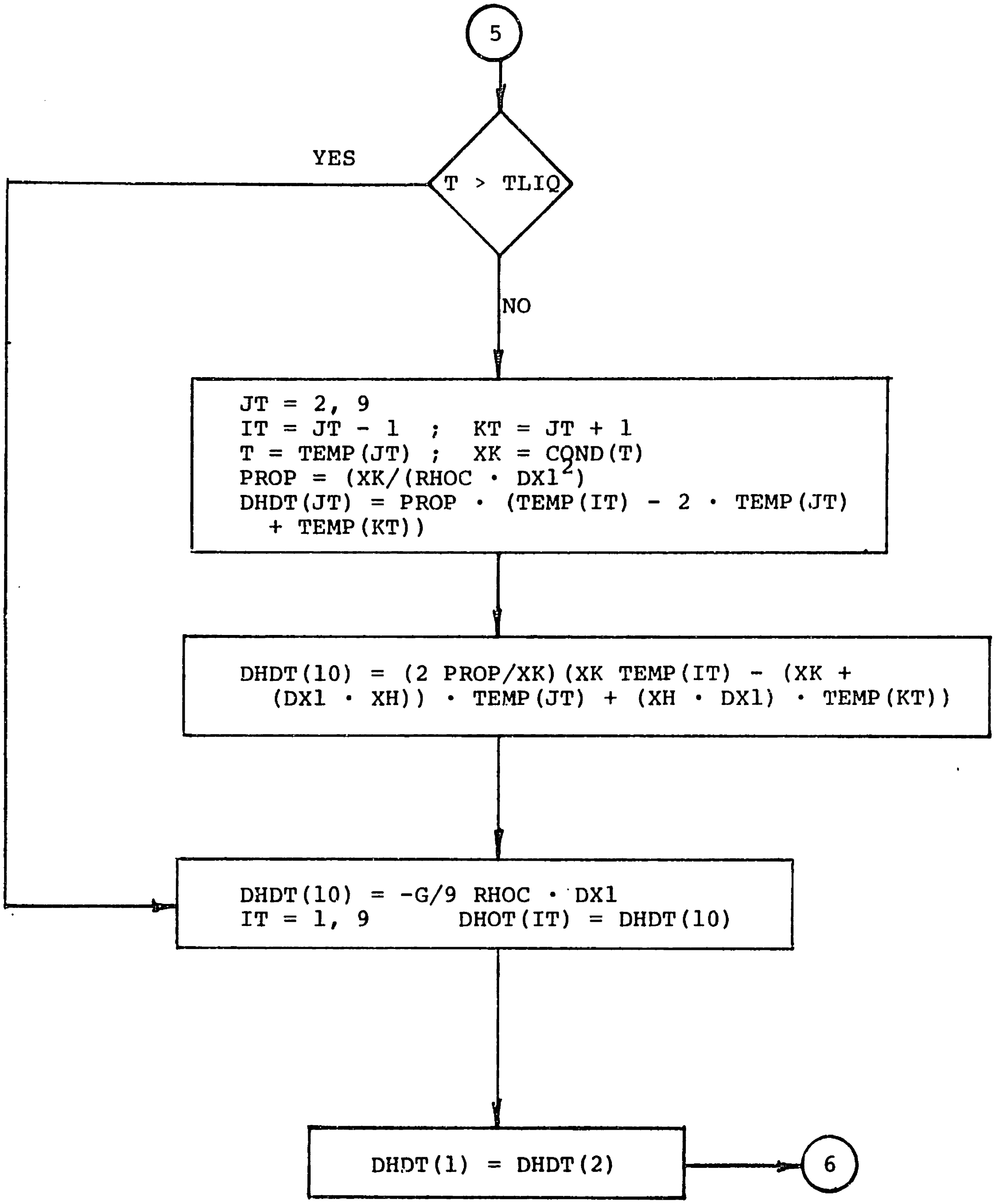
5
YES
T > TLIQ
NO
JT = 2, 9
IT = JT - 1 ; KT = JT + 1
T = TEMP(JT) ; XK = COND(T)
PROP = (XK/(RHOC · DX1^2)
DHDT(JT) = PROP · (TEMP(IT) - 2 · TEMP(JT) + TEMP(KT))
DHDT(10) = (2 PROP/XK)(XK TEMP(IT) - (XK + (DX1 · XH)) · TEMP(JT) + (XH · DX1) · TEMP(KT))
DHDT(10) = -G/9 RHOC · DX1
IT = 1, 9 DHOT(IT) = DHDT(10)
DHDT(1) = DHDT(2)
6

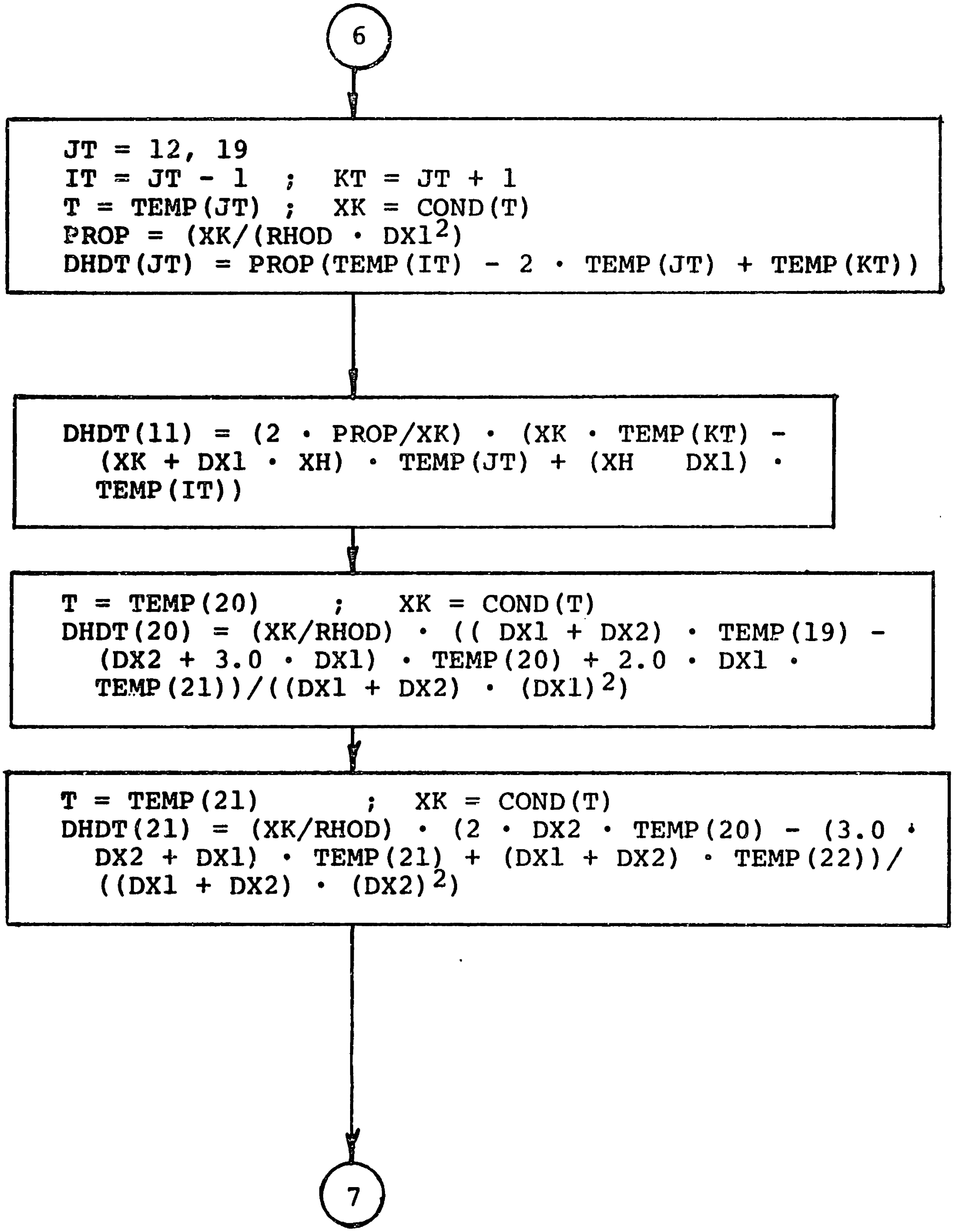

```
JT = 12, 19
IT = JT - 1  ;  KT = JT + 1
T = TEMP(JT)  ;  XK = COND(T)
PROP = (XK/(RHOD · $DX1^2$)
DHDT(JT) = PROP(TEMP(IT) - 2 · TEMP(JT) + TEMP(KT))
```

```
DHDT(11) = (2 · PROP/XK) · (XK · TEMP(KT) -
  (XK + DX1 · XH) · TEMP(JT) + (XH   DX1) ·
  TEMP(IT))
```

```
T = TEMP(20)    ;    XK = COND(T)
DHDT(20) = (XK/RHOD) · (( DX1 + DX2) · TEMP(19) -
  (DX2 + 3.0 · DX1) · TEMP(20) + 2.0 · DX1 ·
  TEMP(21))/((DX1 + DX2) · $(DX1)^2$)
```

```
T = TEMP(21)     ;   XK = COND(T)
DHDT(21) = (XK/RHOD) · (2 · DX2 · TEMP(20) - (3.0 ·
  DX2 + DX1) · TEMP(21) + (DX1 + DX2) · TEMP(22))/
  ((DX1 + DX2) · $(DX2)^2$)
```

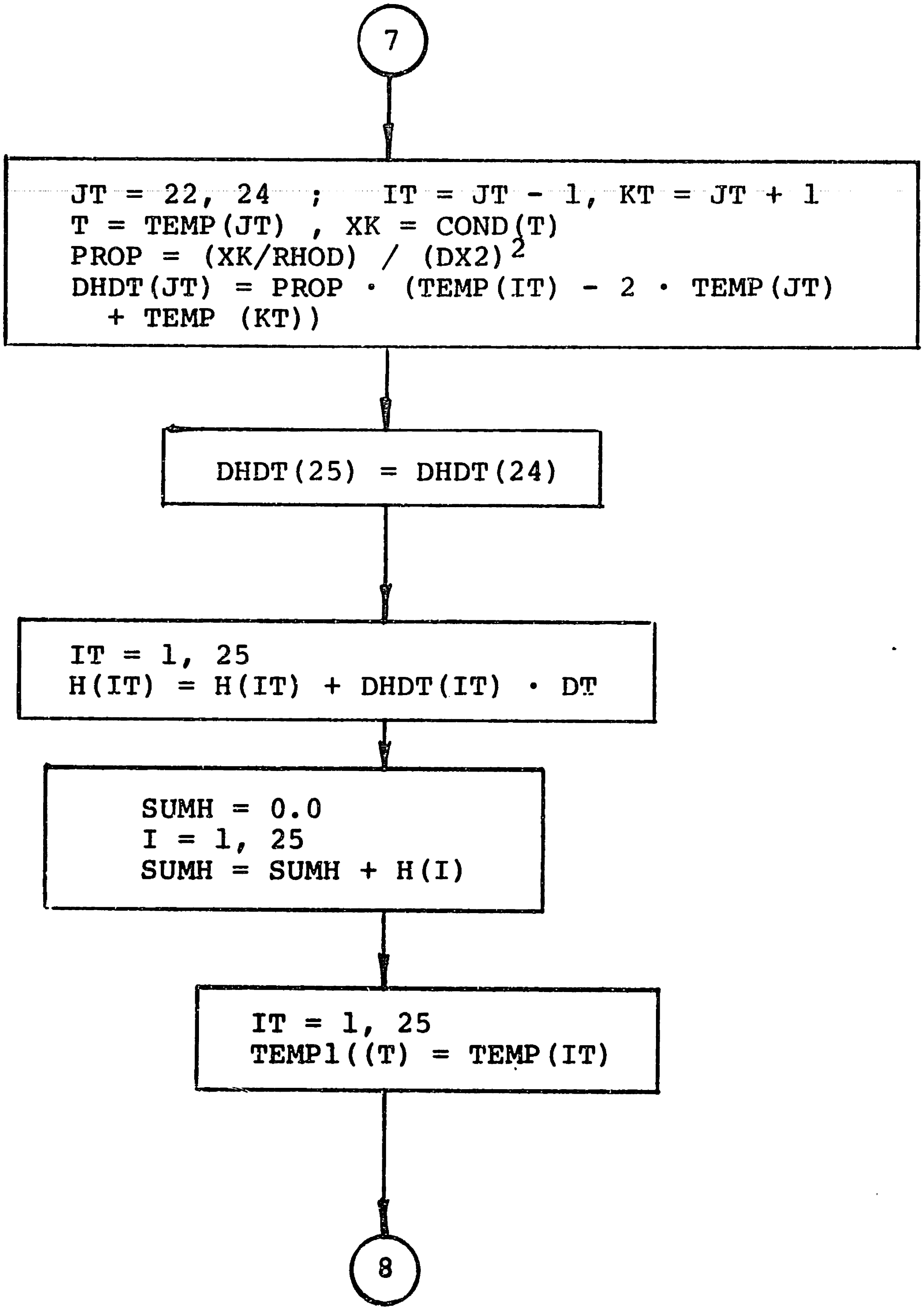
7
JT = 22, 24 ; IT = JT - 1, KT = JT + 1
T = TEMP(JT) , XK = COND(T)
PROP = (XK/RHOD) / $(DX2)^2$
DHDT(JT) = PROP · (TEMP(IT) - 2 · TEMP(JT) + TEMP (KT))
DHDT(25) = DHDT(24)
IT = 1, 25
H(IT) = H(IT) + DHDT(IT) · DT
SUMH = 0.0
I = 1, 25
SUMH = SUMH + H(I)
IT = 1, 25
TEMP1((T) = TEMP(IT)
8

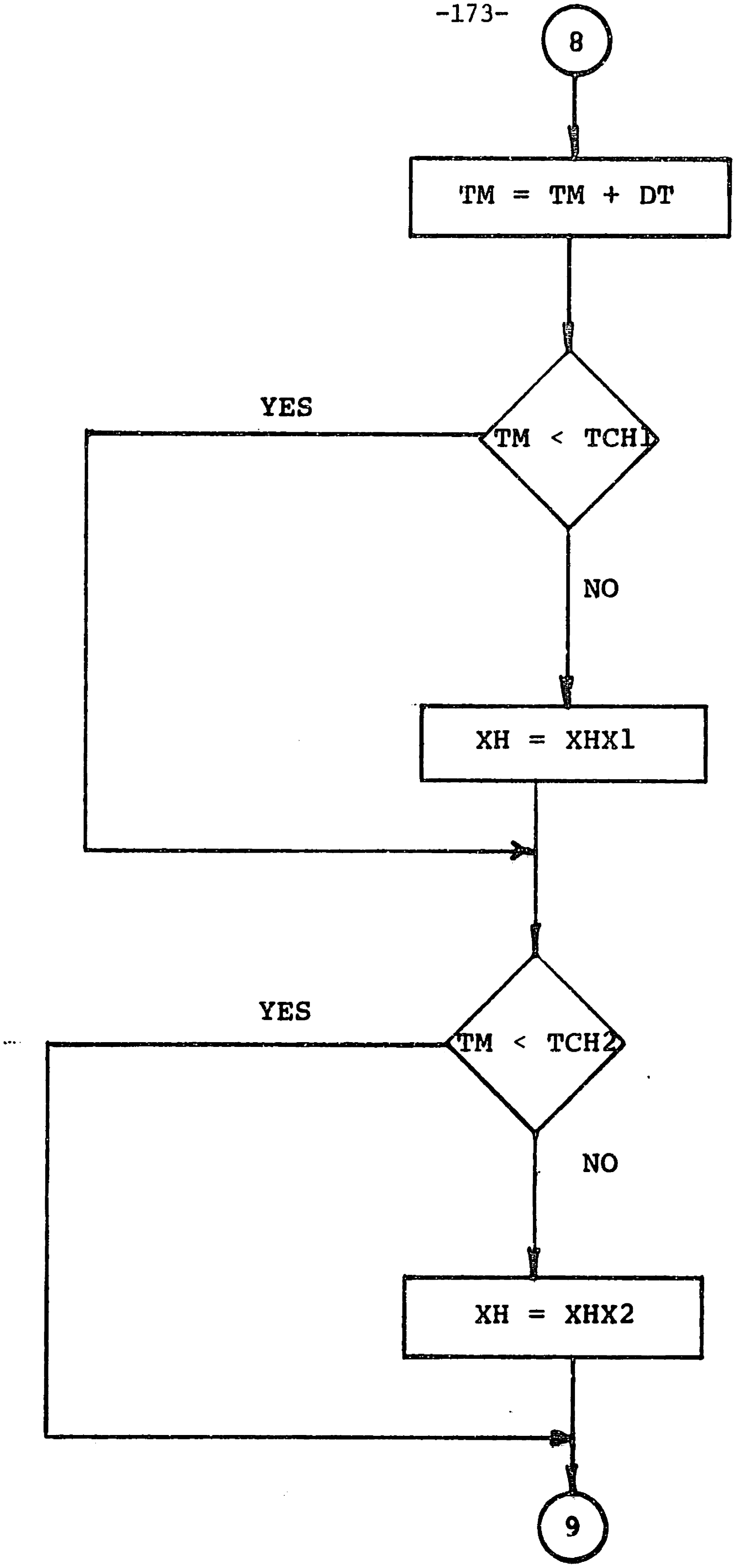
8
TM = TM + DT
YES
TM < TCH1
NO
XH = XHX1
YES
TM < TCH2
NO
XH = XHX2
9

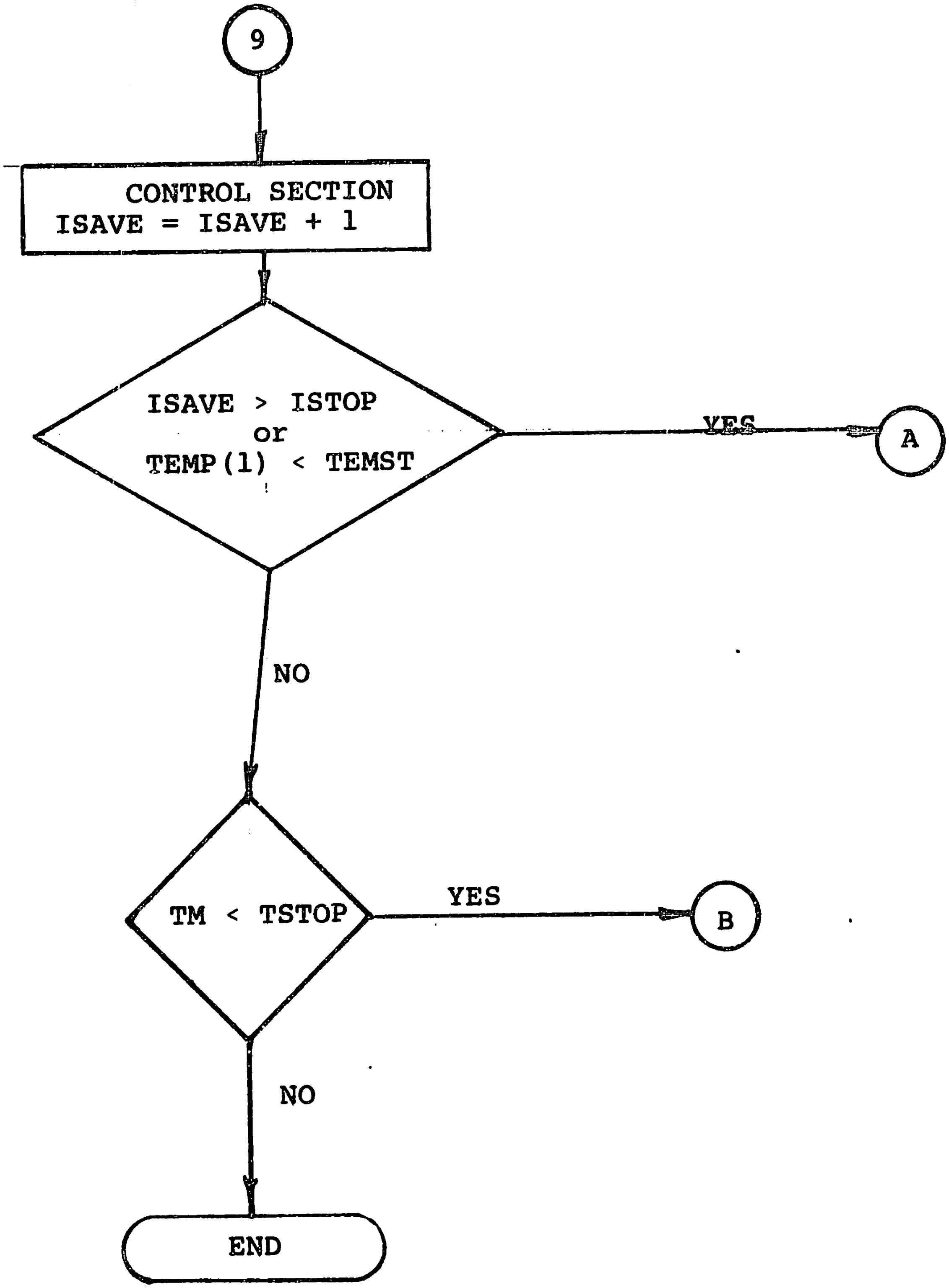
9
CONTROL SECTION
ISAVE = ISAVE + 1
ISAVE > ISTOP
or
TEMP(1) < TEMST
YES
A
NO
TM < TSTOP
YES
B
NO
END

```
//' 'BACKMAN',CLASS=A,REGION=192K
/*SRI STANDARD
/*MAIN TIME=2,LINES=9
//STEP1    EXEC WATFIV
//C.SYSIN DD *
$JOB              BACKMAN,TIME=2
      DIMENSION H(25),TEMP1(25),TEMP(25),DHDT(25),RATE(25),GRAD(25)
      DIMENSION TIM(25),RATEM(25)
C
C
 1    FORMAT(4F10.0)
 2    FORMAT('0T=',E10.3,'           H=',F7.3,'           DX1=',F10.3,
    2 '           DX2=',E10.3)
 3    FORMAT('           I=',I2,'           T=',F7.2,'           DTDX=',
    2 E10.3,'           DTDT=',E10.3,'           H=',F7.2)
 4    FORMAT('            TIME=',E10.3,'           TMAX=',F7.2)
 5    FORMAT('            SUMH=',E10.3,'           SUMDH=',E10.3)
 6    FORMAT('            TIME=',E10.3,'           DTDTMAX=',E10.3)
C
C
C  THE FOLLOWING CONSTANTS CONTROL BOTH THE PRINTING INTERVAL AND
C   TERMINATION OF EACH RUN
      TEMST=0.0
      ISTOP=1002
      IZ=10
      TSTOP=30.0
      IC=0
      ICST=5
C
C
C  MATERIAL CONSTANTS: RHOD= DIE DENSITY, RHOC= CASTING DENSITY, TLIQ=
C     LIQUIDUS TEMPERATURE.
      RHOD=7.8
      RHOC=7.1
      TLIQ=1303.0
C
C  THE MESH IN THIS PROGRAM HAS TWO DIFFERENT SPACINGS: NEAR THE INTERFACE
C    SPACING=DX1, NEAR THE EXTERIOR DIE SURFACE SPACING= DX2
      DX1=.03527
      DX2=.44148
 1111 CONTINUE
      IF(IC.GT.ICST) GO TO 1400
      IC=IC+1
      READ(5,1) XH,DT,TO,TD
      READ(5,1) XHX1,TCH1,XHX2,TCH2
C
C
C  INITIALIZATION SECTION:
      TMAX=0.0
      DO 50 I=11,15
 50   RATEM(I)=0.0
      SUMH=0.0
      SUMDH=0.0
      H(1)=ENTHA(TO)
      DO 100 I=2,10
 100  H(I)=H(1)
      H(11)=ENTHA(TD)
      DO 200 I=12,25
 200  H(I)=H(11)
      IP2=IZ
      TSAVE=0
      TM=0,000
 250  CONTINUE
C
C  TEMPERATURE DETERMINATION: HERE THE ENTHALPY AT EACH NODE IS CONVERTED
C     TO TEMPERATURE USING THE APPROPRIATE THERM FUNCTION
      DO 300 IT=1,10
 300  TEMP(IT)=THERM(H(IT))
      DO 400 IT=11,25
 400  TEMP(IT)=THERM(H(IT))
C
C  MAXIMUM TEMPERATURE : TMAX= THE MAXIMUM TEMPERATURE AT THE INTERFACE
      IF(TEMP(11).LT.TMAX) GO TO 450
      TIME=TM
      TMAX=TEMP(11)
 450  CONTINUE
C
C  RATE SECTION: THIS SECTION CALCULATES THE RATE OF HEATING IN THE
C     DIE AT LOCATIONS NEAR THE INTERFACE
      IF(TM.EQ.0.000) GO TO 550
      DO 500 IR=1,25
 500  RATE(IR)=(TEMP(IR)-TEMP1(IR))/DT
      GO TO 600
 550  CONTINUE
      DO 575 IR=1,25
 575  RATE(IR)=0.00
 600  CONTINUE
C
C  MAXIMUM RATE: RATEM = THE MAXIMUM RATE OF DIE HEATING FOR NODES11-15
      DO 610 I=11,15
      IF(RATE(I).LT.RATEM(I)) GO TO 610
      TIM(I)=TM
      RATEM(I)=RATE(I)
 610  CONTINUE
      IP2=IP2+1
      IF(IP2.LT.17) GO TO 775
      IP2=0
C
C  SECTION FOR DETERMINING THE THERMAL GRADIENT WITHIN THE DIE
      DO 625 IG=11,14
      IG2=IG+1
 625  GRAD(IG)=(TEMP(IG)-TEMP(IG2))/DX1
C
C
C  PRINTING SECTION
      WRITE(6,2) TM,XH,DX1,DX2
      DO 700 I=1,25
 700  WRITE(6,3) I,TEMP(I),GRAD(I),RATE(I),H(I)
      WRITE(6,4) TIME,TMAX
      DO 750 I=11,15
      WRITE(6,6) TIM(I),RATEM(I)
 750  CONTINUE
      WRITE(6,5) SUMH,SUMDH
C
C  G= FLUX OF HEAT ACROSS THE INTERFACE
 775  G=(TEMP(10)-TEMP(11))*XH
C
C
C
```

```
C  HEAT FLOW SIMULATION: IN THIS SECTION THE APPROPRIATE NODAL EQUATIONS ARE
C     APPLIED THROUGHOUT THE MESH: INCLUDING BOUNDARY POINTS
C  THE NODE PTS. 1-1-10 ARE WITIN THE CASTING: 11 AND 12 ON EITER SIDE OF THE
C     INTERFACE: 12-25 ARE WITHIN THE DIE.
C  IF T.GT. TLIQ THE PROGRAM ASSUMES COMPLETE LIQUID CONVECTION
       IF (TEMP(1).GT.TLIQ) GO TO 900
       DO 850 JT=2,10
       IT=JT-1
       KT=JT+1
       T=TEMP(JT)
       XK=COND(T)
       PROP=(XK/(RHOC*(DX1**2)))
       IF(JT.EQ.10) GO TO 800
       DHDT(JT)=PROP*(TEMP(IT)-2.0*TEMP(JT)+TEMP(KT))
       GO TO 850
 800   DHDT(10)=(2.0*PROP/XK)*(XK*TEMP(IT)-(XK+DX1*XH)*TEMP(JT)+
     2 (XH*DX1)*TEMP(KT))
 850   CONTINUE
       DHDT(1)=DHDT(2)
       GO TO 950
 900   DHDT(10)=Q/(RHOC*9.0*DX1)*(-1.0)
       DO 925 IT=1,9
 925   DHDT(IT)=DHDT(10)
 950   CONTINUE
       DO 1050 JT=11,12
       IT=JT-1
       KT=JT+1
       T=TEMP(JT)
       XK=COND(T)
       PROP=(XK/(RHOD*(DX1**2)))
       IF(JT.EQ.11) GO TO 1000
       DHDT(JT)=PROP*(TEMP(IT)-2.0*TEMP(JT)+TEMP(KT))
       GO TO 1050
 1000  DHDT(11)=(2.0*PROP/XK)*(XK*TEMP(KT)-(XK+DX1*XH)*TEMP(JT)+
     2 (XH*DX1)*TEMP(IT))
 1050  CONTINUE
       T=TEMP(20)
       XK=COND(T)
       DHDT(20)=(XK/RHOD)*((DX1+DX2)*TEMP(19)-(DX2+3.0*DX1)*TEMP(20)+
     2 2.0*DX1*TEMP(21))/((DX1+DX2)*DX1*DX1)
       T=TEMP(21)
       DHDT(21)=(XK/RHOD)*(2.0*DX2*TEMP(20)-(3.0*DX2+DX1)*TEMP(21)+
     2 (DX1+DX2)*TEMP(22))/((DX1+DX2)*DX2*DX2)
       DO 1100 JT=22,24
       IT=JT-1
       KT=JT+1
       T=TEMP(JT)
       XK=COND(T)
       PROP=(XK/(RHOD*(DX2**2)))
 1100  DHDT(JT)=PROP*(TEMP(IT)-2.0*TEMP(JT)+TEMP(KT))
       DHDT(25)=DHDT(24)
       DO 1200 IT=1,25
 1200  H(IT)=H(IT)+DHDT(IT)*DT
       SUMDH=0.0
       DO 1225 I=1,25
 1225  SUMDH=SUMDH+DHDT(I)
       SUMH=0.0
       DO 1275 I=1,25
 1275  SUMH=SUMH+H(I)
C  THE ARRAY TEMPI IS STORED IN ORDER TO CALCULATE THE RATE ARRAY
```

```
      DO 1300 IT=1,25
 1300 TEMP1(IT)=TEMP(IT)
C TM= TIME DURING THE RUN: HERE IT IS AUGMENTED BY THE TIME INTERVAL
      TM=TM+DT
C  IN THIS SECTION THE VALUE OF H IS CHANGED TO SIMULATE CHANGES IN
C     THE CHARACTER OF THE INTERFACE
      IF(TM.LT.TCH1) GO TO 1301
      XH=XHX1
 1301 CONTINUE
      IF(TM.LT.TCH2) GO TO 1302
      XH=XHX2
 1302 CONTINUE
 1305 CONTINUE
C
C  CONTROL SECTION:
      ISAVE=ISAVE+1
      IF(ISAVE.LT.102) GO TO 1335
      I7=100
 1335 CONTINUE
      IF(ISAVE.GT.ISTOP) GO TO 1111
      IF(TEMP(1).LT.TEMST) GO TO 1111
      IF(TM.LT.TSTOP) GO TO 250
 1400 CONTINUE
      RETURN
      END
      FUNCTION COND(T)
C  THIS FUNTION CALCULATES THE THERMAL CONDUCTIVITY OF STEEL WITH TEMPERATURE
      IF(T.GT.877.00) GO TO 1010
      COND=.156-(1.03*.0001)*T
      GO TO 2010
 1010 COND=.065
 2010 CONTINUE
      RETURN
      END
      FUNCTION ENTHA(T)
C  THIS FUNCTION REPRESENTS THE ENTHALPY OF STEEL
      IF(T.GT.520.0) GO TO 1020
      ENTHA=T/7.8491
      GO TO 9020
 1020 IF(T.GT.950.0) GO TO 2020
      ENTHA=(T-201.8)/4.8031
      GO TO 9020
 2020 IF(T.GT.1150.0) GO TO 3020
      ENTHA=(T+137.5)/6.98125
      GO TO 9020
 3020 IF(T.GT.1155.0) GO TO 4020
      ENTHA=(T-1150.0)/.217+184.42
      GO TO 9020
 4020 IF(T.GT.1160.0) GO TO 5020
      ENTHA=T-1155.0+207.42
      GO TO 9020
 5020 IF(T.GT.1260.0) GO TO 6020
      ENTHA=(T-1160.0)/2.63+212.42
      GO TO 9020
 6020 IF(T.GT.1303.0) GO TO 7020
      ENTHA=(T-1260.0)/1.65+250.42
      GO TO 9020
 7020 ENTHA=(T-1303.0)/5.585+ 276.42
 9020 CONTINUE
```

```
      RETURN
      END
      FUNCTION THERM(H)
C  THIS FUNCTION CONVERTS ENTHALPY VALUES TO TEMPERATURE FOR STEEL
      IF(H.GT.66.25) GO TO 1030
      THERM=(7.8491)*H
      GO TO 7030
 1030 IF(H.GT.155.774) GO TO 2030
      THERM=201.8+(4.8031)*H
      GO TO 7030
 2030 IF(H.GT.184.422) GO TO 3030
      THERM=-137.5+(6.98125)*H
      GO TO 7030
 3030 IF(H.GT.207.42) GO TO 4030
      THERM=1150.0+.217*(H-184.42)
      GO TO 7030
 4030 IF(H.GT.212.42) GO TO 5030
      THERM=1155.0+(H-207.42)
      GO TO 7030
 5030 IF(H.GT.250.42) GO TO 6030
      THERM=1160.0+2.63*(H-212.42)
      GO TO 7030
 6030 IF(H.GT.276.42) GO TO 8030
      THERM=1260.0+1.65*(H-250.42)
      GO TO 7030
 8030 THERM=1303.0+5.585*(H-276.42)
 7030 CONTINUE
      RETURN
      END
$ENTRY
.1200000  .0050000  1200.00   420.00
$STOP
/*
```

```
// 'HACKMAN',CLASS=A,REGION=192K
/*SRT STANDARD
/*MAIN TIME=2,LINES=4
//STEP1     EXEC WATFIV
//C.SYSIN DD *
$JOB               HACKMAN,TIME=2
      DIMENSION H(25),TEMP1(25),TEMP(25),DHDT(25),RATE(25),GRAD(25)
      DIMENSION TIM(25),RATEM(25)
C
C
 1    FORMAT(4F10.0)
 2    FORMAT('0T=',F10.3,'             H=',F7.3,'             DX1=',E10.3,
     2 '               DX2=',E10.3)
 3    FORMAT('             I=',I2,'             T=',F7.2,'             DTDR=',
     2 E10.3,'             DTDT=',E10.3,'             H=',F7.2)
 4    FORMAT('              TIME=',E10.3,'              TMAX=',F7.2)
 5    FORMAT('              SUMH=',E10.3,'              SUMDH=',E10.3)
 6    FORMAT('              TIME=',E10.3,'              DTDTMAX=',E10.3)
C
C
C  THE FOLLOWING CONSTANTS CONTROL BOTH THE PRINTING INTERVAL AND
C   TERMINATION OF EACH RUN
      TEMST=0.0
      ISTOP=1002
      IZ=10
      TSTOP=30.0
      IC=0
      ICST=5
C
C
C  MATERIAL CONSTANTS: RHOD= DIE DENSITY, RHOC= CASTING DENSITY, TLIQ=
C     LIQUIDUS TEMPERATURE.
      RHOD=7.8
      RHOC=8.94
      TLIQ=1002.0
C
C  THE MESH IN THIS PROGRAM HAS TWO DIFFERENT SPACINGS: NEAR THE INTERFACE
C    SPACING=DX1, NEAR THE EXTERIOR DIE SURFACE SPACING= DX2
      DX1=.03527
      DX2=.44149
 1111 CONTINUE
      IF(IC.GT.ICST) GO TO 1600
      IC=IC+1
      READ(5,1) XH,DT,TO,TD
      READ(5,1) XHX1,TCH1,XHX2,TCH2
C
C
C  INITIALIZATION SECTION:
      TMAX=0.0
      DO 50 I=11,15
 50   RATEM(I)=0.0
      SUMH=0.0
      SUMDH=0.0
      H(1)=ENCOP(TO)
      DO 100 I=2,10
 100  H(I)=H(1)
      H(11)=ENTHA(TD)
      DO 200 I=12,25
 200  H(I)=H(11)
```

```
      IP2=17
      ISAVE=0
      TM=0.000
 250  CONTINUE
C
C  TEMPERATURE DETERMINATION: HERE THE ENTHALPY AT EACH NODE IS CONVERTED
C    TO TEMPERATURE USING THE APPROPRIATE THERM FUNCTION
      DO 300 IT=1,10
 300  TEMP(IT)=THERCU(H(IT))
      DO 400 IT=11,25
 400  TEMP(IT)=THERM(H(IT))
C
C  MAXIMUM TEMPERATURE : TMAX= THE MAXIMUM TEMPERATURE AT THE INTERFACE
      IF(TEMP(11).LT.TMAX) GO TO 450
      TIME=TM
      TMAX=TEMP(11)
 450  CONTINUE
C
C  RATE SECTION: THIS SECTION CALCULATES THE RATE OF HEATING IN THE
C    DIE AT LOCATIONS NEAR THE INTERFACE
      IF(TM.EQ.0.000) GO TO 550
      DO 500 IR=1,25
 500  RATE(IR)=(TEMP(IR)-TEMP1(IR))/DT
      GO TO 600
 550  CONTINUE
      DO 575 IR=1,25
 575  RATE(IR)=0.00
 600  CONTINUE
C
C  MAXIMUM RATE: RATEM = THE MAXIMUM RATE OF DIE HEATING FOR NODES11-15
      DO 610 I=11,15
      IF(RATE(I).LT.RATEM(I)) GO TO 610
      TIM(I)=TM
      RATEM(I)=RATE(I)
 610  CONTINUE
      IP2=IP2+1
      IF(IP2.LT.17) GO TO 775
      IP2=0
C
C  SECTION FOR DETERMINING THE THERMAL GRADIENT WITHIN THE DIE
      DO 625 IG=11,19
      IG2=IG+1
 625  GRAD(IG)=(TEMP(IG)-TEMP(IG2))/DX1
C
C
C  PRINTING SECTION
      WRITE(6,2) TM,XH,DX1,DX2
      DO 700 I=1,25
 700  WRITE(6,3) I,TEMP(I),GRAD(I),RATE(I),H(I)
      WRITE(6,4) TIME,TMAX
      DO 750 I=11,15
      WRITE(6,6) TIM(I),RATEM(I)
 750  CONTINUE
      WRITE(6,5) SUMH,SUMDH
C
C  G= FLUX OF HEAT ACROSS THE INTERFACE
 775  G=(TEMP(10)-TEMP(11))*XH
C
C
```

```
C
C  HEAT FLUX SIMULATION: IN THIS SECTION THE APPROPRIATE NODAL EQUATIONS ARE
C     APPLIED THROUGHOUT THE MESH: INCLUDING BOUNDARY POINTS
C  THE NODE PTS. 1-1-10 ARE WITIN THE CASTING: 11 AND 12 ON EITER SIDE OF THE
C     INTERFACE: 12-25 ARE WITHIN THE DIE
C  IF T.GT. TLIQ THE PROGRAM ASSUMES COMPLETE LIQUID CONVECTION
        IF (TEMP(1).GT.TLIQ) GO TO 900
        DO 850 JT=2,10
        IT=JT-1
        KT=JT+1
        T=TEMP(JT)
        XK=CONDCU(T)
        PROP=(XK/(RHOC*(DX1**2)))
        IF(JT.EQ.10) GO TO 800
        DHDT(JT)=PROP*(TEMP(IT)-2.0*TEMP(JT)+TEMP(KT))
        GO TO 850
 800    DHDT(10)=(2.0*PROP/XK)*(XK*TEMP(IT)-(XK+DX1*XH)*TEMP(JT)+
      2 (XH*DX1)*TEMP(KT))
 850    CONTINUE
        DHDT(1)=DHDT(2)
        GO TO 950
 900    DHDT(10)=G/(RHOC*9.0*DX1)*(-1.0)
        DO 925 IT=1,9
 925    DHDT(IT)=DHDT(10)
 950    CONTINUE
        DO 1050 JT=11,19
        IT=JT-1
        KT=JT+1
        T=TEMP(JT)
        XK=COND(T)
        PROP=(XK/(RHOD*(DX1**2)))
        IF(JT.EQ.11) GO TO 1000
        DHDT(JT)=PROP*(TEMP(IT)-2.0*TEMP(JT)+TEMP(KT))
        GO TO 1050
 1000   DHDT(11)=(2.0*PROP/XK)*(XK*TEMP(KT)-(XK+DX1*XH)*TEMP(JT)+
      2 (XH*DX1)*TEMP(IT))
 1050   CONTINUE
        T=TEMP(20)
        XK=COND(T)
        DHDT(20)=(XK/RHOD)*((DX1+DX2)*TEMP(19)-(DX2+3.0*DX1)*TEMP(20)+
      2 2.0*DX1*TEMP(21))/((DX1+DX2)*DX1*DX1)
        T=TEMP(21)
        DHDT(21)=(XK/RHOD)*(2.0*DX2*TEMP(20)-(3.0*DX2+DX1)*TEMP(21)+
      2 (DX1+DX2)*TEMP(22))/((DX1+DX2)*DX2*DX2)
        DO 1100 JT=22,24
        IT=JT-1
        KT=JT+1
        T=TEMP(JT)
        XK=COND(T)
        PROP=(XK/(RHOD*(DX2**2)))
 1100   DHDT(JT)=PROP*(TEMP(IT)-2.0*TEMP(JT)+TEMP(KT))
        DHDT(25)=DHDT(24)
        DO 1200 IT=1,25
 1200   H(IT)=H(IT)+DHDT(IT)*DT
        SUMDH=0.0
        DO 1225 I=1,25
 1225   SUMDH=SUMDH+DHDT(I)
        SUMH=0.0
        DO 1275 I=1,25
 1275  SUMH=SUMH+H(I)
C  THE ARRAY TEMP1 IS STORED IN ORDER TO CALCULATE THE RATE ARRAY
       DO 1300 IT=1,25
 1300  TEMP1(IT)=TEMP(IT)
C TM= TIME DURING THE RUN, HERE IT IS AUGMENTED BY THE TIME INTERVAL
       TM=TM+DT
C  IN THIS SECTION THE VALUE OF H IS CHANGED TO SIMULATE CHANGES IN
C     THE CHARACTER OF THE INTERFACE
       IF(TM.LT.TCH1) GO TO 1301
       XH=XHX1
 1301  CONTINUE
       IF(TM.LT.TCH2) GO TO 1302
       XH=XHX2
 1302  CONTINUE
 1305  CONTINUE
C
C  CONTROL SECTION:
       ISAVE=ISAVE+1
       IF(ISAVE.LT.102) GO TO 1335
       I7=100
 1335  CONTINUE
       IF(ISAVE.GT.ISTOP) GO TO 1111
       IF(TEMP(1).LT.TEMST) GO TO 1111
       IF(TM.LT.TSTOP) GO TO 250
 1400  CONTINUE
       RETURN
       END
       FUNCTION COND(T)
C  THIS FUNTION CALCULATES THE THERMAL CONDUCTIVITY OF STEEL WITH TEMPERATURE
       IF(T.GT.377.00) GO TO 1010
       COND=.156-(1.03*.0001)*T
       GO TO 2010
 1010  COND=.055
 2010  CONTINUE
       RETURN
       END
       FUNCTION CONDCU(T)
C     THIS FUNCTION CALCULATES THE THERMAL CONDUCTIVITY FOR COPPER
       CONDCU=.9796-.0001724*T
       RETURN
       END
       FUNCTION ENTHA(T)
C  THIS FUNCTION REPRESENTS THE ENTHALPY OF STEEL
       IF(T.GT.520.0) GO TO 1020
       ENTHA=T/7.8491
       GO TO 9020
 1020  IF(T.GT.950.0) GO TO 2020
       ENTHA=(T-201.8)/4.8031
       GO TO 9020
 2020  IF(T.GT.1150.0) GO TO 3020
       ENTHA=(T+137.5)/6.98125
       GO TO 9020
 3020  IF(T.GT.1155.0) GO TO 4020
       ENTHA=(T-1150.0)/.217+184.42
       GO TO 9020
 4020  IF(T.GT.1160.0) GO TO 5020
       ENTHA=T-1155.0+207.42
       GO TO 9020
 5020  IF(T.GT.1260.0) GO TO 6020
```

```
      ENTHA=(T-1160.0)/2.63+212.42
      GO TO 9020
 6020 IF(T.GT.1303.0) GO TO 7020
      ENTHA=(T-1260.0)/1.65+250.42
      GO TO 9020
 7020 ENTHA=(T-1303.0)/5.585+ 276.42
 9020 CONTINUE
      RETURN
      END
      FUNCTION ENCOP(T)
C   THIS FUNCTION REPRESENTS THE ENTHALPY OF COPPER
      IF(T.GT.785.0)  GO TO 1040
      ENCOP=.1027*T-4.61
      GO TO 3040
 1040 IF(T.GT.1002.0) GO TO 2040
      ENCOP=.2627*T-130.22
      GO TO 3040
 2040 ENCOP=.1212*T+11.56
 3040 CONTINUE
      RETURN
      END
      FUNCTION THERM(H)
C  THIS FUNCTION CONVERTS ENTHALPY VALUES TO TEMPERATURE FOR STEEL
      IF(H.GT.66.25) GO TO 1030
      THERM=(7.8491)*H
      GO TO 7030
 1030 IF(H.GT.155.774) GO TO 2030
      THERM=201.8+(4.8031)*H
      GO TO 7030
 2030 IF(H.GT.184.422) GO TO 3030
      THERM=-137.5+(6.98125)*H
      GO TO 7030
 3030 IF(H.GT.207.42) GO TO 4030
      THERM=1150.0+.217*(H-184.42)
      GO TO 7030
 4030 IF(H.GT.212.42) GO TO 5030
      THERM=1155.0+(H-207.42)
      GO TO 7030
 5030 IF(H.GT.250.42) GO TO 6030
      THERM=1160.0+2.63*(H-212.42)
      GO TO 7030
 6030 IF(H.GT.276.42) GO TO 8030
      THERM=1260.0+1.65*(H-250.42)
      GO TO 7030
 8030 THERM=1303.0+5.585*(H-276.42)
 7030 CONTINUE
      RETURN
      END
      FUNCTION THERCU(H)
C   THIS FUNCTION CONVERTS ENTHALPY VALUES TO TEMPERATURE FOR COPPER
      IF(H.GT.76.0) GO TO 1060
      THERCU=9.737*H+44.88
      GO TO 3060
 1060 IF(H.GT.133.0) GO TO 2050
      THERCU=3.806*H+495.69
      GO TO 3060
 2060 THERCU=8.25*H-95.37
 3060 CONTINUE
      RETURN
```

BIOGRAPHICAL NOTE

The author was born in Boston, Massachusetts on June 15, 1949. After completing high school studies at Phillips Academy, Andover, Massachusetts, he entered the Massachusetts Institute of Technology where he received his S.B. and S.M. degrees in the Department of Metallurgy and Materials Science in 1972. His thesis, under the supervision of Professor Merton C. Flemings, was entitled "The Effect of Zirconium on the Solidification of Al-Cu-Zr Alloys". As an undergraduate he received financial support from the Foundry Educational Foundation.

He immediately continued his graduate education in the Solidification group at M.I.T. under the joint supervision of Professors Robert Mehrabian and Merton C. Flemings. In 1974 he received a Harris Foundation Stipend.

In 1971 he married the former Susan Carter who is currently a nurse at the Massachusetts General Hospital.